Lígia Sauaya Pereira

Reconstruction of the ocean circulation in the subtropical western South Atlantic during the last 40,000 years

Thesis presented as a partial fulfilment of the requirements for the degree of Doctor of Science in Oceanography at the Oceanographic Institute, University of São Paulo, in the area of Geological Oceanography.

Supervisor: Prof. Dr. Rubens Cesar Lopes Figueira

.

São Paulo
2018

Lígia Sauaya Pereira

Reconstruction of the upper ocean circulation in the subtropical western South Atlantic during the last 40,000 years

Corrected version

Thesis presented as a partial fulfilment of the requirements for the degree of Doctor of Science in Oceanography at the Oceanographic Institute, University of São Paulo, in the area of Geological Oceanography.

Evaluated in: _____/_____/_____

_____
Prof(a). Dr(a).

_____
Prof(a). Dr(a).

_____
Prof(a). Dr(a).

_____
Prof(a). Dr(a).

Table of Contents

List of Figures

List of Tables

List of Acronyms

AAIW	Antarctic Intermediate Water
AABW	Antarctic Bottom Water
AC	Agulhas Current
ACC	Antarctic Circumpolar Current
AIM	Antarctic Isotope Maxima
AMOC	Atlantic Meridional Overturning Circulation
B-A	Bølling-Allerød
BC	Brazil Current
BCC	Brazilian Coastal Current
BGC	Benguela Current
BMC	Brazil-Malvinas Confluence
CSM	Cape Santa Marta
D-O	Dansgaard-Oeschger Events
HS	Heinrich Stadials
ITCZ	Intertropical Convergence Zone
LGM	Last Glacial Maximum
MAT	Modern Analog Technique
MC	Malvinas Current
NADW	North Atlantic Deep Water
PPW	Plata Plume Water
SAC	South Atlantic Current
SACW	South Atlantic Central Water
SACZ	South Atlantic Convergence Zone
SASH	South Atlantic Subtropical High
SASM	South American Summer Monsoon
SEC	South Equatorial Current
SSS	Sea Surface Salinity
SST	Sea Surface Temperature
STF	Subtropical Front
TW	Tropical Water
YD	Younger Dryas

Abstract

The Atlantic meridional overturning circulation (AMOC) has a central role in the interhemispheric transport of heat and changes in its intensity are known to have profound impact on global climate. Disturbances in the AMOC are also supposedly associated with the past changes in marine productivity and oceanic uptake of atmospheric carbon dioxide, which contributed to the global climate changes that led to the termination of the last glacial cycle. Although the South Atlantic Ocean constitutes an important pathway for the return flow of the AMOC, the changing impacts of the AMOC especially in the subtropical western South Atlantic still remain elusive. In this study, high-resolution records of upper water column properties and productivity have been applied to reconstruct the evolution of oceanographic conditions in the subtropical western South Atlantic covering the last 40,000 years. The proxy records employed here are based both on faunal assemblages and on the stable oxygen isotopic composition of planktonic foraminifera from a marine sediment core collected off southern Brazilian continental margin (27°S). The main findings of the present study reveal, for the first time, enhanced primary productivity in the subtropical western South Atlantic during Heinrich Stadials along the last glacial, when the AMOC showed reduced strength. Additionally, this study reveals decreased primary productivity over the Last Glacial Maximum and the Younger Dryas, when the AMOC showed only moderate reductions. The most outstanding productivity decline is depicted after the Holocene inception, when the AMOC recovered its strength. Further, the findings of the present work also reveal that rather overall glacial-like conditions prevailed at the onset of the Holocene, before complete reinvigoration of the AMOC. Full interglacial configuration would only establish at approximately 9,000 years, when the AMOC fully recovered; although such interglacial setting would be abruptly interrupted during the Mid Holocene, accompanying a sudden reduction of the AMOC. Those findings suggest that the impact of the AMOC on the subtropical western South Atlantic would have played a critical role not only over the last glacial, but also throughout the glacial-interglacial transition and even under full interglacial conditions. The main hypothesis of this research is that the observed changes were triggered by the dynamics of the Brazil Current primarily driven by disturbances in the AMOC.

Keywords: paleoceanography, paleoproductivity, planktonic foraminifera, Atlantic meridional overturning circulation (AMOC), Brazil Current, South Atlantic.

Resumo

A célula de revolvimento meridional do Atlântico (AMOC) desempenha um papel central no transporte inter-hemisférico de calor e mudanças em sua intensidade têm profundo impacto sobre o clima global. Distúrbios na AMOC supostamente também estariam associados a alterações pretéritas na produtividade marinha e absorção oceânica de dióxido de carbono atmosférico, que contribuíram para mudanças no clima global e levaram à terminação do último ciclo glacial. Embora o Atlântico Sul constitua importante rota para o fluxo de retorno da AMOC, impactos de alterações na AMOC especialmente na porção subtropical do Atlântico Sudoeste ainda permanecem elusivos. Neste estudo, registros de alta resolução de propriedades da camada superior da coluna de água e de produtividade foram utilizados para reconstruir a evolução de condições oceanográficas na porção subtropical do Atlântico Sudoeste ao longo dos últimos 40,000 anos. Os indicadores empregados se baseiam na composição de assembleias faunísticas e de isótopos estáveis de oxigênio em foraminíferos planctônicos de testemunho sedimentar marinho coletado na margem continental sul do Brasil (27°S). Os principais resultados deste estudo revelam, pela primeira vez, aumento de produtividade primária na porção subtropical do Atlântico Sudoeste durante *Heinrich Stadials* ao longo do último glacial, quando a AMOC apresentou reduzida intensidade. Adicionalmente, o presente estudo revela diminuição de produtividade primária durante o Último Máximo Glacial e *Younger Dryas*, quando a AMOC apresentou apenas moderada redução. O declínio de produtividade mais proeminente é observado após o início do Holoceno, quando a AMOC recuperou sua intensidade. Os resultados do presente trabalho também revelam que, de modo geral, condições similares ao glacial prevaleceram no princípio do Holoceno, antes de completa retomada da AMOC. Plenas condições interglaciais apenas teriam se estabelecido há cerca de 9,000 anos, quando a AMOC foi completamente revigorada; embora plena configuração interglacial tenha sido abruptamente interrompida em meados do Holoceno, acompanhando repentina redução da AMOC. Estes resultados sugerem que o impacto da AMOC na porção subtropical do Atlântico Sudoeste teria desempenhado um papel crítico não apenas durante o último glacial, mas também ao longo da transição glacial-interglacial e mesmo sob plenas condições interglaciais. A principal hipótese deste estudo é de que as mudanças observadas foram ocasionadas por dinâmicas da Corrente do Brasil primariamente induzidas por distúrbios na AMOC.

Palavras-chave: paleoceanografia, paleoprodutividade, foraminíferos planctônicos, célula de revolvimento meridional do Atlântico (AMOC), Corrente do Brasil, Atlântico Sul.

Chapter 1

Introduction

1.1 Context

The last glacial-interglacial transition was marked by a pronounced rise in global temperatures and increased carbon dioxide content in the atmosphere. As an important greenhouse gas, atmospheric carbon dioxide has a strong impact on the Earth's climate system, modulating the transitions from glacial to interglacial climate states (SIGMAN; BOYLE, 2000; BROVKIN *et al.*, 2007). Such impact on global climate is clearly evidenced in ice core records (PETIT *et al*., 1999) showing an outstanding increase of approximately 90 ppm in the atmospheric carbon dioxide content during the termination of the last glacial cycle (MONNIN *et al*., 2001). The mechanisms associated to that internal change in the Earth's climate system along glacial-interglacial cycles, yet, still remain elusive (BERNARDELLO, 2014; SCHMITTNER; LUND, 2015).

It is a consensus, however, that the ocean plays a critical role in the regulation of the Earth's carbon cycle as an important carbon reservoir (PETERSON; LISIECKI; STERN, 2014). The ocean carbon uptake is propitiated by the interplay between distinct processes that take place at the air-sea interface (LEVY *et al*., 2013). Physical properties related to the enhanced solubility of carbon dioxide in cooler seawater foster carbon storage by deeper and colder water masses at abyssal depths, a process commonly referred to as 'physical pump' (GRUBER; SARMIENTO, 2002; ARCHER *et al*., 2004). Marine biological activity resulting in a vertical flux of organic carbon to the seafloor also represents an important mechanism of carbon sink at oceanic depths, a process widely known as 'biological pump' (MIX, 1989; THOMSEN *et al*., 2017). Altogether, both mechanisms boost carbon storage into the deep ocean, playing a crucial role in the regulation of global climate (SIGMAN; BOYLE, 2000; MORRISON; FRÖLICHER; SARMIENTO, 2015).

Part of the carbon stored in the seafloor returns to the surface through the upwelling of deeper and nutrient-rich waters, which fuel most of biological productivity in the global ocean (SARMIENTO *et al*., 2010). In regions where carbon-rich deep water masses emerge to the surface a great excess of carbon dioxide stored in the seafloor is released to the atmosphere (MARINOV *et al*., 2006; SKINNER *et al*., 2010). Hence, upwelling also has a key importance to global climate.

Disturbances in the ocean circulation affecting carbon dioxide uptake largely impact the global carbon cycle and thereby the Earth's climate system. It has been suggested (SCHMITTNER; LUND, 2015; HERTZBERG *et al*., 2016) that changes in the oceanic biological pump efficiency supposedly governed by perturbations in the Atlantic meridional overturning circulation (AMOC) (MARIOTTI *et al*., 2012; MENVIEL *et al*., 2014) would have induced the atmospheric carbon rise recorded during the termination of the last glacial cycle (PETIT *et al*., 1999; MONNIN *et al*., 2001). Particularly in the western South Atlantic, however, the evolution of marine productivity along the last glacial-interglacial cycle is still poorly constrained. The coupling between marine productivity changes and disturbances in the AMOC therefore still remains unclear (ANDERSON *et al*., 2009; SCHMITTNER; LUND, 2015).

Along with marine productivity, the seawater temperature also directly affects solubility and ocean carbon uptake. Variabilities in seawater temperature are tightly linked to the AMOC, which transports a substantial amount of heat from low to high latitudes widely modulating ocean heat redistribution and storage (GANACHAUD; WUNSCH, 2003; BARKER *et al.*, 2009). Disturbances in the AMOC thus severely impact both ocean heat transport and carbon uptake, thereby affecting global climate (BROECKER *et al*., 1998; BÖHM *et al.*, 2015). Glacial terminations are known to be marked by a reinvigoration of the Atlantic overturning circulation (AMOC 'warm mode') largely fostered by the reestablishment of the Indian-Atlantic interoceanic connection ('warm route') through the 'leakage' of warm and salty waters from the Agulhas Current (KNORR; LOHMANN, 2003; PEETERS, *et al*., 2004). Still, especially on the western South Atlantic, little is known about the effect of the Agulhas leakage under such transient climate conditions (PIVEL *et al*., 2013; SANTOS *et al.*, 2017b).

The western South Atlantic is the pathway for (sub) surface warm and salty waters from the Indian Ocean reaching the Atlantic, which recirculate in the anticyclonic South Atlantic subtropical gyre and are transported poleward by the Brazil Current (BC) when approaching the western boundary of the gyre (STRAMMA; ENGLAND, 1999; TOMCZAK; GODFREY 2003). The South Atlantic is also the flow path of the deepest water masses of the global ocean formed in the high latitudes of the North Atlantic, which strongly impact the AMOC; and the Southern Ocean, where abyssal waters store most of the global oceanic carbon (GARZOLI; MATANO, 2011). It is also one of the regions where those nutrient-enriched waters originated in the Southern Ocean emerge to the surface (ANDERSON *et al*., 2009).

Nevertheless, particularly in the western South Atlantic upwelling regions, where higher primary productivity occurs, reconstructions of past productivity changes are so far scarce or limited in temporal resolution and coverage (PORTILHO-RAMOS *et al*., 2015; LESSA *et al*., 2017). Likewise, the reconstruction of past oceanographic changes in the subtropical western South Atlantic associated with the inflow of warm and salty waters from the Indian Ocean throughout transient climate conditions are still poorly documented (PIVEL *et al*., 2013; SANTOS *et al.*, 2017b).

Paleoceanographic reconstructions are crucial to unravel potential links between anomalies of temperature and marine productivity correlated to disruptions in the AMOC. The scarcity of high-resolution records challenge the understanding of the underlying mechanisms associated to boundary conditions as those that led to past glacial-interglacial transitions. Also, limited spatial and temporal coverage records constrain not only the development and support for conceptual models, but also the validation of climate model simulations that might provide more accurate prediction of future climate changes (KOHFELD, *et al*, 2013; VÖLKER; KÖHLER, 2013).

Such understanding proves to be critical in light of the ongoing anthropogenic carbon emissions and global warming (SCHEFFER; BROVKIN; COX, 2006; TORN; HARTE, 2006). Evidences from ice core and deep-sea sediment records show that atmospheric carbon dioxide concentration has varied by up to 40% over the past few hundred

thousand years (MIX, 1989). Also, an increased inflow of Indian Ocean waters to the South Atlantic over the past few decades has been indicated both by observations (CAI, 2006) and by modelling results (BIASTOCH *et al*., 2009) in response to anthropogenic forcing. A persistent change in the Agulhas system is projected to accelerate in the near future possibly altering the AMOC evolution, and thus affecting global climate (SEN GUPTA *et al.*, 2009; BEAL *et al*., 2011; CALEY *et al*., 2012). It was within such a context that motivation has greatly aroused to develop the present research.

1.2 Objectives

The main objective of this work was to reconstruct the evolution of paleoceanographic conditions in the subtropical western South Atlantic throughout the last glacial-interglacial cycle aiming to evaluate potential links between upper ocean changes and disturbances in the AMOC. In order to fulfil that aim, high-resolution records from a highly productive region of the western South Atlantic have been applied. Also, the recorded changes have been assessed under distinct background climate conditions within the last glacial and the Holocene, covering the last 40,000 years. The following specific objectives were set as to accomplish the main goal of this study:

(i) Assess marine primary productivity evolution in the upwelling region off Cape Santa Marta (27^{o}S) based on the faunal composition of planktonic foraminiferal assemblages;

(ii) Estimate anomalies of temperature in the upper water column applying the Modern Analog Technique (MAT) derived from planktonic foraminiferal associations;

(iii) Evaluate sea surface salinity changes employing the oxygen isotopic composition of ice-volume corrected seawater ($\delta^{18}O_{ivc\text{-}ssw}$) as a salinity proxy;

(iv) Examine underlying shifts in the upper water column stratification through planktonic foraminiferal oxygen isotope records;

(v) Analyse the impact of Agulhas leakage using planktonic foraminiferal species typical for Agulhas fauna as a tracer.

1.3 Outline

After setting the context and aims of the present research in this introductory Chapter 1, an overview of the last glacial-interglacial background climate conditions is presented in Chapter 2. The modern environmental setting in the study area is outlined in Chapter 3. The methodology applied in the present research is described in Chapter 4 and the results are presented in the following Chapter 5. The outcomes yielded in the framework of this research are further discussed in Chapter 6, and the main findings are summarised in Chapter 7.

Chapter 2

Last Glacial-Interglacial Cycle

Changes in the global climate system are primarily forced by cyclic oscillations in the Earth's orbital parameters (i.e., eccentricity, obliquity or tilt, precession), the so-called Milankovitch cycles (Fig. 1), which affect seasonality and location of solar radiation reaching the Earth. Such cyclic changes in the orbital geometry impacting the advance and retreat of ice sheets and glaciers resulted in the succession of glacial and interglacial periods within the Quaternary (Fig. 2) (HAYS; IMBRIE; SHACKLETON, 1976).

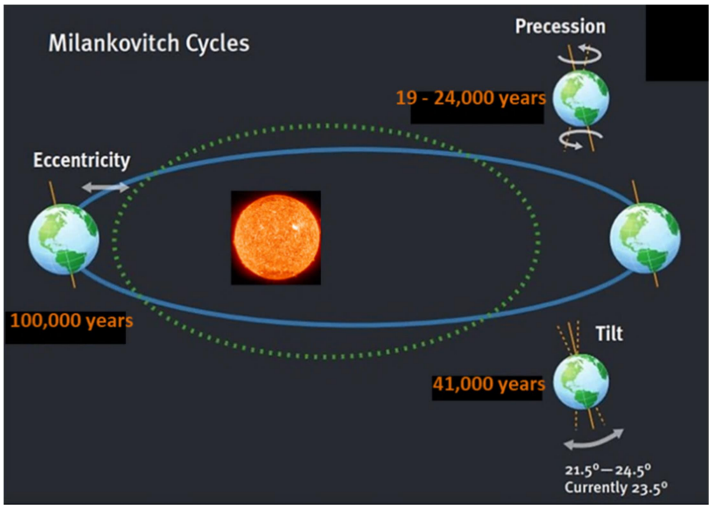

Figure 1 – Schematic elements of Milankovitch cycles (Source: The COMET Program).

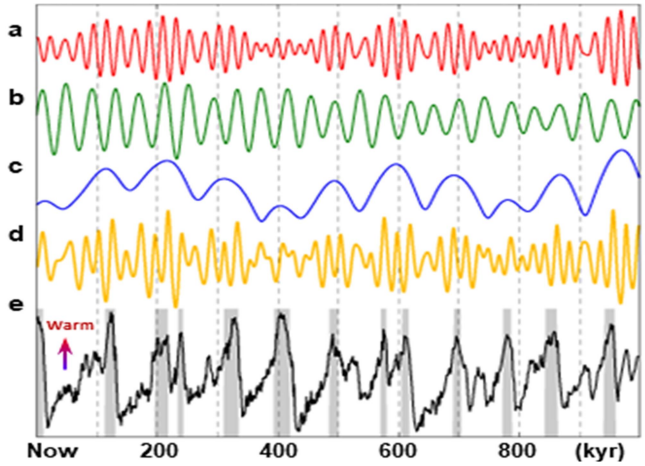

Figure 2 – Milankovitch cycles and glaciation stages. (a) precession (orientation of Earth's axis); (b) obliquity (tilt of Earth's axis); (c) eccentricity; (d) solar forcing (65°N summer); (e) stages of glaciation (grey band: warm interglacials) (adapted from BERGER; WEFER, 1992).

Superimposed to the long-term trend dictated by astronomical parameters (i.e., orbital timescale), short-term (i.e., suborbital timescale) climate changes also marked the course of the last glacial cycle (Fig. 3) (RAHMSTORF, 2001).

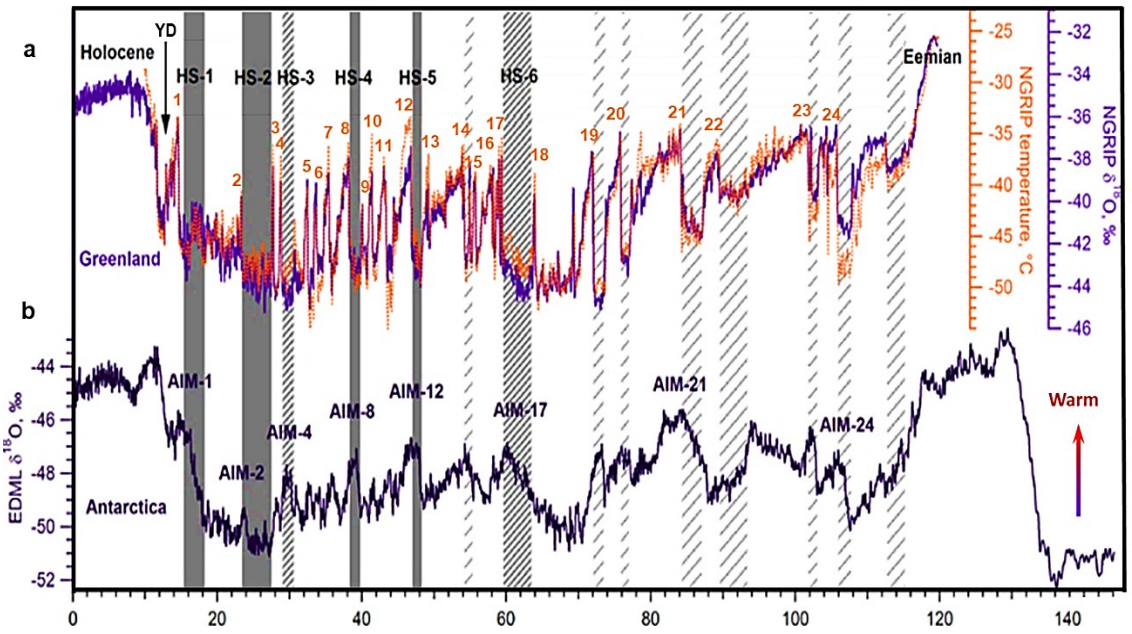

Figure 3 – Chronology of major climatic events along the last glacial. (a) Dansgaard-Oeschger (D-O): events of rapid warming (interstadials) in Greenland (orange numbers), detected both in oxygen isotope ($\delta^{18}O$) records from the NGRIP ice core (light purple line) (NGRIP MEMBERS, 2004) and in the temperature reconstruction for NGRIP drilling site (orange dots) (KINDLER *et al.*, 2014). Heinrich Stadials (HS): periods of prolonged cooling (stadials) in the northern latitudes culminating in major events (grey bars: mostly of Laurentide origin; dark grey hatch bars: mostly of European origin) (HEINRICH, 1988) and also minor episodes (light grey hatch) (CHAPMAN; SHACKLETON, 1999) of iceberg discharge in the North Atlantic, recorded in ice rafted debris (IRD) layers of marine sediment cores. Younger Dryas (YD): interval of sudden return to glacial conditions in the northern hemisphere, mirrored in the NGRIP ice core and also in pollen records of cold-tolerant *Dryas octopetala* wildflowers; (b) Antarctic Isotope Maxima (AIM): warming events in Antarctica depicted in $\delta^{18}O$ records from the EDML ice core (dark purple line) (EPICA COMMUNITY MEMBERS, 2006) (Source: Creative Commons).

Abrupt climate changes in the northern hemisphere initially detected in ice core records from Greenland (Fig. 3a) were characterised by brief intervals of pronounced warming (interstadials), the so-called Dansgaard-Oeschger (D-O) events, that interrupted prolonged periods of intense cooling (DANSGAARD *et al.*, 1984; OESCHGER *et al.*, 1984). Parallel to the D-O events, long lasting time periods of low temperatures (stadials) culminated in episodes of massive iceberg discharge in the North Atlantic recorded in marine sediment cores (HEINRICH, 1988). Such episodic events within glacial stadials, known as Heinrich Stadials (HS), took place in the cold spells

immediately contiguous to D-O warmings. The increasingly warming trend toward the Holocene after the glacial maxima receding was temporarily reversed by an interval of sudden return to glacial conditions in the northern latitudes. Such event of abrupt cooling, referred to as the Younger Dryas (YD), was named after the signature of pollen records from the cold-tolerant alpine-tundra wildflower *Dryas octopetala*, signalling its rapid northward expansion over that period (ALLEY, 2000; CARLSON, 2013).

In contrast to the rapid changes recorded in the high northern latitudes, temperature oscillations in the southern hemisphere were rather gradual (Fig. 3b), as evidenced by Antarctic ice core records (EPICA COMMUNITY MEMBERS, 2006). Also, the episodic warming intervals in the southern high latitudes, termed as Antarctic Isotopic Maxima (AIM), were not synchronous with the events of abrupt temperature rise in its northern counterparts. Instead, the coupling between D-O and AIM events show opposite directions, rather occurring approximately out of phase. Such anti-correlated pattern between both hemispheres has been attributed to drastic reorganisations of the ocean circulation linked to variabilities in the AMOC, which acts to redistribute heat across the Atlantic. Disruptions in the AMOC would have affected the interhemispheric transport of heat, dictating the pace of anomalous temperature swings at millennial timescale and resulting in the seesawing of heat between the hemispheres along the last glacial (CROWLEY, 1992; BROECKER, 1998; BLUNIER; BROOK, 2001).

The AMOC constitutes the Atlantic portion of the global ocean conveyor belt, a global system of currents driven by the thermohaline circulation, which encircles the globe redistributing heat around the global ocean (Fig. 4). The thermohaline circulation is induced by density gradients defined by seawater temperature and salinity. Less dense warm surface waters flowing poleward cool along its pathway by losing heat to the atmosphere. Once reaching the pole, they also get saltier since salt does not freeze as sea ice forms, so that it drains into the surrounding seawater. Surface waters hence become denser and sink into the deep ocean. Less dense surface waters then move to replace the sinking seawater, thereby fuelling the thermohaline circulation. It is estimated that a cubic meter of seawater may take about a thousand years to complete its pathway along the global conveyor belt (RAHMSTORF, 2006).

Figure 4 – Schematic representation of the global ocean conveyor belt (Source: National Oceanographic Centre).

As a component of the global conveyor belt, the AMOC transports substantial amount of heat from the tropics toward the northern high latitudes, the equivalent of 1.3 PW (1 PW = 10^{15} W), accounting for 25% of the global meridional heat transport (GANACHAUD; WUNSCH, 2003). AMOC disturbances thus strongly impact the cross-equatorial transport of heat (Fig. 5) and thereby the global climate system.

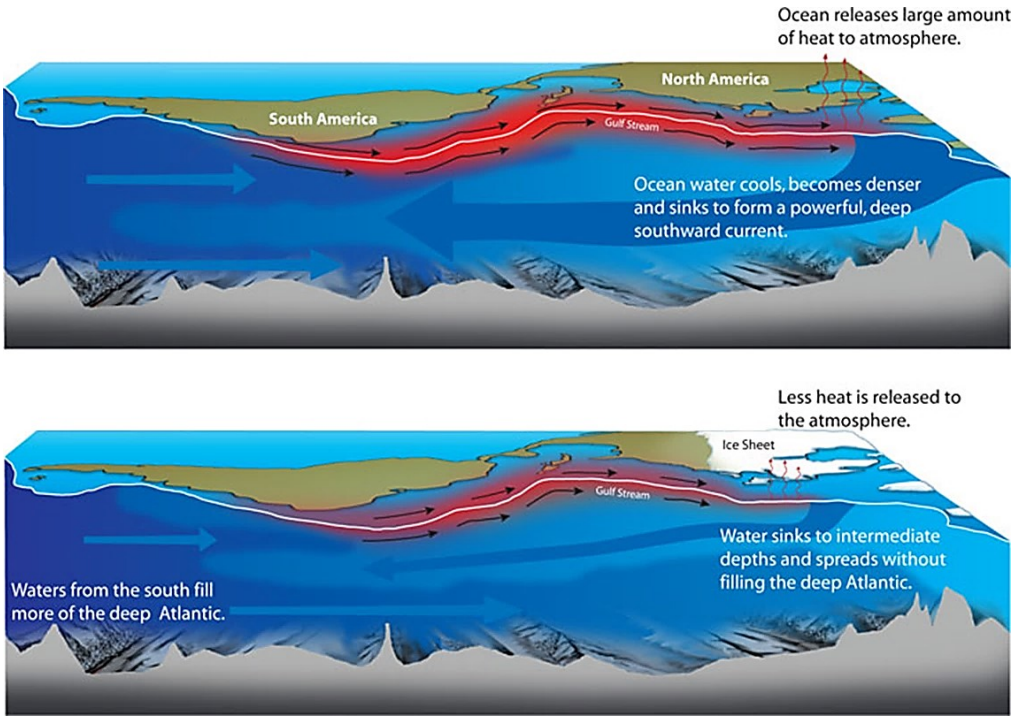

Figure 5 – Transect of the Atlantic Ocean and schematic illustration of Atlantic meridional overturning circulation (AMOC) disturbance (Source: Woods Hole Oceanographic Institute).

The primary control of such cross-equatorial heat transported by the AMOC is determined by the imbalance between the deep water masses formed in the high latitudes of the North Atlantic (i.e., North Atlantic Deep Water - NADW) and the Southern Ocean (i.e., Antarctic Bottom Water - AABW). Reduced NADW production, and ultimately the AMOC slowdown, results in a decreased northward export of heat (Fig. 5). As a consequence, heat is stored southward. This leads therefore to the northern latitudes cooling and ensuing southern hemisphere warming. Such interhemispheric coupling has been coined as the 'bipolar seesaw' (Fig. 6) (CROWLEY, 1992; STOCKER, 1998; BROECKER, 1998).

The notion of a bipolar asynchrony determined by such disturbances in the ocean circulation modulating the leads and lags between the two hemispheres (Fig. 6a) has also been reinforced by climate modelling results (Fig. 6b). Simulation experiments show that artificially induced AMOC shutdown in fact results in a widespread northern hemisphere cooling and correlated southward warming (VELLINGA; WOOD, 2002; ZHANG; DELWORTH, 2005; JAESCHKE *et al*., 2007).

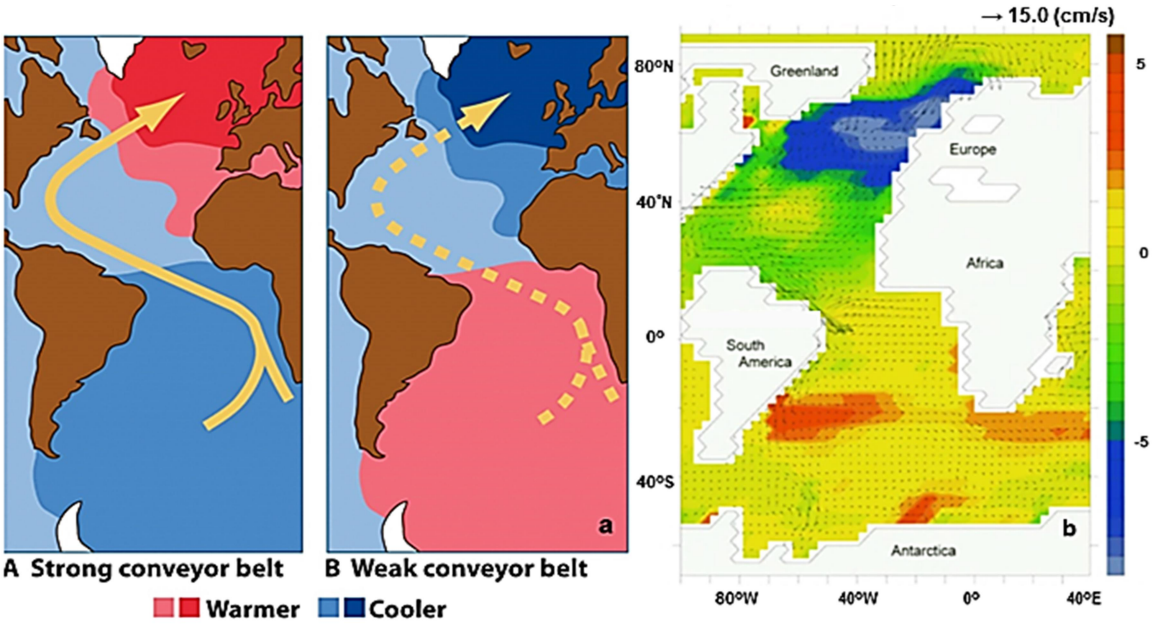

Figure 6 – The bipolar seesaw. (a) schematic representation of the conceptual model of a thermal 'bipolar seesaw' associated with disturbances in the strength of the Atlantic conveyor belt (RUDDIMAN, 2008); (b) result of a simulation experiment performed with a coupled ocean-atmosphere model showing anomalous temperature in ^{o}C (colour shading) across the Atlantic under induced AMOC shutdown. The arrow at the top indicates a velocity of 15 cm/s (adapted from JAESCHKE *et al*., 2007).

Transient global climate models also indicate that the most severe impact on climate resulting from disruptions in the ocean circulation particularly takes place in the North Atlantic sector, where the NADW is formed (Fig. 7). This further reiterates the critical importance of the AMOC as a sensitive part of the global ocean circulation and therefore of the global climate system (VELLINGA; WOOD, 2002; ZHANG; DELWORTH, 2005).

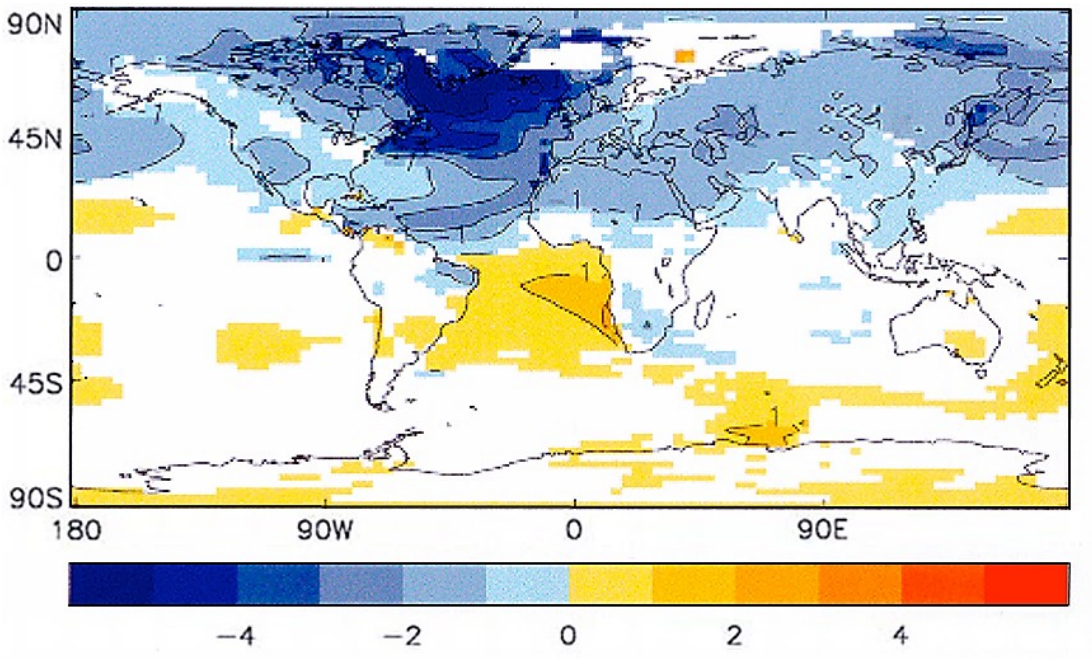

Figure 7 – Global climate impact of a collapse in the Atlantic thermohaline circulation. The impact is depicted in the surface air temperature change in ^{o}C (colour shading) derived from a coupled ocean-atmospheric circulation model (VELLINGA; WOOD, 2002).

Climate models further evidence that the thermohaline circulation is a highly nonlinear system. As it was first described by STOMMEL (1961) in a pioneer modelling study, such nonlinearity is most importantly driven by seawater salinity. This implies that when anomalies in seawater salinity reach a critical threshold the thermohaline circulation is suddenly transposed to another equilibrium state, which would thus result in abrupt climate changes (RAHMSTORF, 2006).

Shifts in seawater salinity may trigger either positive or negative feedbacks in the thermohaline circulation and ultimately in the climate system. A positive salinity feedback occurs when strengthened thermohaline circulation transports more salt

northward, enhancing deep water formation in the northern high-latitudes, thereby fuelling the thermohaline circulation and the transport of heat. Conversely, a negative feedback induced by critical salinity decrease leads to reduced deep-water production, acting instead to weaken the thermohaline circulation and redistribution of heat (DE VRIES; WEBER, 2005; RAHMSTORF, 2006).

Disturbances in the Atlantic deep water circulation along the last glacial would have been mainly reflected by three major modes of ocean circulation prevailing at distinct intervals throughout that period (Fig. 8) (RAHMSTORF, 2002).

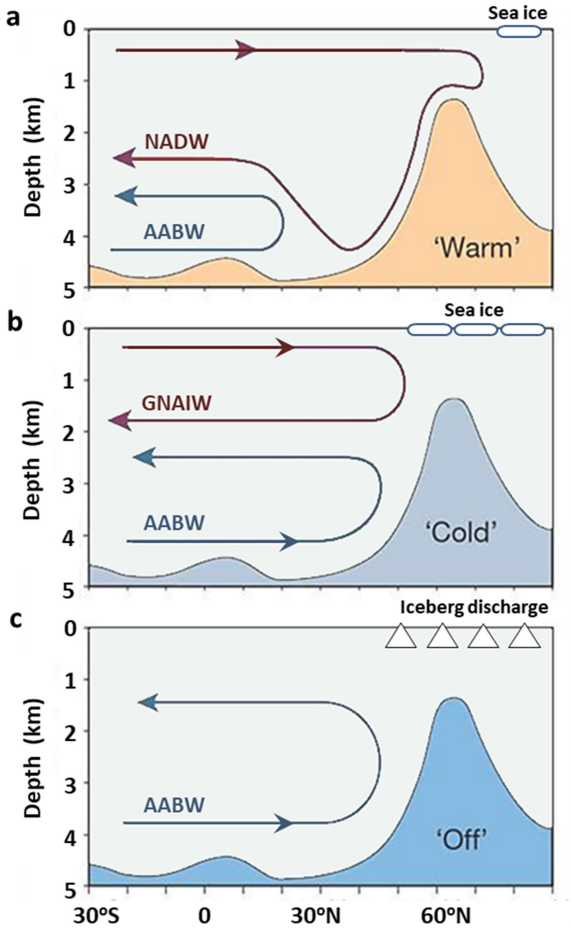

Figure 8 – Schematic modes of the AMOC during the last glacial period. The diagrams show the interplay between northern- (red) and southern-sourced (blue) waters defining the distinct AMOC modes. (a) the 'warm' (or interglacial) mode is dominated by active and deep NADW formation in the North Atlantic; (b) the 'cold' (or glacial) mode is characterised by active, but rather shoaled northern-sourced water flowing at intermediate depths (i.e., Glacial North Atlantic Intermediate Water – GNAIW, a 'glacial' type of NADW), and by the AABW advection from the Southern Ocean; (c) the 'off' mode is featured by a shutdown (i.e., collapse or no significant formation) of the NADW), and the prevalence of the AABW in the North Atlantic (modified from RAHMSTORF, 2002).

Reconstructions of the AMOC strength and geometry based on radiogenic isotope tracers (i.e., $^{231}Pa/^{230}Th$ and $^{143}Nd/^{144}Nd$) both in marine sediment and foraminiferal records from the Atlantic Ocean (BÖHM *et al.*, 2015; HOWE *et al.*, 2016b) indicate that a sustained NADW production would have predominated over most of the last glacial cycle. Deviations from such overall pattern, as when the AMOC 'cold' mode (Fig. 8b) would rather have prevailed, seem to be restricted to relatively brief intervals of harshest glacial conditions (LIPPOLD *et al.*, 2009; BÖHM *et al.*, 2015; HOWE *et al.*, 2016b). Over time periods as the Last Glacial Maximum (LGM) (23-19 kyr), when huge continental ice sheets reached maximum coverage stretching over vast extensions of the northern latitudes (CLARK *et al.,* 2009), shallower northern-sourced waters (GNAIW) seemly flowed toward the Southern Ocean. At that time, increased southern-sourced waters (AABW) would have instead filled large portions of the deep North Atlantic, as it has also been inferred from paleonutrient tracers (i.e., $\delta^{13}C$ - carbon isotope records) (Fig. 9).

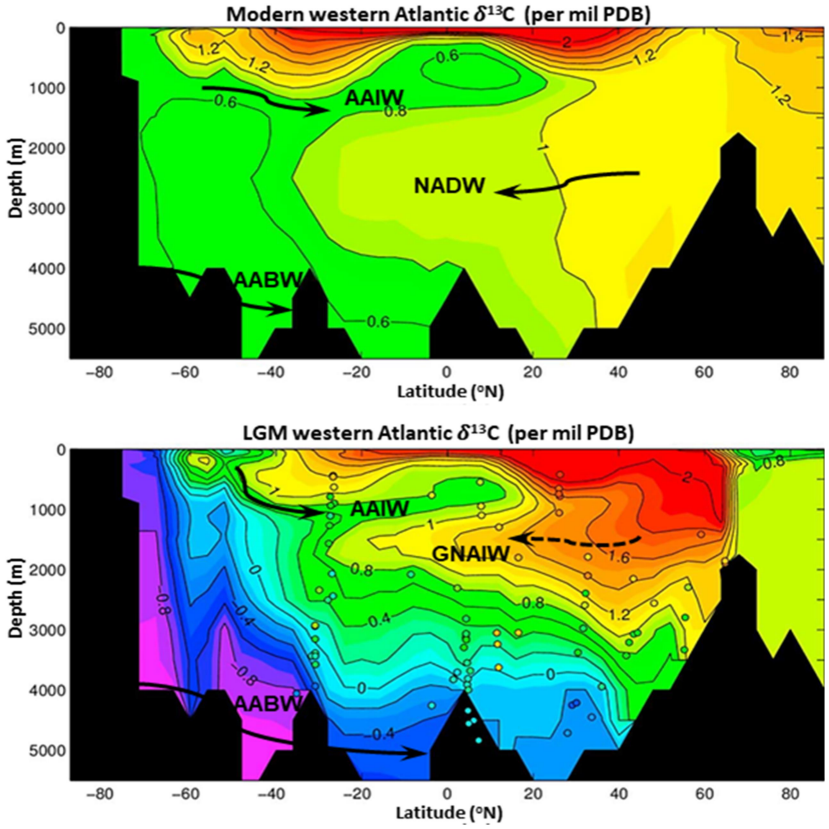

Figure 9 – Atlantic Ocean circulation in the modern day (top) and during the Last Glacial Maximum (LGM) (bottom). Reconstruction of the Atlantic Ocean circulation as inferred from GEOSECS western Atlantic $\delta^{13}C$ records (KROOPNICK, 1985) and decoupled in a water mass decomposition model (adapted from GEBBIE, 2014).

Further, the signature of radiogenic isotope tracers also indicate that disturbances in the AMOC would have accompanied abrupt climatic events in the northern hemisphere throughout the last glacial, such as D-O interstadials, Heinrich stadials, and the YD event (McMANUS *et al*., 2004; LIPPOLD *et al.*, 2009; BÖHM *et al.*, 2015). The high temporal resolution of some North Atlantic records (BÖHM *et al.*, 2015) has allowed to detect marked changes in the AMOC along with much brief events as the D-O interstadials. During those D-O events of warming in the northern hemisphere, active AMOC would have preponderated.

Most outstanding episodes of anomalous AMOC, however, would have taken place during HS events of massive meltwater pulses stemming from iceberg discharges (McMANUS *et al*., 2004; LIPPOLD *et al.*, 2009; BÖHM *et al.*, 2015). Notably those HS near glacial maxima (i.e. HS1, HS2) would have resulted in drastic AMOC slowdown or collapse, i.e., the AMOC 'off' mode (Fig. 8c) (BÖHM *et al.*, 2015). Over such periods of extreme glacial cooling, the progressive advance of major continental ice sheets would have caused them to become unstable and collapse when reaching a critical mass (MacAYEAL, 1993). Also, there is evidence of a significant, but less pronounced AMOC slowdown during shorter or less severe intervals of glacial cooling, as other HS and the YD (12.9-11.5 kyr) (McMANUS *et al*., 2004; BÖHM *et al.*, 2015; LYNCH-STIEGLITZ, 2017). It seems that prodigious volume of icebergs release and massive freshwater inflow into the North Atlantic would be demanded as to severely reduce the NADW formation and lead the AMOC to the edge of a collapse (BÖHM *et al.*, 2015).

The abrupt events detected along the last glacial have been described as such as the NADW production persisting over most of the last glacial would have enhanced the northward heat transport, culminating at times in episodic events of much pronounced warming in the northern high latitudes and triggering D-O interstadials. Eventually, after some D-O events of warming and ensuing ice melting, significant sea level rise might possibly have also proceeded to corrode and undercut ice shelves, enhancing freshwater influx to the North Atlantic and resulting in Heinrich events. Such process might have accounted for the apparent link between HS and D-O events. HS would then

reduce the NADW production and thus the AMOC strength, leading to a bipolar climate swing and reversing the process (MASLIN; SEIDOV; LOWE, 2001; BARKER *et al.* 2009). The thermal boundary across the Southern Ocean imposed by the Antarctic Circumpolar Current (Fig. 10) might have acted, however, to slowdown the transmission of the northern climate signal to Antarctica. That would apparently explain the contrasting feature of more gradual AIM and abrupt D-O events detected in ice core records (SCHMITTNER; SAENKO; WEAVER, 2003; BARKER *et al.*, 2009). Like the results of climate models, marine sediment core records therefore also support the notion of a seesaw alternation in the Atlantic heat piracy modulating hemispheric heat partitioning.

Prolonged warming in Antarctica propitiated by the long lasting HS1 (18-14.6 kyr) following the initial rise of boreal summer insolation (~19 kyr) (CARLSON; WINSOR, 2012) would have resulted in a remarkable retreat of ice sheets and sea ice coverage. The dwindling effect of ice, in turn, would have diminished the surface albedo and the ocean insulation from the overlying atmosphere, thereby enhancing air-sea exchange and carbon dioxide outgassing to the atmosphere. Both feedback mechanisms would have amplified the internal response of the climate system to cyclic changes in external orbital forcing, affecting the Earth's heat budget and leading to global temperature rise.

Further, the increased inflow of warm and salty waters into the Atlantic through the Agulhas leakage (Fig. 10) along the glacial-interglacial transition would have boasted the NADW production, triggering the reactivation of the interglacial mode of the Atlantic overturning circulation, i.e., the AMOC 'warm' mode (Fig. 8a) (KNORR; LOHMANN, 2003; PEETERS, *et al*., 2004; BEAL *et al*., 2011). The enhanced influx of warm and salty waters from the Indian Ocean over this transitional period would have been propitiated by a southward displacement of the Subtropical Front (STF) induced by a poleward migration of the southern westerly winds (BARD; RICKABY, 2009; BIASTOCH *et al*., 2009; BEAL *et al*., 2011).

As a highly nonlinear system particularly sensitive to drastic changes in seawater salinity, the Atlantic overturning circulation would have been again severely disturbed and pushed to a threshold (MASLIN; SEIDOV; LOWE, 2001; RAHMSTORF, 2006).

Opposing to drastic salinity decreases triggered by icebergs upsurge and freshwater inputs over glacial boundary conditions, however, vast amounts of salt into the Atlantic fostering the AMOC recovery instead (PEETERS *et al.*, 2004) would have forced the climate system to cross a critical boundary, leading to the termination of the last glacial period and to the Holocene inception at ca. 11 kyr ago.

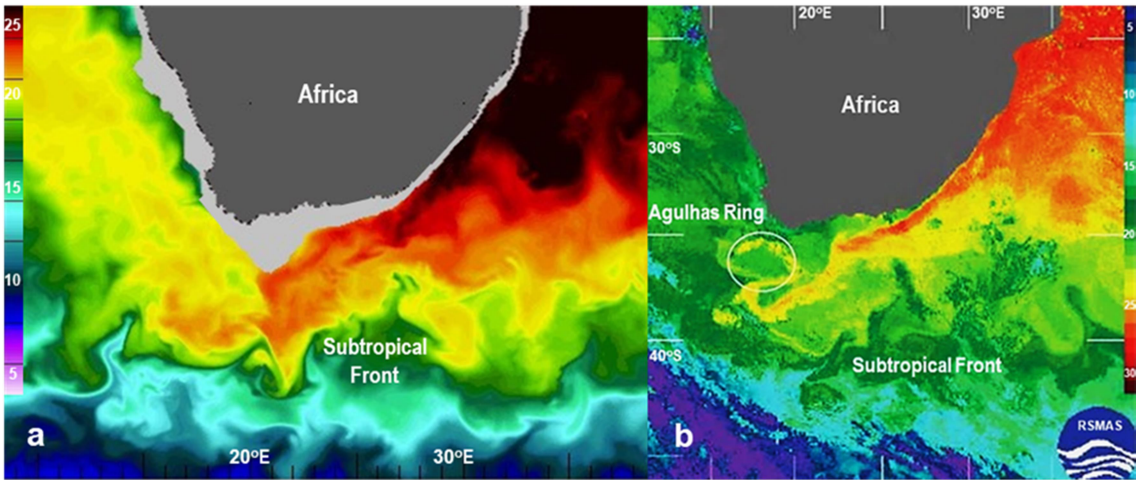

Figure 10 – The leakage of the Agulhas Current into the Atlantic Ocean. (a) the infrared satellite image depicts the thermal contrast in °C (colour shading) between the Agulhas Current (right) and the eastern South Atlantic waters (left) at the southern tip of Africa (modified from Naval Oceanographic Office); (b) the infrared satellite image (RSMAS) further depicts the Agulhas leakage propelled by the intermittent shedding of eddies breaking off from the current after its retroflection, forming the 'Agulhas rings'. The image particularly shows the detachment of the Agulhas ring 'Astrid' surrounded by a warm water filament (white circle) two months after the Agulhas retroflection (adapted from PEETERS *et al.*, 2004). The Subtropical Front (STF) demarks a frontal zone delimitating warmer subtropical waters from the cooler Antarctic Circumpolar Current (ACC).

Chapter 3

Regional Setting

The study area (Fig. 11) is located at the southernmost portion of an arc-shaped embayment in the Brazilian continental margin extending from 23-28°S, known as the South Brazilian Bight (ZEMBRUSCKI, 1979).

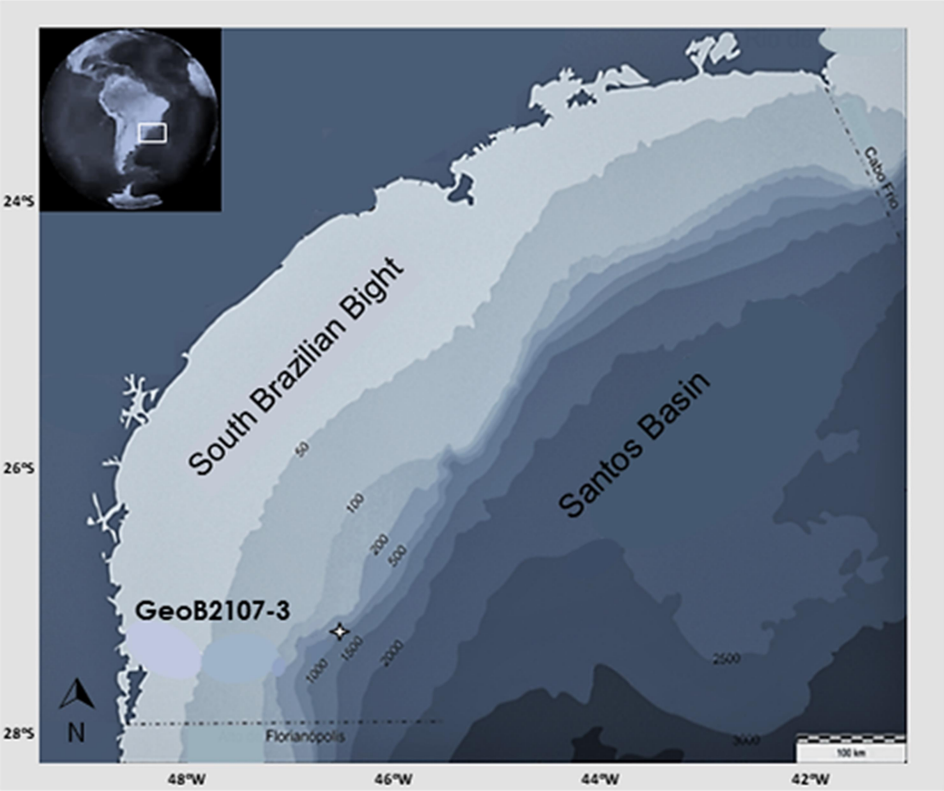

Figure 11 – Map of the study area and location of the marine sediment core GeoB2107-3 (star) investigated in this study (modified from NUNES; VIVIERS; LANA, 2004).

That sector of the Brazilian margin delimits a major sedimentary basin, the Santos Basin, which stretches from the Cabo Frio High (23°S) to the Florianopolis High (28°S). In the Santos Basin, the wide continental shelf reaching up to 230 km northward becomes narrower (~100 km) toward the study area, where the isobaths of 50 m is located only 5 km away from the coast (CAMPOS *et al*., 2013). The study area is also marked by an abrupt shift in the coastline orientation from NE-SW to N-S (Fig. 11).

During the Quaternary, sedimentary processes would have been controlled by events of sea level rise and retreat that led to the drowning and exposure of the continental shelf (ROCHA *et al*., 1975; MAHIQUES, *et al*., 2004). In general terms, sedimentation would have predominantly occurred during periods of lower sea level, when the shelf exposure would have favoured terrigenous input. Conversely, it would be progressively reduced along with the sea level rise toward the Holocene (KOWSMANN; COSTA, 1979). At the present, sedimentary processes in the study area are mostly influenced by the interplay between the meandering flow of the Brazil Current (BC) and the seasonal northward intrusion of the Plata Plume Water (PPW) (Fig. 15a; b) (MAHIQUES, *et al*., 2004). Such processes foster the establishment of highly productive zones (BRANDINI *et al*., 2014), enhancing the deposition of organic matter (GAETA; BRANDINI, 2006) that is reflected in the high carbon content in the sediments (MAHIQUES, *et al*., 2004).

3.1 Continental Climate

The region off Cabo Frio (Fig. 11) marks the transition between tropical (north) and subtropical (south) climate regimes (ROCHA *et al*., 1975). The continental climate in the southeastern South America is defined as subtropical humid (ASP *et al*., 2009), but with a strong seasonality resulting in intense summer precipitation (Fig. 12a) (ZHOU; LAU, 1998) and less pronounced winter rainfall (Fig. 12b) (VERA; VIGLIAROLO; BERBERY, 2002). During austral summer, intensified northeasterly trades cause the southward migration of the Intertropical Convergence Zone (ITCZ), a major tropical rain belt, enhancing convective activity over northern South America (GRIMM; VERA; MECHOSO, 2004). Tropical moisture is transported further southeast by the South American low-level jet, a NW-SE convective band that extends toward the subtropical South Atlantic forming the South Atlantic Convergence Zone (SACZ) (CARVALHO; JONES; LIEBMANN, 2004), an important element of the South American summer monsoon (SASM) (ZHOU; LAU, 1998). During austral winter, equatorward incursions of mid-latitude cold fronts associated with the displacement of the semi-permanent South Atlantic Subtropical High pressure cell (SASH) toward the continent induce the inland inflow of moisture from the Atlantic Ocean, resulting in episodic cyclonic storms (HASTENRATH, 1991; VERA; VIGLIAROLO; BERBERY, 2002).

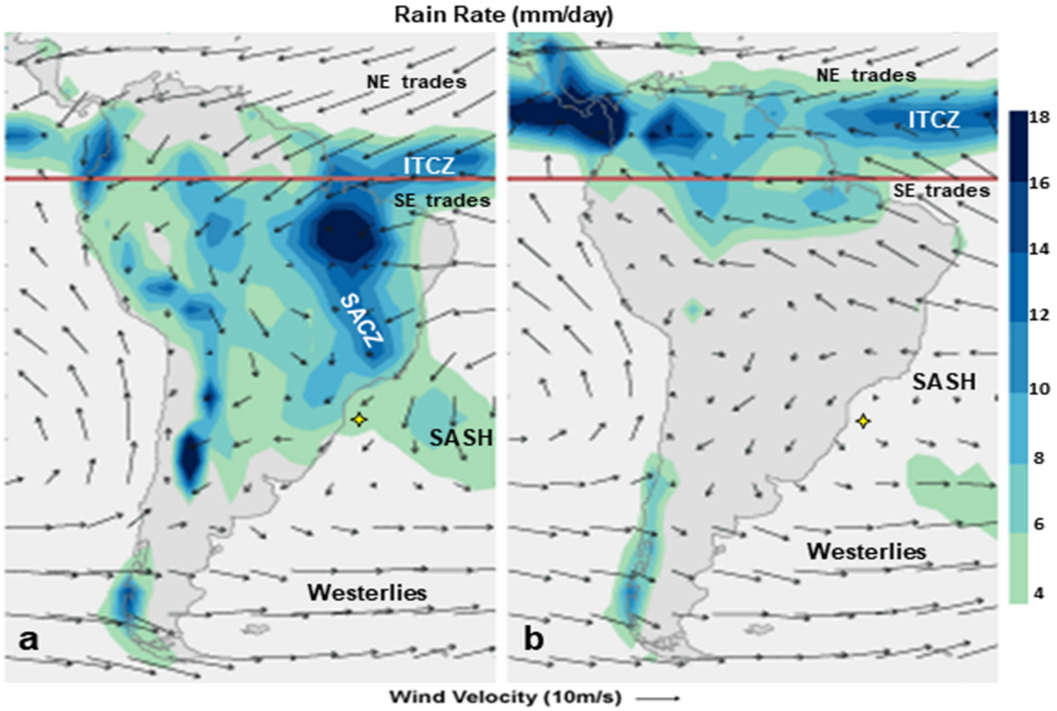

Figure 12 – Atmospheric circulation over South America. Schematic representation showing the average surface wind velocity (vectors) and rain rate (colour shaded) for: (a) January (austral summer); and (b) July (austral winter). The atmospheric features are labelled as: SASH - South Atlantic Subtropical High pressure cell, NE trades - northeasterly trade winds, SE trades - southeasterly trade winds, Westerlies - westerly winds, ITCZ - Intertropical Convergence Zone, SACZ - South Atlantic Convergence Zone. The location of the marine sediment core GeoB2107-3 (yellow star) is also indicated (modified from NASA Earth Observatory).

3.2 Upper Water Column Properties

In the study area, the modern mean annual sea surface temperature (SST) is ca. 23ºC (LOCARNINI *et al*., 2013) (Fig. 13a). Nevertheless, the SST rather shows a marked annual cycle with an amplitude of ca. 4°C, whereby warmer waters prevail during the austral summer. Such seasonal SST variability is attributed to the annual cycle of insolation and to changes in the BC flow, which is in turn determined by the intensity of solar radiation and also by the wind regime (PETERSON; STRAMMA, 1991; PROVOST; GARCIA; GARÇON, 1992).

Conversely, sea surface salinity (SSS) presents reduced annual cycle with an amplitude of ca. 0.2 psu, whereby higher values preponderate during the austral winter. The mean SSS in the study area is ca. 36.5 psu (ANTONOV *et al*., 2010) (Fig. 13b).

Also in the study area, vertical profiles of nutrients distribution in the water column show that high phosphate, nitrate and silicate contents in the upper layer present a linear correlation with lower temperatures (<20^{o}C isotherm), reflecting the upwelling of colder and nutrient-rich SACW waters (BRAGA *et al*., 2008; BRANDINI *et al*., 2014).

Additionally, vertical profiles show that higher concentrations of phosphate and silicate prevailing in winter correlate with low-salinity shallower waters, mirroring the freshening induced by seasonal northward PPW intrusions and associated continental-sourced input toward the study area. Such PPW displacements reaching the CSM in winter rather display a nitrate-depleted content due to its rapid absorption by phytoplankton along the southernmost portion of the Brazilian margin (BRAGA *et al*., 2008; BRANDINI *et al*., 2014).

Vertical profiles of temperature, salinity, and nutrient content show that nutrient enrichment of the upper water column in the study area is strongly associated with hydrodynamic and seasonal processes resulting from the interplay between the BC meanders and PPW waters. Such processes propitiate the fertilisation of oligotrophic waters off CSM, fostering primary production and supporting both phyto- and zooplanktonic community, as well as fishery off CSM (MATSUURA, 1986; BRANDINI *et al*, 2014). The evidences of nutrient enrichment in the upper water column (BRAGA, *et al*., 2008), favouring the establishment of highly productive zones off CSM (BRANDINI *et al*, 2014), is further corroborated by depositional processes resulting in enhanced organic matter and carbon contents in marine sediments (MAHIQUES, *et al*., 2004; GAETA; BRANDINI, 2006).

Modern nutrient content in the core site location is displayed by a vertical profile of the water column (Fig. 13c) showing the distribution of phosphate concentrations with depth. The hydrodynamic processes enhancing nutrient input to the euphotic zone and fostering local productivity are further described in section 3.4.

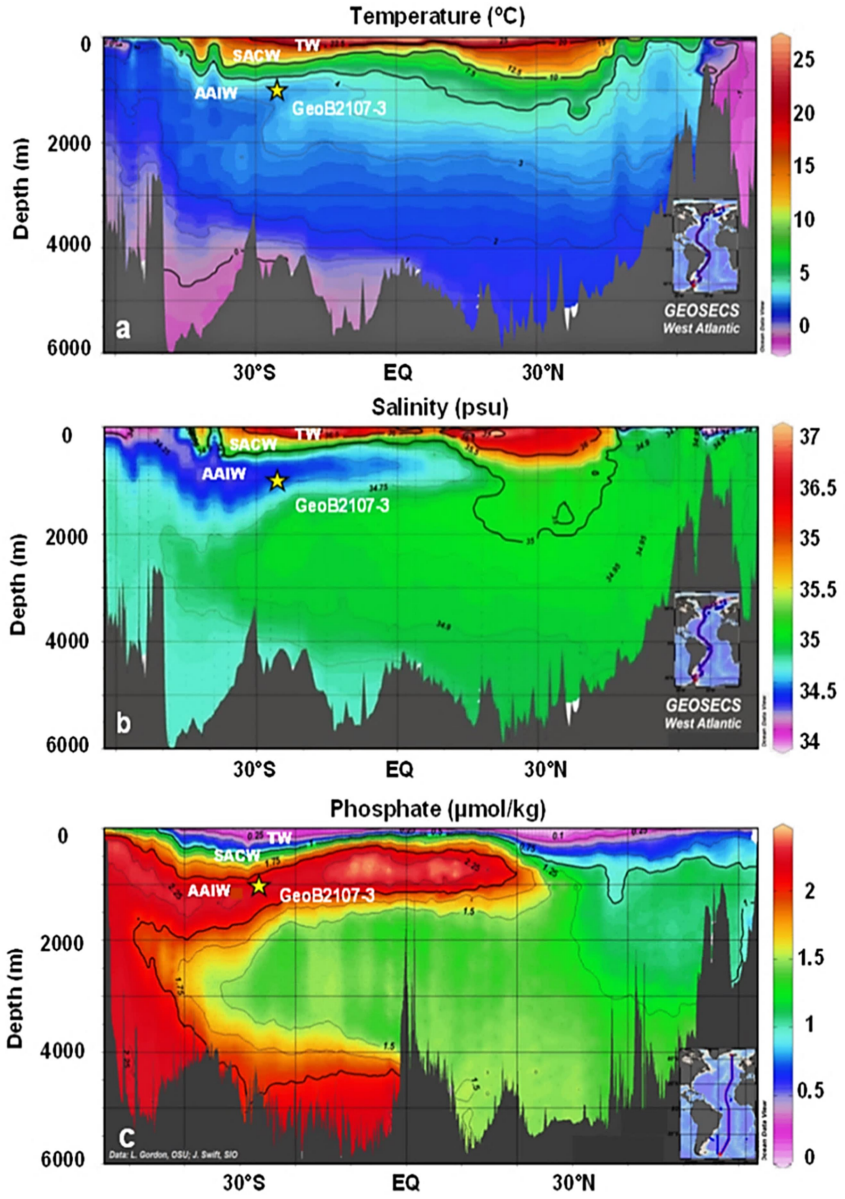

Figure 13 – Latitudinal transect of the Atlantic Ocean and vertical profiles of water column properties. (a) temperature (°C); (b) salinity (psu); and (c) nutrient (phosphate) content (µmol/kg) (colour shading). The location of the marine sediment core GeoB2107-3 (yellow star) is indicated together with the water masses transported by the Brazil Current (BC), namely the Tropical Water (TW) and the South Atlantic Central Water (SACW). The water mass bathing the core site at intermediate depth, i.e., the Antarctic Intermediate Water (AAIW) is also shown (modified from GEOSECS and eWOCE).

3.3 Upper Ocean Circulation

The upper ocean circulation in the study area is dominated by the BC. At largescale, the BC integrates the western portion of the anticyclonic South Atlantic Subtropical Gyre

(Fig. 14) (STRAMMA; ENGLAND, 1999; TALLEY *et al*., 2011). At mesoscale, the BC meandering flow modulates the surface circulation (Fig. 15a; b).

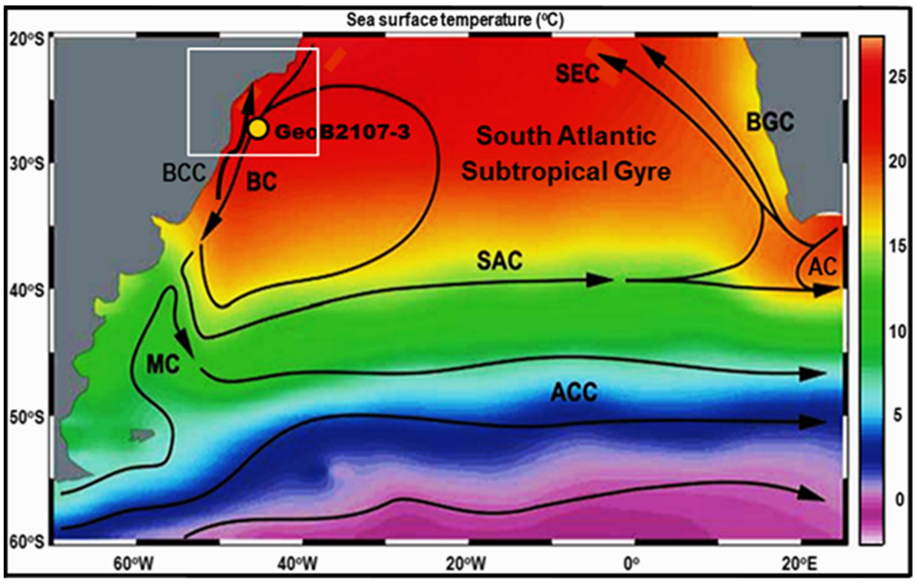

Figure 14 –Schematic largescale upper ocean circulation in the subtropical South Atlantic (black lines) (modified from STRAMMA; ENGLAND, 1999). The currents are labelled as: AC-Agulhas Current, ACC-Antarctic Circumpolar Current, BC-Brazil Current, BCC-Brazilian Coastal Current, BGC-Benguela Current, MC-Malvinas Current, SAC-South Atlantic Current, and SEC-South Equatorial Current. Mean annual temperatures at the surface in °C (colour shading) (CONKRIGHT *et al*., 2002) and location of the investigated marine sediment core GeoB2107-3 (yellow circle) are also shown (modified from CHIESSI *et al*., 2008).

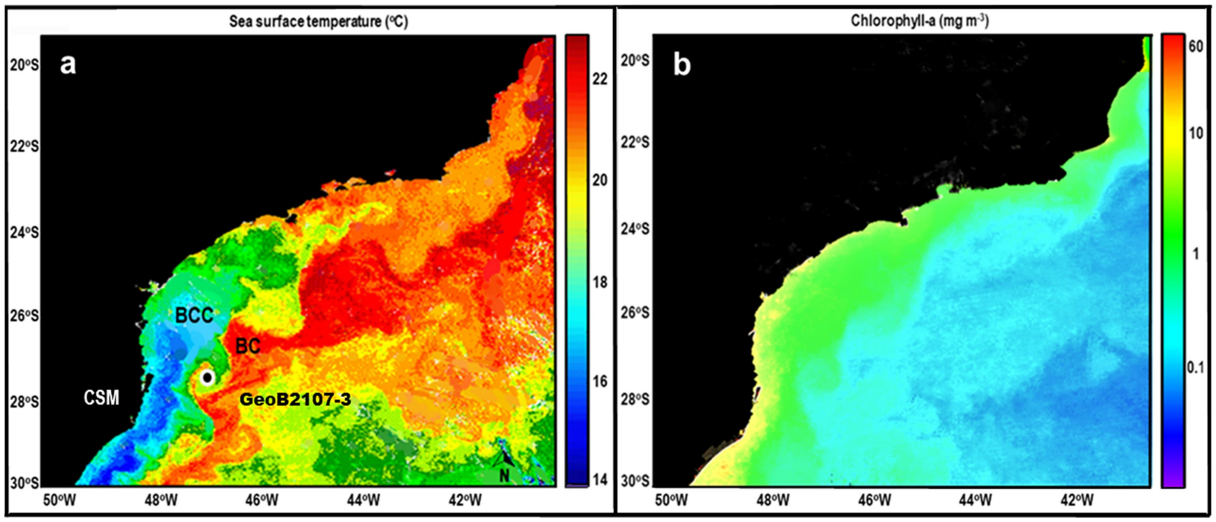

Figure 15 – Mesoscale upper ocean circulation off Cape Santa Marta (CSM). The satellite winter images show the mesoscale circulation defined by the Brazil Current (BC) meandering flow. (a) infrared satellite image (AVHRR/NOAA) depicts the development of the Santa Marta cyclonic vortex, delineated by a thermal contrast in °C (colour shading) between the BC and the Brazilian Coastal Current (BCC); (b) ocean colour satellite image (VIIRS-SNPP/NOAA) depicts the development of Santa Marta cyclonic vortex delineated by the surface chlorophyll-*a* content in mg m^{-3} (colour shading) mirroring phytoplankton bloom and primary productivity.

The BC originates from the southern branch of the South Equatorial Current (SEC), which bifurcates between 10-15°S when approaching the Brazilian continental margin (PETERSON; STRAMMA, 1991; STRAMMA; ENGLAND, 1999). As a western boundary current, the BC flows southward along the Brazilian margin transporting tropical warm, salty and nutrient-depleted waters (PETERSON; STRAMMA, 1991; SILVEIRA *et al*., 2000). Around 38°S, the BC converges with the northward flowing Malvinas Current (MC), which transports cold, less saline and nutrient-rich subantarctic waters towards the tropics (PETERSON *et al*., 1996; SILVEIRA *et al*., 2000). At the Brazil-Malvinas Confluence (BMC), both the BC and the MC are deflected and flow eastward as the South Atlantic Current (SAC) and as the northern branch of the Antarctic Circumpolar Current (ACC), respectively (OLSON *et al*., 1988; SILVEIRA *et al*., 2000). The SAC contributes to the Benguela Current (BGC), which feeds the SEC, completing the gyre (STRAMMA; ENGLAND, 1999; TALLEY *et al*., 2011).

In its origin, the BC transports warm, salty and oligotrophic Tropical Water (TW) (>20°C; 36 psu) in the mixed layer (< 100 m water depth) (Fig. 13a-c). South of 20°S, the BC incorporates colder, less saline and nutrient-rich South Atlantic Central Water (SACW) (6-20°C; 34.6-36 psu) in the permanent thermocline (100-600 m water depth) (Fig. 13a-c), becoming increasingly stronger and deeper (STRAMMA; ENGLAND, 1999; SILVEIRA *et al*., 2000; CIRANO *et al*., 2006). The SACW originates at the southwestern boundary of the South Atlantic subtropical gyre from cold, fresh sub-Antarctic waters formed in the Pacific Ocean and advected eastward by the ACC. As the SACW reaches the eastern boundary of the gyre, it also receives the contribution of warm, saltier subsurface waters from the Indian Ocean transported by the Agulhas Current (AC) (STRAMMA; ENGLAND, 1999; TOMCZAK; GODFREY, 2003).

At intermediate depths, the study site is bathed by the cold, low-salinity and nutrient-rich Antarctic Intermediate Water (AAIW) (2-6°C; 34.3 psu), which originates along the Antarctic Polar Front from Antarctic surface waters and flows northward below the thermocline (600-1200 m water depth) (Fig. 13a-c) (STRAMMA; ENGLAND, 1999; SILVEIRA *et al*., 2000). After reaching the BMC, the AAIW is deflected eastward integrating the gyre (SILVEIRA *et al*., 2008). The AAIW constitutes an important

component of the thermohaline circulation as the upper branch of the AMOC (LUMPKIN; SPEER, 2007; TALLEY *et al*., 2011).

On the continental shelf, the northward flow of the Brazilian Coastal Current (BCC) transports cold, low-salinity and nutrient-enriched waters (Figs. 14; 15a; b) originated from continental runoff, with a strong contribution of PPW. The BCC is largely responsible for the terrigenous nutrient input to the study area, which is modulated by continental climatic conditions (PIOLA *et al*., 2005; RAZIK *et al*., 2015).

3.4 Primary Productivity

Primary productivity in the study area is tightly linked to the BC dynamics, which promotes a regional upwelling system yearlong. As the BC flows southward bordering the shelf break, abrupt shifts in the bottom topography resulting from the shelf narrowing and changes in coastline orientation (Fig. 11) produce instabilities in the BC, causing the development of meanders and vortices (Fig. 15a; b) (PALMA; MATANO, 2009; CAMPOS *et al*., 2013). Cyclonic vortices as observed off CSM exhibit a clockwise and upward vertical flux, which induces the SACW upwelling at the shelf break as the meander moves, injecting nutrient-rich waters into the euphotic zone (BRANDINI *et al*., 2014; SATO, 2015). During austral summer, this persistent shelf break upwelling mechanism is enhanced by coastal upwelling events driven by upwelling-favourable northeasterly (NE) winds (MATSUURA, 1986; CASTELÃO; CAMPOS; MILLER, 2004; PALMA; MATANO, 2009). Alongshelf NE winds cause an offshore displacement of the TW, inducing nutrient-rich SACW to emerge onto the shelf (PALMA; MATANO; PIOLA, 2008; BRANDINI *et al*., 2014). The synergy of both upwelling mechanisms acts in such a way that the SACW is first uplifted to shallower depths by BC shelf break upwelling and then pumped to the surface by NE wind-driven coastal upwelling (PALMA; MATANO, 2009; CAMPOS *et al*., 2013).

Besides this regional upwelling system, perennial fluvial discharge of small rivers (ASP *et al*., 2009) induces the intrusion of nutrient-rich waters over the shelf throughout the year (NOERNBERG; KAMPEL; BRANDINI, 2007; BRANDINI *et al*., 2014). During austral winter, a seasonal change in the regional wind field from NE to SW (i.e.

southwesterly downwelling-favourable winds) also propels the northward incursion of PPW waters (Fig. 15a), today the main source of terrigenous input to the subtropical Southwestern Atlantic (PIOLA *et al*., 2005; PALMA; MATANO; PIOLA, 2008; RAZIK *et al*., 2015). As the BC moves along the Brazilian margin, the intense mesoscale activity associated to its meandering flow impels those nutrient-rich shelf waters transported by the BCC toward the continental slope off CSM (Fig. 15b) (BRANDINI *et al*., 2014 MATANO *et al*., 2014). The interplay between the BC cyclonic vortices and BCC continental-sourced nutrient supply constitutes an important process for the fertilization of tropical oligotrophic waters, providing a new source of nutrients for marine primary production, thereby favouring phytoplankton blooms and strongly impacting marine ecosystem off CSM (BRAGA *et al*., 2008; MATANO *et al*., 2014; BRANDINI *et al*., 2014).

Chapter 4

Methodology

4.1 Marine Sediment Core: Preliminary Procedures

The marine sediment core GeoB2107-3 investigated in this study was recovered from the continental slope off southeastern South America (27º10'S, 46º27'W, 1048 m water depth) during R/V Meteor cruise M23/2 (BLEIL *et al*., 1994). In the present study, it was analysed the uppermost 251 cm of the 783 cm long sediment core. The sediment core was sampled at 1 cm intervals. All samples were wet-sieved (150 μm mesh) and oven-dried at 50^{o}C for radiocarbon (^{14}C), stable oxygen isotope (δ^{18}O), and micro-paleontological (planktonic foraminiferal assemblage) analyses. The procedures adopted for the respective analyses are described in the following sections.

4.2 Age Model

The age model for the analysed section of core GeoB2107-3 was based on 12 accelerator mass spectrometry radiocarbon ages performed on the shallow-dwelling planktonic foraminifera *Globigerinoides sacculifer* (HEIL, 2006). Radiocarbon analyses were conducted at the Leibniz Laboratory for Radiometric Dating and Stable Isotope Research at the University of Kiel, Germany. The age-depth model was originally published by HENDRY *et al*. (2012) using the Marine09 calibration curve (REIMER *et al.*, 2009), and more recently by HOWE *et al*. (2016a; b), GU *et al*. (2017), and PORTILHO-RAMOS *et al*. (2018) with the Marine13 calibration curve (REIMER *et al.*, 2013). All radiocarbon ages here were converted into calibrated ages using the online version of the software Calib 7.1 (STUIVER; REIMER; REIMER, 2017) and the Marine13 calibration curve (REIMER *et al.*, 2013), applying a marine reservoir correction (ΔR) of 35 years (http://calib.org/marine/getref.php?RefNo¼135, STUIVER; REIMER; REIMER, 2017). The age model was constructed based on linear interpolation of the calibrated ages, and reported with 2σ uncertainties. All ages are indicated as calibrated years before present (cal yr BP, present is 1950 AD).

4.3 Micropaleontological Analyses: Planktonic Foraminiferal Assemblages

The reconstruction of past paleoceanographic conditions was partially based on the faunal composition of planktonic foraminiferal assemblages. Due to the distinct habitats of planktonic foraminiferal species, shifts in the faunal composition of the assemblages provide valuable information of past changes in oceanographic conditions (WEFER *et al*., 1999; KUCERA, 2007). In this study, the faunal composition of planktonic foraminiferal assemblages was applied to reconstruct paleotemperature (Section 4.3.1), paleoproductivity (Section 4.3.2), and the leakage of the Agulhas Current into the Atlantic (Section 4.3.3).

For that purpose, about 300 tests of planktonic foraminifera per sample were hand-picked under a binocular microscope from the sediment fraction larger than 150 μm. The sampling intervals varied from 1 to 7 cm of the uppermost 251 cm of core GeoB2107-3. The sampling criterion adopted for the micropaleontological analyses was based on the variability of the sedimentation rates. Aiming to achieve a mean temporal resolution of ~300 kyr (~180 kyr for HS and the YD), the micropaleontological analyses were performed at sampling intervals of 1 cm under time periods of lowest sedimentation rates; whereas wider sampling intervals were applied for time periods of higher sedimentation rates (because, in this case, ages do not vary so much with depth).

After taxonomical identification (based mainly on BÉ, 1977; HEMLEBEN; SPINDLER; ANDERSON, 1989; KEMLE-VON MÜCKE; HEMLEBEN, 1999) and census counts of all specimens within the assemblages, the faunal composition and relative abundance of each species were derived. The micropaleontological analyses were performed in the Laboratory of Environmental Bioindicators of the Oceanographic Institute at the University of São Paulo, Brazil.

4.3.1 Reconstruction of Paleotemperature

The paleotemperatures were estimated based on the faunal composition of planktonic foraminiferal assemblages and applying the Modern Analog Technique (MAT)

performed with the software C2 (JUGGINS, 2007). This technique establishes an analogy between fossil and modern samples based on a given calibration dataset and selects those with most similar faunal composition as analogues for modern oceanographic conditions. The basic assumption here was that temperature of the ambient seawater primarily controls the foraminiferal assemblages. The planktonic foraminiferal calibration dataset applied here comprised 891 surface samples of the Atlantic Ocean between 90°N and 60°S from the MARGO Project database (KUCERA *et al*., 2005; PORTILHO-RAMOS *et al*., 2015). The modern annual temperature values for 10 m, 50 m, and 100 m water-depths were extracted and calibrated from the World Ocean Atlas (WOA) (LOCARNINI *et al*., 2013). The squared chord distance was employed for the MAT transfer function as a similarity measure and the weighted mean of the best 10 modern analogues was applied as reconstruction result. Using the leave-one-out cross-validation method, the root mean square error of prediction (RMSEP) of the transfer function was calculated as 1.8°C (R^2 = 0.92), 1.9°C (R^2 = 1.01), and 2.0°C (R^2 = 1.15) for 10 m, 50 m and 100 m, respectively.

4.3.2 Reconstruction of Paleoproductivity

The relative abundance of the eutrophic planktonic foraminiferal species *Globigerina bulloides* and *Globigerinita glutinata* in the faunal assemblages was used as a proxy for marine productivity. The preference for nutrient-enriched and highly productive environments represents the most important aspect particularly defining the distribution of these non-symbiont bearing species (SCHIEBEL; HEMLEBEN, 2005; ODA; YAMASAKI, 2005; SOUTO *et al*., 2011). Being primarily herbivorous, they proliferate when nutrients are introduced in the euphotic zone (e.g., upwelling regions), favouring primary production (e.g., phytoplankton blooms) (ORTIZ; MIX; COLLIER, 1995; SCHIEBEL; HEMLEBEN, 2005; METCALFE *et al*., 2015). For this reason, both species are considered indicative of upwelling systems (NAIDU; BABU; RAO, 1992; PEETERS; BRUMMER; GANSSEN, 2002; SOUTO *et al*., 2011) and have been widely applied as proxies of marine productivity in paleoceanographic reconstructions (ORTIZ; MIX; COLLIER, 1995; PORTILHO-RAMOS *et al*., 2015; LESSA *et al*., 2017).

Additionally, the species *Globorotalia inflata*, *Neogloboquadrina dutertrei*, and *Globorotalia truncatulinoides* (dextral coiling), which are also primarily herbivorous and thrive in productive environments (BÉ, 1977; HEMLEBEN; SPINDLER; ANDERSON, 1989; ORTIZ; MIX; COLLIER, 1995; TOLEDO; COSTA; PIVEL, 2007) were also analysed. Those species, however, are strongly influenced as well by environmental conditions other than productivity, such as seawater temperature, upper water column stratification, and surface mixing (HEMLEBEN; SPINDLER; ANDERSON, 1989; CHIESSI *et al.*, 2007; CLÉROUX, *et al*., 2009). Therefore, they were analysed together with other upper water column properties.

4.3.3 Reconstruction of Agulhas Leakage

Past glacial-interglacial transitions were marked by the reestablishment of the Indian-Atlantic interoceanic connection and enhanced Agulhas leakage (KNORR; LOHMANN, 2003; PEETERS, *et al*., 2004). Together with the Agulhas warm and salty waters inflow to the South Atlantic, the detachment of the Agulhas rings (Fig. 10b) also propels the dispersal of a typical planktonic foraminiferal fauna (PEETERS *et al*., 2004; CALEY *et al*., 2012).

Paleostudies show that this typical Agulhas fauna was virtually absent in South Atlantic records over the past glacial periods, reappearing along with the re-opening of the 'warm water route' and the onset of interglacial periods (PEETERS *et al*., 2004; CALEY *et al*., 2012; FERREIRA *et al*., 2012). The reseeding of such specific fauna in the Atlantic thus seems to be tightly dependant on migration via Agulhas waters, and its signature therefore has been largely used as a tracer of Agulhas leakage (FLORES; GERSONDE; SIERRO, 1999; PEETERS *et al*., 2004; MARTINEZ-MENDEZ *et al*., 2010; CALEY *et al*., 2012).

In this study, the relative abundance of the planktonic foraminiferal species *Globorotalia menardii, Pulleniatina obliquiloculata*, *Orbulina universa* and *Globigerinoides conglobatus* in the assemblages was applied as a proxy of the Agulhas leakage. The reappearance of such species in the western South Atlantic is usually

related to the leakage of Agulhas waters (GIRAUDEAU, 1993; PEETERS *et al*., 2004). The species *P. obliquiloculata* is typical from tropical Indo-Pacific oceans (BÉ, 1977; UJIIÉ; ISHITANI, 2016). Although generally rare and underrepresented in the foraminiferal assemblages (KEMLE-VON MÜCKE; HEMLEBEN, 1999), the variability of this species in the core site indicates that it is strongly affected by relatively large-amplitude abundance changes. This species therefore was also applied as a proxy of Agulhas leakage. All those above mentioned species are also indicative of warm, oligotrophic waters, and well stratified upper water column (BÉ, 1977; HEMLEBEN; SPINDLER: ANDERSON, 1989; WATKINS; MIX; WILSON, 1996; SCHIEBEL; HEMLEBEN, 2017) and, as such, were further applied to reconstruct paleoceanographic changes along the Holocene.

4.4 Geochemical Analyses: Stable Oxygen Isotope

To reconstruct additional upper water column properties in the past, the $\delta^{18}O$ composition of the planktonic foraminiferal species *Globigerinoides ruber* (white *sensu stricto*) and *Globorotalia truncatulinoides* (dextral coiling) was also applied. Those species have been commonly used for such purpose providing that they typically inhabit distinct water depths within the upper water column. The shallow-dwelling species *G. ruber* is known to reflect environmental conditions at the top of the mixed layer (ca. 30-50 m) (RAVELO; FAIRBANKS, 1992; CHIESSI *et al*., 2007), whereas the deeper-dwelling species *G. truncatulinoides* records the conditions below the mixed layer at the permanent thermocline (ca. 200-400 m) (MULITZA *et al*., 1997; CHIESSI *et al*., 2007).

About ten tests of *G. ruber* (white) within the size range 250–350 μm, and three tests of *G. truncatulinoides* (dextral) within the size range of 550-600 μm were hand-picked under a binocular microscope at sampling intervals of 1 cm of the uppermost 251 cm of core GeoB2107-3 (HEIL, 2006). The $\delta^{18}O$ analyses were performed on a Finnigan MAT 252 mass spectrometer equipped with an automatic carbonate preparation device at the Center for Marine Environmental Sciences (MARUM). Isotopic results are reported in the usual delta notation relative to the Vienna Pee Dee Belemnite (VPDB).

Data were calibrated against an inhouse standard (Solnhofen limestone), itself calibrated against the NBS19 standard. Estimates for standard deviation in isotopic measurements for $\delta^{18}O$ were lower than ±0.07‰ within the measuring period.

In this study, the stable oxygen isotopic composition of *G. ruber* (white) and *G. truncatulinoides* (dextral) planktonic foraminiferal tests was applied to reconstruct the ice-volume corrected oxygen isotopic composition of surface seawater ($\delta^{18}O_{ivc\text{-}ssw}$), a proxy for paleosalinity (Section 4.4.1), and past upper ocean stratification (Section 4.4.2).

4.4.1 Reconstruction of $\delta^{18}O_{ivc\text{-}ssw}$: a Proxy for Paleosalinity

The $\delta^{18}O$ composition of planktonic foraminiferal shells records the $\delta^{18}O$ of the surrounding seawater in which they calcify. As such, foraminiferal $\delta^{18}O$ composition varies depending both on the salinity and temperature of the surrounding seawater, as well as on the water volume locked up in ice sheets. Considering those distinct variants, it is possible to indirectly determine the paleosalinity of the surrounding seawater at the time that foraminiferal shell was formed. The ice-volume corrected (ivc) estimates of the surface seawater (ssw) oxygen isotopic composition ($\delta^{18}O_{ivc\text{-}ssw}$) has been therefore usually applied as a proxy for paleosalinity (CHIESSI *et al.*, 2015). In this study, the reconstruction of past changes in the upper ocean salinity was based on the MAT-derived paleotemperature estimates (Section 5.2.1), as well as on the oxygen isotopic composition of *G. ruber* (white) shells ($\delta^{18}O_{G.\ ruber}$), using the paleotemperature equation from MULITZA *et al*. (2003):

$$[SST\ (^{o}C) = -\ 4.44\ x\ (\delta^{18}O_{G.\ ruber} - \delta^{18}O_{sw}) + 14.20]$$

It was then applied the Vienna Pee Dee Belemnite (VPDB) to Vienna Standard Mean Ocean Water (VSMOW) conversion factor of 0.27‰ (HUT, 1987) and the sea-level curve from WAELBROECK *et al*. (2002). The uncertainties of the $\delta^{18}O_{sw}$ approach typically result in 1σ error of ca. 0.3‰ for $\delta^{18}O_{ivc\text{-}ssw}$ (MOHTADI *et al*., 2014). Higher $\delta^{18}O_{ivc\text{-}ssw}$ values are indicative of enhanced sea surface salinity (CHIESSI *et al*., 2015).

4.4.2 Reconstruction of Past Upper Ocean Stratification

Seawater temperature and salinity affect the density and stability of the water column. Because planktonic foraminiferal species record in their $\delta^{18}O$ composition the ambient temperature and $\delta^{18}O$ of the surrounding seawater ($\delta^{18}O$ of the upper ocean being linearly correlated to salinity), the stable oxygen isotope difference ($\Delta\delta^{18}O$) between deep- and shallow-dwelling planktonic foraminifera can be interpreted as a record of past changes in the vertical density gradient at the upper water column (MULITZA *et al*., 1997). The $\Delta\delta^{18}O$ has thus been largely used as a proxy for upper ocean stratification in paleoclimate studies, whereby high values yielded are interpreted as indicative of strong stratification (MULITZA *et al*., 1997; ARZ *et al.*, 2001). The $\delta^{18}O$ values of the deep-dwelling *G. truncatulinoides* (dextral) (MULITZA *et al*., 1997; CHIESSI *et al*., 2007) and shallow-dwelling *G. ruber* (white) (RAVELO; FAIRBANKS, 1992; CHIESSI *et al*., 2007) were applied here for $\Delta\delta^{18}O$ estimation ($\Delta\delta^{18}O_{G.truncatulinoides\text{-}G.ruber}$).

Chapter 5

Results

5.1 Age Model

The radiocarbon ages (HEIL, 2006), as well as the calibrated ages used to produce the age model of core GeoB2107-3 are presented in Table 1 and Fig. 16.

Table 1 –Radiocarbon ages used to produce age model of marine sediment core GeoB2107-3.

Depth (cm)	Species	Age (^{14}C yr BP)	+Error (yr)	-Error (yr)	Calibrated age (cal yr BP)	± Error (yr)	Lab ID
3	*G. sacculifer*	1590	30	30	1120	100	KIA 14534
33	*G. sacculifer*	5340	40	40	5660	100	KIA 14533
63	*G. sacculifer*	8995	55	55	9620	150	KIA 14532
73	*G. sacculifer*	11890	80	80	13320	150	KIA 14530
103	*G. sacculifer*	13030	80	80	14910	400	KIA 14528
148	*G. sacculifer*	19100	130	120	22530	280	KIA 22409
163	*G. sacculifer*	19810	150	150	23320	400	KIA 14525
178	*G. sacculifer*	24250	200	200	27890	390	KIA 22408
193	*G. sacculifer*	25750	240	240	29380	650	KIA 22407
203	*G. sacculifer*	31180	460	430	34690	790	KIA 16166
223	*G. sacculifer*	33380	580	540	37120	1350	KIA 16164
253	*G. sacculifer*	35990	870	780	40110	1600	KIA 16165

The analysed section of core GeoB2107-3 spans the period from 0.85 to 40 cal kyr BP. The age model adopted here is the same as that recently published by HOWE *et al*. (2016a; b), GU *et al*. (2017), and PORTILHO-RAMOS *et al*. (2018) using the Marine13 calibration curve (REIMER *et al*., 2013), which produced ages similar to those previously published by HENDRY *et al*. (2012) using the Marine09 curve (REIMER *et al*., 2009). Those age models show a maximum difference of ca. 0.8 kyr.

Sedimentation rates of the investigated core section (Fig. 16) show four peaks occurring at/or close to HS4, HS3, and the end of HS1, as well as at the onset of the LGM. Maximum values of 20.7 cm/kyr occurred from 14.8 until 13.4 cal kyr BP, and minimum values of 1.85 cm/kyr occurred from 35 until 30.1 cal kyr BP. The mean temporal resolution for the faunal assemblages is ca. 300 yr, with intervals of ca. 180 yr for HS and the YD. The mean temporal resolution for all other data is ca. 120 yr.

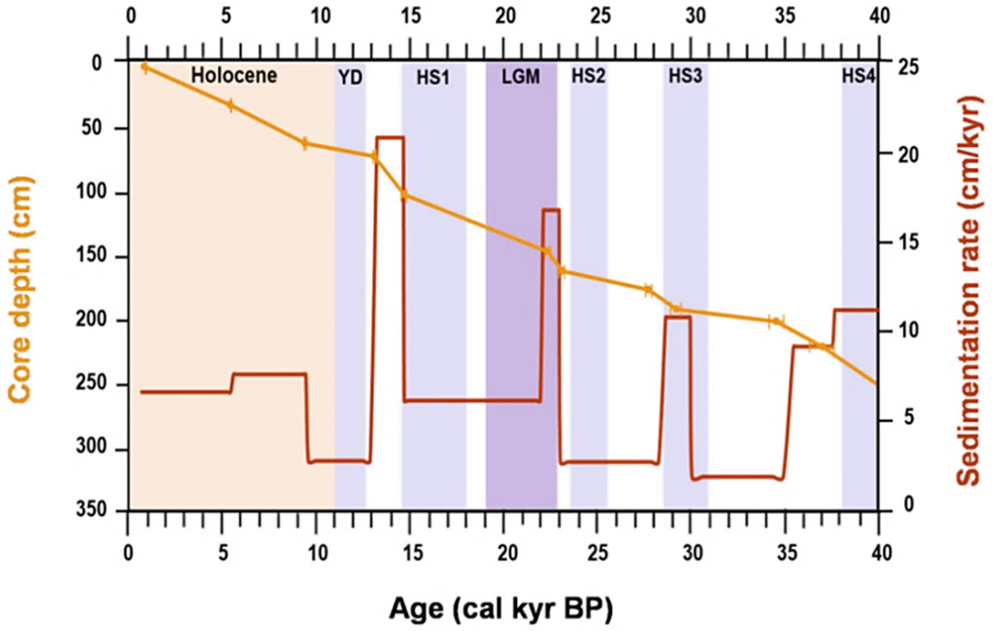

Figure 16 – Age-depth model and sedimentation rates of marine sediment core GeoB2107-3. The blue bars correspond to Heinrich Stadials (HS) and the Younger Dryas (YD) (SARNTHEIN *et al*., 2001), the lilac bar refers to the Last Glacial Maximum (LGM), and the light pink bar to the Holocene.

5.2 Micropaleontological Analyses: Planktonic Foraminiferal Assemblages

Altogether, twenty six planktonic foraminiferal species were identified in the assemblages (Tab. 2). However, only five species showed higher mean relative percentages (i.e., >3%) in the faunal composition of assemblages, namely the (sub) tropical species *Globigerinoides ruber* (white and pink) and *Globigerinoides sacculifer*; and the transitional species *Globigerinita glutinata*, *Globigerina bulloides*, and *Globorotalia inflata* (KUCERA, 2007). Those five species accounted for 79.2% of total planktonic foraminiferal assemblage (Tab. 3; Fig. 17).

Table 2 –Faunal composition of planktonic foraminiferal assemblages.

	Planktonic Foraminiferal Species
1.	*Candeina nitida* (d'Orbigny, 1839)
2.	*Globigerina bulloides* (d'Orbigny, 1826)
3.	*Globigerina falconensis* (Blow, 1959)
4.	*Globigerinella calida* (Parker, 1962)
5.	*Globigerinella digitata* (Brady, 1879)
6.	*Globigerinella sifonifera* (d'Orbigny, 1839)
7.	*Globigerinita glutinata* (Egger, 1895)
8.	*Globigerinita uvula* (Ehrenberg, 1861)
9.	*Globigerinoides conglobatus* (Brady, 1879)
10.	*Globigerinoides ruber* (pink and white) (d'Orbigny, 1839)
11.	*Globigerinoides sacculifer* (Brady, 1877)
12.	*Globorotalia crassaformis* (Galloway and Wissler, 1927)
13.	*Globorotalia hirsuta* (d'Orbigny, 1839)
14.	*Globorotalia inflata* (d'Orbigny, 1839)
15.	*Globorotalia menardii* (d'Orbigny, 1865)
16.	*Globorotalia scitula* (Brady, 1882)
17.	*Globorotalia truncatulinoides* (d'Orbigny, 1839)
18.	*Globoturborotalia rubencens* (Hofker, 1956)
19.	*Hastigerina digitata* (Rhumbler, 1911)
20.	*Neogloboquadrina dutertrei* (d'Orbigny, 1839)
21.	*Neogloboquadrina pachyderma* (Ehrenberg, 1861)
22.	*Orbulina universa* (d'Orbigny, 1839)
23.	*Pulleniatina obliquiloculata* (Parker and Jones, 1865)
24.	*Sphaeroidinella dehiscens* (Parker and Jones, 1865)
25.	*Turborotalia humilis* (Brady, 1884)
26.	*Turborotalia quinqueloba* (Natland, 1938)

Table 3 –Relative abundances of planktonic foraminiferal species in the assemblages.

Species	Abundance (%)				
	40 kyr			Glacial	Holocene
	Mean	Minimum	Maximum	Mean	Mean
***G. ruber* (white)**	22.7	2.9	36.6	24.7	15.6
***G. ruber* (pink)**	19.6	6.6	56.5	15.4	34.5
G. glutinata	12.4	0.3	25.9	13.9	7.1
G. bulloides	12.3	0	23.6	14.6	3.9
G. inflata	6.1	0	16.2	7.5	1.1
G. sacculifer	6.1	1.9	15.6	5.6	8.0
G. sifonifera	3.0	0.6	8.2	2.8	5.0
G. rubencens	2.5	0	7.5	2.9	0.7
G. menardii	2.0	0	18.0	0.1	8.8
N. pachyderma	1.9	0	8.2	2.4	0.3
N. dutertrei	1.8	0	6.1	1.9	1.4
O. universa	1.8	0	14.0	0.5	6.4
***G. truncatulinoides* (dextral)**	1.7	0	8.0	1.6	2.3
G. calida	1.6	0	6.1	1.8	0.9
G. scitula	1.2	0	3.6	1.5	0.3
G. conglobatus	1.0	0	7.1	0.5	2.7
***G. truncatulinoides* (sinistral)**	0.7	0	3.7	0.9	0
G. hirsuta	0.4	0	1.9	0.3	0.6
G. falconensis	0.3	0	2.3	0.4	0.1
G. crassaformis	0.3	0	1.1	0.3	0.1
G. uvula	0.2	0	1.2	0.3	0
P. obliquiloculata	0.1	0	1.0	0	0.2
T. quinqueloba	0.1	0	0.8	0.2	0.1
C. nitida	0	0	0.5	0	0.1
T. humilis	0	0	0.5	0	0
G. digitata	0	0	0.3	0	0
H. digitata	0	0	0.3	0	0
S. dehiscens	0	0	0.3	0	0

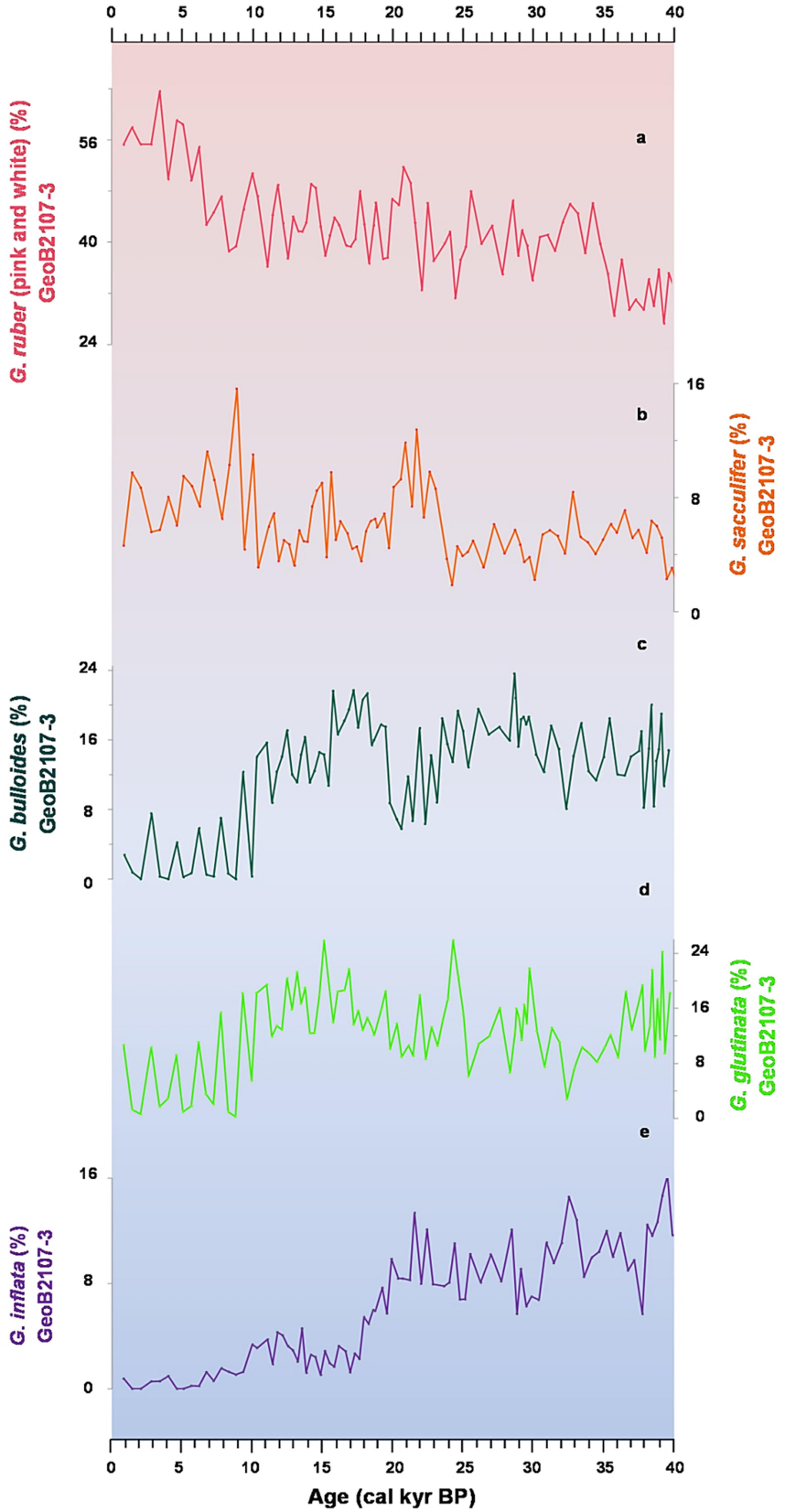

Figure 17 – Main planktonic foraminiferal species in the assemblages during the last 40 kyr. (a) *Globigerinoides ruber* (white; pink); (b) *Globigerinoides sacculifer*; (c) *Globigerina bulloides*; (d) *Globigerinita glutinata*; (e) *Globorotalia inflata* (this study).

The dominant species in the assemblages was *G. ruber* (white and pink) with mean relative abundance of 42.3% over the past 40 cal kyr BP. The species displayed a glacial-interglacial pattern, showing the lowest mean percentage (40.1%) during the glacial and highest average (50.1%) over the Holocene (Tab. 3; Fig. 17a).

The *G. ruber* species was followed by *G. glutinata* and *G. bulloides*, which showed mean percentages of 12.4% and 12.3%, respectively along the last 40 cal kyr BP. Unlike *G. rube*r, however, *G. glutinata*, and *G. bulloides* presented higher abundances during the glacial with mean percentages of 13.9% and 14.6%, respectively, and decreasing over the Holocene with mean percentages of 7.1% and 3.9%, respectively (Tab. 3; Fig. 17c; d). Superimposed to a long-term glacial-interglacial trend, both species also displayed a markedly short-term pattern, which is further described in section 5.2.2.

Finally, the species *G. sacculifer* and *G. inflata* showed the same mean percentage (6.1%) over the last 40 cal kyr BP both displaying a glacial-interglacial pattern, but in opposite directions. The species *G. sacculifer* recorded lower mean abundance (5.6%) along the glacial, increasing during the Holocene (8.0%); whereas *G. inflata* showed higher abundance (7.5%) over the glacial and a sharp decline (1.1%) toward the Holocene (Tab. 3; Fig. 17b; e). The species *G. sacculifer* also showed an outstanding increase over the LGM, which is referred as well in section 5.2.2.

5.2.1 Reconstruction of Paleotemperature

The evolution of sea surface temperatures (i.e., 10 m) off CSM over the last 40 cal kyr BP shows 4 distinct phases: (i) most of the last glacial (40-23 cal kyr BP), when the lowest temperatures (19.1-20.6ºC; mean 19.8ºC) were recorded; (ii) the LGM (23-19 cal kyr BP), marked by a temperature rise (20.1-22.8ºC; mean 21.2ºC), i.e., the highest temperature for the last glacial; (iii) the deglaciation (19-11 cal kyr BP), showed an overall slight increase of temperatures (20.1-22.2ºC; mean 20.9ºC), but with a sharp rise at the boundary of the Holocene; and (iv) the Holocene (last 11 cal kyr BP), marked by the highest temperatures (20.2-26.2ºC; mean 24.6ºC) (Fig. 18).

The temperature estimates at subsurface levels (i.e., 50 m and 100 m) follow the same trend of the sea surface temperatures (i.e., 10 m) (Fig. 18). The average temperature estimates at 10 m, 50 m and 100 m are summarised in Tab. 4.

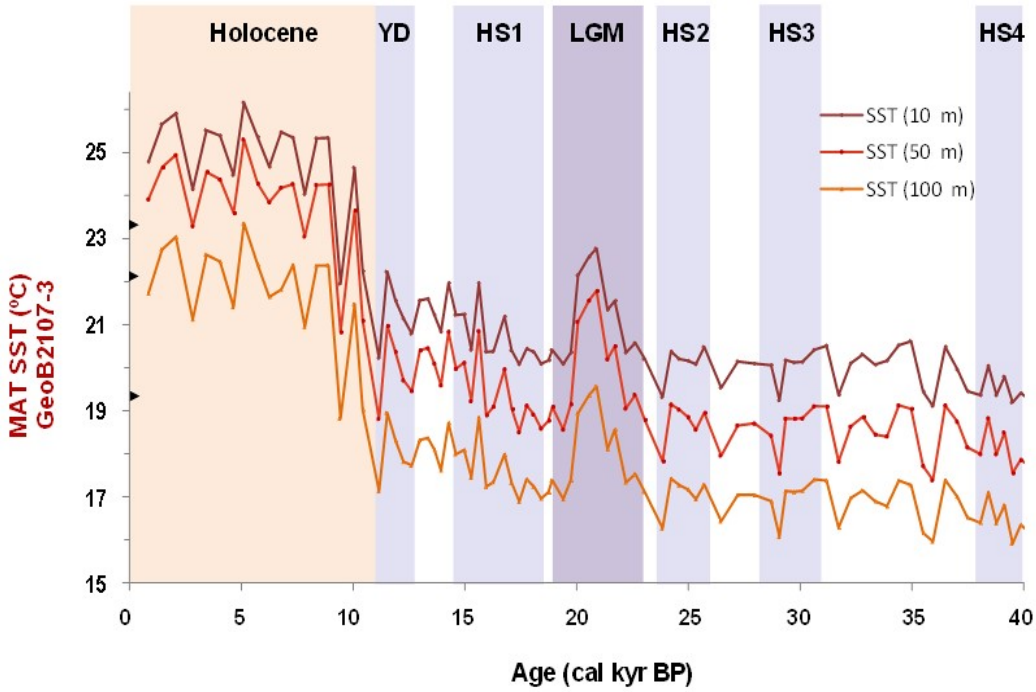

Figure 18 – Modern Analog Technique (MAT)-derived temperature estimates for 10 m, 50 m, and 100 m water depths (this study). The modern mean annual temperatures in the core site at 10 m, 50 m, and 100 m water depths (LOCARNINI *et al.*, 2013) are also shown (y-axis: black triangles). The blue bars correspond to Heinrich Stadials (HS) and the Younger Dryas (YD) (SARNTHEIN *et al.*, 2001), the lilac bar refers to the Last Glacial Maximum (LGM), and the light pink bar to the Holocene.

Table 4 –MAT-derived temperature averages for 10 m, 50 m, and 100 m water depths.

Period	**Depth**		
	10 m	**50 m**	**100 m**
Glacial (40-23 kyr)	19.8ºC	18.5 ºC	16.8ºC
LGM (23-19 kyr)	21.2ºC	20.0ºC	18.1ºC
Deglaciation (19-11 kyr)	20.9ºC	19.6ºC	17.8ºC
Holocene (last 11 kyr)	24.6ºC	23.5ºC	21.5ºC

Compared to the modern mean annual temperatures of 23.3°C (10 m), 22°C (50 m), and 19.3°C (100 m) at the core site (LOCARNINI *et al.*, 2013) (Fig. 18; black triangles), the MAT-derived mean temperature estimates of 24.6°C (10 m), 23.5°C (50 m), and 21.5°C (100 m) obtained at the core (Tab. 4) are mostly within the yielded temperature uncertainties (i.e., root mean square error of prediction – RMSEP) of 1.8°C (10 m), 1.9°C (50 m), and 2.0°C (100 m) (Section 4.3.1).

5.2.2 Reconstruction of Paleoproductivity

The faunal composition of the planktonic foraminiferal assemblages showed the dominance of the symbiont-bearing species *G. ruber* (white and pink) and *G. sacculifer* (Fig. 17a; b), typical for warm and oligotrophic waters (KUCERA, 2007). Altogether, those species accounted for nearly half (48.4%) of the specimens over the past 40 cal kyr BP (Tab. 3). However, non-symbiont-bearing species typical for eutrophic waters, like *G. glutinata* and *G. bulloides* also contributed significantly to the faunal composition of the assemblages (Fig. 17c; d). Together, they constituted 24.7% of the specimens during the 40 cal kyr BP, being only outnumbered by the *G. ruber* species (Tab. 3).

Along the glacial, the highest mean percentages recorded by *G. glutinata* and *G. bulloides* accounted for almost a third (28.5%) of the identified specimens (Tab. 3). During the LGM, however, a sharp decrease in abundance was recorded by *G. glutinata* (8.9%) culminating at ca. 20 cal kyr BP, when *G. bulloides* reached the lowest percentage of the glacial (5.8%) (Figs. 17c; d; 19). The marked drop in abundance of both eutrophic species over the LGM was coeval with a steep increase of *G. sacculifer* (13%) (Fig. 17b). Along the interglacial, the highest percentages of *G. glutinata* and *G. bulloides* (18.2% and 14.1%, respectively) were found at the rise of the Holocene (ca. 10 cal kyr BP), with a sharp drop in abundance of both species thereafter (Figs. 17c; d; 19).

Superimposed to this long-term trend, peaks of *G. glutinata* and *G. bulloides* were recorded during HS (Fig. 19).

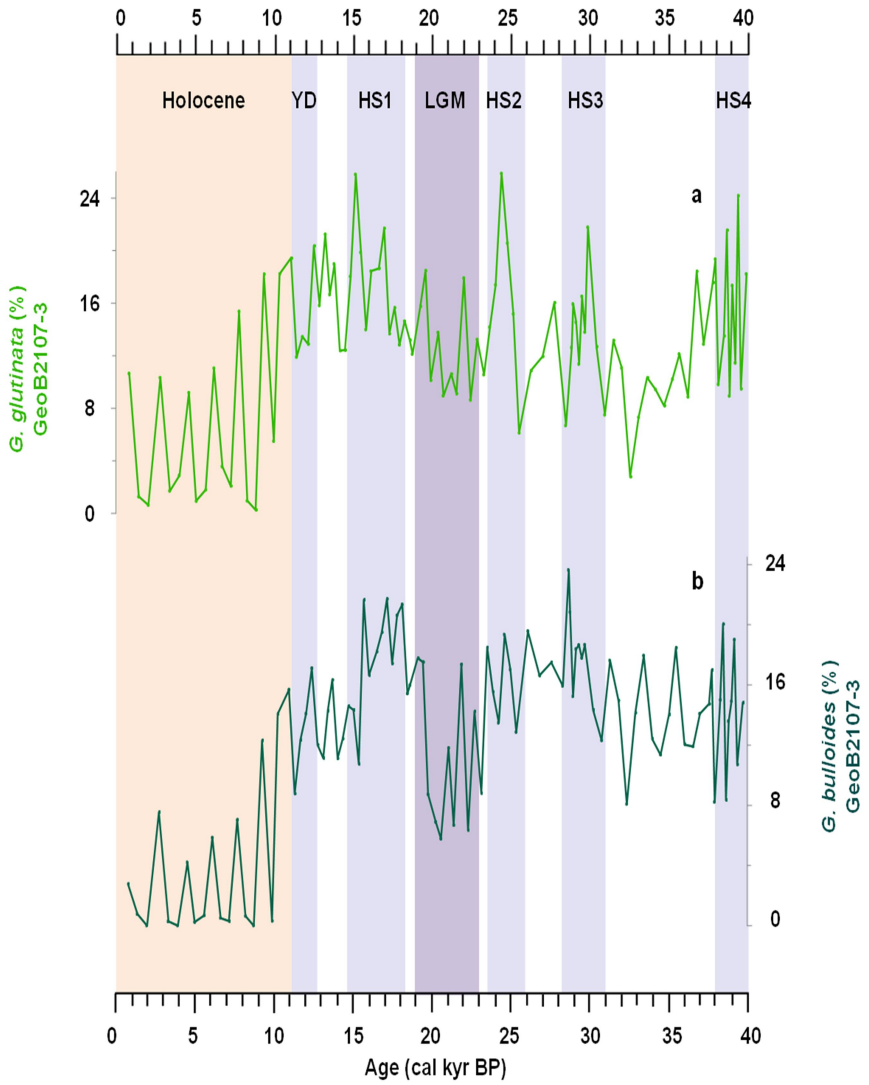

Figure 19 – Eutrophic planktonic foraminiferal species. (a) *Globigerinita glutinata*; (b) *Globigerina bulloides* (this study). The blue bars correspond to Heinrich Stadials (HS) and the Younger Dryas (YD) (SARNTHEIN *et al*., 2001), the lilac bar refers to the Last Glacial Maximum (LGM), and the light pink bar to the Holocene.

The highest percentages of *G. glutinata* during the last 40 cal kyr BP clearly match with all HS (HS4: 24.2%; HS3: 21.8%; HS2: 25.9%; HS1: 25.8%). Also, maximum relative abundance of *G. bulloides* over the last 40 cal kyr BP was reached at HS3, with higher peaks of ca. 20% exhibited during HS periods (HS4: 20%; HS3: 23.6%; HS2: 19.3%; HS1: 21.7%). Conversely, a drop in abundance of *G. glutinata* (from 20.3% to 11.9%) and *G. bulloides* (from 17.1% to 8.8%) occurred at shorter (i.e., millennial) timescale during the YD.

Other species that usually thrive in productive environments, such as *G. inflata*, *G. trucatulinoides* (dextral), and *N. dutertrei* only displayed a clear trend at the long-term glacial-interglacial timescale. The highest relative abundances of 16.2%, 8.0%, and 6.1%, respectively (Tab. 3) were recorded by those species during the glacial and toward the glacial-interglacial transition, abruptly declining with the inception of full interglacial conditions.

5.2.3 Reconstruction of Agulhas Leakage

After the onset of the Holocene, a faunal turnover was depicted in the composition of the planktonic foraminiferal assemblages. Along with an overall decline of eutrophic species, pronounced increase of typical Agulhas fauna was found (Fig. 20). The maximum percentages of the species *G. menardii* (18.0%), *O. universa* (14.0%), *G. conglobatus* (7.1%), and *P. obliquiloculata* (1.0%) (Tab. 3) were recorded when full interglacial conditions stablished. Over the Mid Holocene, however, a drop in the relative abundances of those species culminated at ca. 5 cal kry BP, a period marked by the lowest percentages of *G. conglobatus* and a temporary absence of *P. obliquiloculata*.

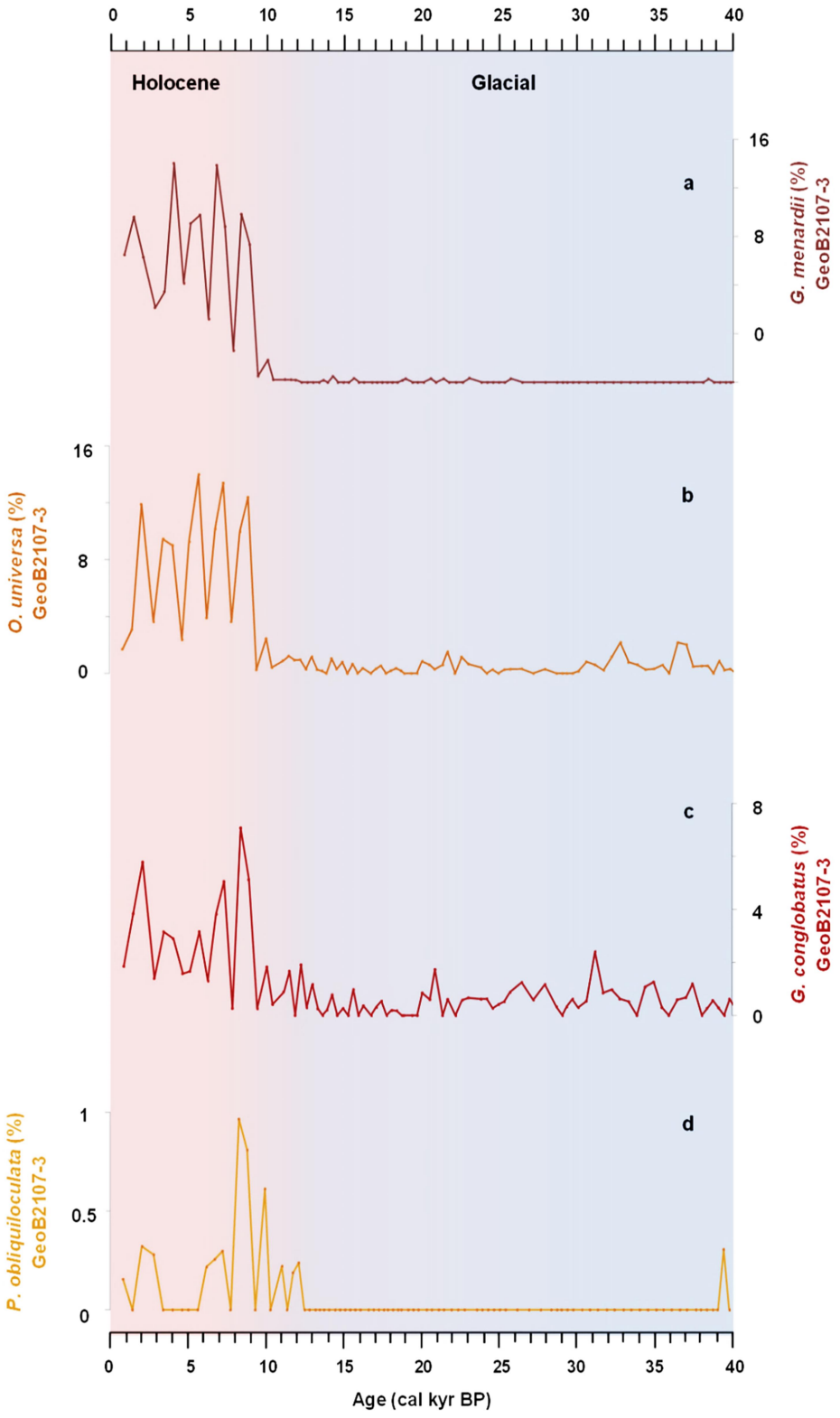

Figure 20 – Agulhas leakage fauna. (Sub) tropical planktonic foraminiferal species (KUCERA, 2007) virtually absent during the glacial and flourishing with the Holocene inception. (a) *Globorotalia menardii*; (b) *Orbulina universa*; (c) *Globigerinoides conglobatus*; and (d) *Pulleniatina obliquiloculata* (this study).

5.3 Geochemical Analyses: Stable Oxygen Isotopes

The *G. ruber* $\delta^{18}O$ values (Fig. 21a) ranged from 0.4 to -1.1‰. Major $\delta^{18}O_{G.\ ruber}$ decreases throughout the glacial period were found along the LGM and HS1, with amplitudes of ca. 1.0‰. At the boundary between HS1 and the Bølling-Allerød (B-A) event (14.6-12.9 kyr), a sharp increase with an amplitude of 0.7 ‰ was recorded. A decreasing trend in the *G. ruber* $\delta^{18}O$ values was observed thereafter, but with an increase recorded along the Mid Holocene with an amplitude of ca. 0.6‰.

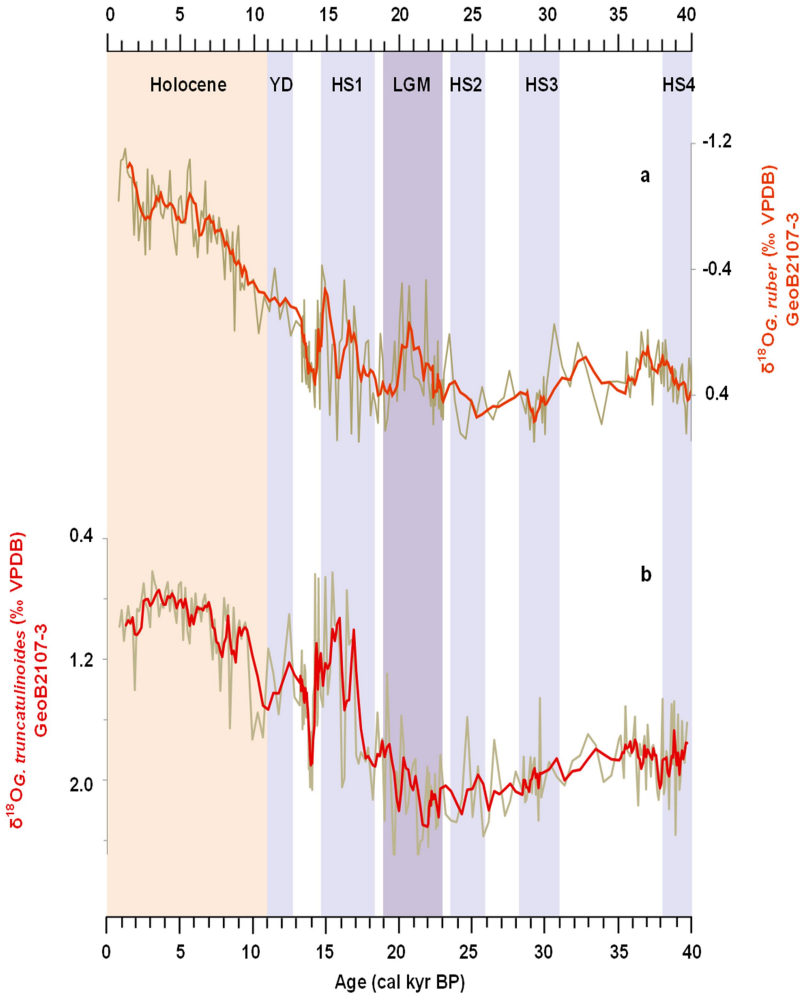

Figure 21 – Stable oxygen isotope records. Foraminiferal stable oxygen isotope records (and five-point running average) from: (a) *G. ruber* (white) ($\delta^{18}O_{G.\ ruber}$); and (b) *G. truncatulinoides* (dextral) ($\delta^{18}O_{G.\ truncatulinoides}$). The blue bars correspond to Heinrich Stadials (HS) and the Younger Dryas (YD) (SARNTHEIN *et al.*, 2001), the lilac bar refers to the Last Glacial Maximum (LGM), and the light pink bar to the Holocene.

The *G. truncatulinoides* $\delta^{18}O$ values (Fig. 21b) spanned from 2.6 to 0.7‰. The lowest $\delta^{18}O_{G.\ truncatulinoides}$ values were recorded during HS1, with amplitude of ca. 1.5‰. Apart from HS1, no clear signal of millennial-scale changes were observed during other HS. A positive excursion with amplitude of ca. 0.6‰ was found over the YD. Along the Holocene, an overall decreasing trend was shown, but with a sharp drop during the Early Holocene with an amplitude of ca. 0.8‰, and a positive excursion during the Late Holocene with an amplitude of ca. 0.7‰.

5.3.1 Reconstruction of $\delta^{18}O_{ivc\text{-}ssw}$: A Proxy for Paleosalinity

The ice-volume corrected $\delta^{18}O_{ssw}$ values (Fig. 22) oscillated between 1.2 and 2.3‰. A marked increase in $\delta^{18}O_{ivc\text{-}ssw}$ values was observed during the LGM, with an amplitude of 0.7‰. High frequency variability in the $\delta^{18}O_{ivc\text{-}ssw}$ values was recorded during the HS1 with amplitudes of ca. 1‰. After HS1, a steady decrease in $\delta^{18}O_{ivc\text{-}ssw}$ values with an amplitude of ca. 1.0‰ was found during the B-A until it reached a low during the YD. At the onset of the Holocene, a sharp increase with ca. 1.0‰ of amplitude was followed by a decreasing trend in $\delta^{18}O_{ivc\text{-}ssw}$ values.

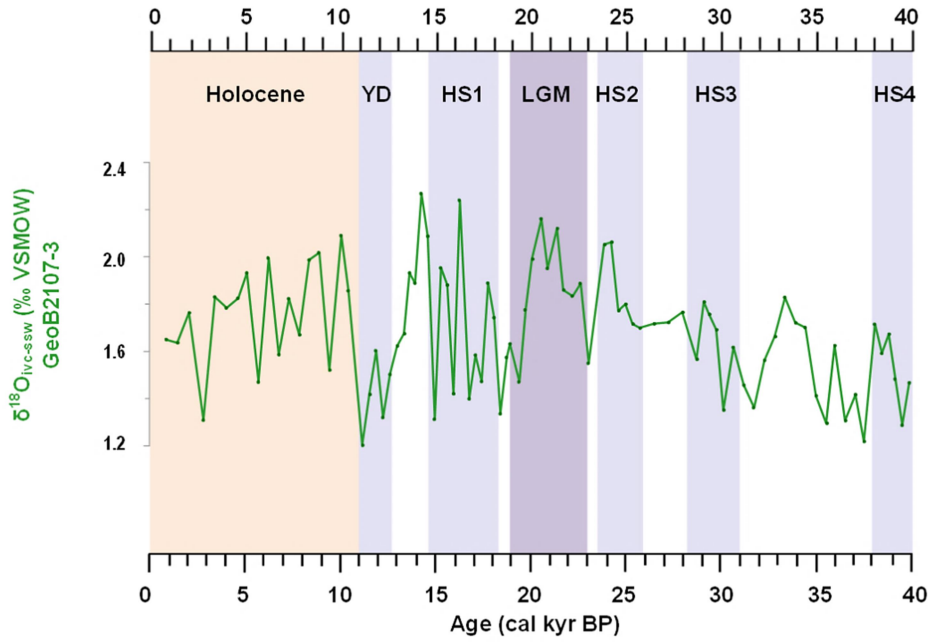

Figure 22 – Ice-volume corrected oxygen isotopic composition of surface seawater ($\delta^{18}O_{ivc\text{-}ssw}$), a proxy for salinity (this study). The blue bars correspond to Heinrich Stadials (HS) and the Younger Dryas (YD) (SARNTHEIN *et al.*, 2001), the lilac bar refers to the Last Glacial Maximum (LGM), and the light pink bar to the Holocene.

5.3.2 Reconstruction of Past Upper Ocean Stratification

Along the glacial, the $\Delta\delta^{18}O$ derived from $\delta^{18}O_{G.\ truncatulinoides}$ and $\delta^{18}O_{G.\ ruber}$ (Fig. 23) showed maximum values over the LGM, with deviations of ca. 0.4‰ with respect to the mean; while minimum values were recorded during HS1, with mean deviations of ca. 0.6‰. Minor changes in the $\Delta\delta^{18}O_{G.truncatulinoides\text{-}G.ruber}$ values were also found within other HS, during HS4 and HS3, with deviations of ca. 0.2 and 0.1 ‰, respectively. Along the interglacial, minimum values were shown at the Holocene inception, whereas maximum values were recorded over the Late Holocene with respective deviations of ca. 0.3‰ and 0.4‰ with respect to the mean.

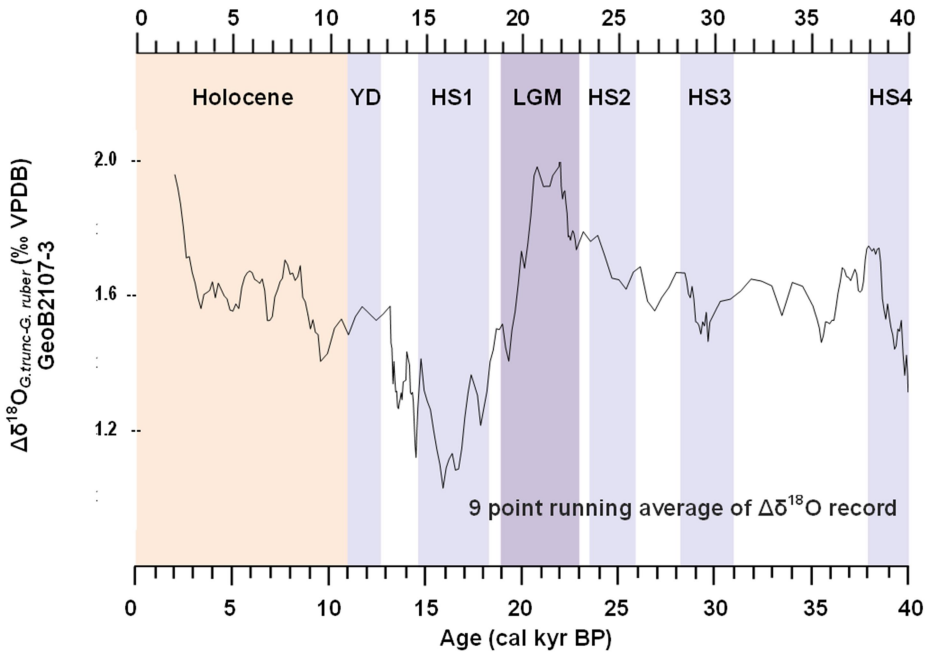

Figure 23 – Stable oxygen isotope difference (nine-point running average) between deep- and shallow-dwelling planktonic foraminifera *G. truncatulinoides* and *G. ruber* ($\Delta\delta^{18}O_{G.truncatulinoides\text{-}G.ruber}$), a proxy for upper ocean stratification (this study). The blue bars correspond to Heinrich Stadials (HS) and the Younger Dryas (YD) (SARNTHEIN *et al*., 2001), the lilac bar refers to the Last Glacial Maximum (LGM), and the light pink bar to the Holocene.

The main results described in this section are summarized in the Figures 24, 25, 26 and 27. In those figures, the proxy records from GeoB2107-3 are plotted together with Bermuda Rise $^{231}Pa/^{230}Th$ records, a proxy for AMOC strength (McMANUS *et al*., 2004; LIPPOLD *et al*., 2009); precession-driven austral summer insolation (BERGER, 1992); global sea-level (WAELBROECK *et al*., 2002); and are also compared with other marine and terrestrial proxy records. The figures 24 and 25 show the results spanning the whole studied period of the last 40 kyr. The Figures 26 and 27 focus on the main results covering the last 11 kyr (i.e., the Holocene evolution following the last glacial-interglacial transition).

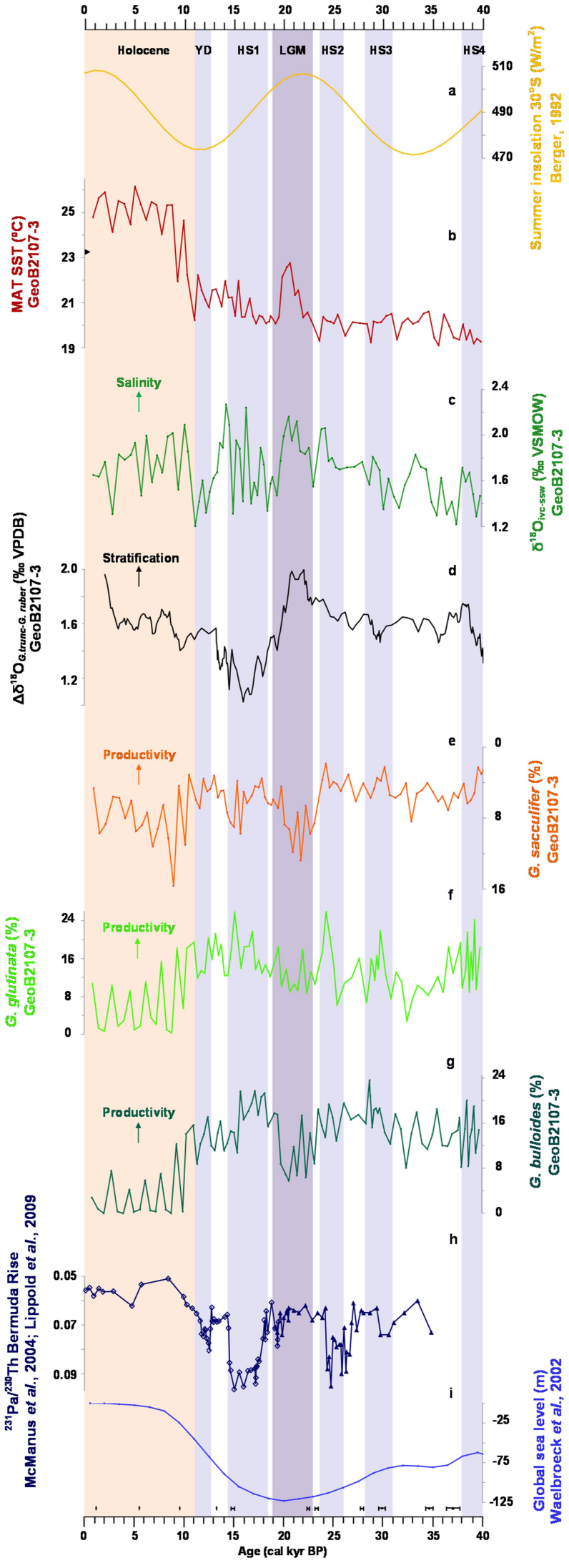

Figure 24 – Proxy records from core GeoB2107-3 plotted together with other records.
(a) Precession-driven February austral summer insolation (30°S) (W/m^2) (BERGER, 1992); **(b)** Modern Analog Technique (MAT)-derived sea surface temperature estimate (this study), and modern mean annual temperature at the core site (y-axis: black triangle) (LOCARNINI *et al.*, 2013); **(c)** Ice-volume corrected oxygen isotopic composition of surface seawater ($\delta^{18}O_{ivc\text{-}ssw}$), a proxy for salinity (this study); **(d)** Stable oxygen isotope difference (nine-point running average) between deep- and shallow-dwelling planktonic foraminifera *G. truncatulinoides* and *G. ruber* ($\Delta\delta^{18}O_{G.truncatulinoides\text{-}G.ruber}$), a proxy for upper ocean stratification (this study); Relative abundances of: **(e)** Oligotrophic *G. sacculifer*; **(f)** Eutrophic *G. glutinata;* and **(g)** *G. bulloides* planktonic foraminifera (this study); **(h)** Bermuda Rise $^{231}Pa/^{230}Th$ records, a proxy for the AMOC strength (open square: McMANUS *et al.*, 2004; solid triangle: LIPPOLD *et al.*, 2009); **(i)** Global sea-level record (WAELBROECK *et al.*, 2002). Black symbols at the bottom of the panel depict calibrated radiocarbon ages. The blue bars correspond to Heinrich Stadials (HS) and the Younger Dryas (YD) (SARNTHEIN *et al.*, 2001); the lilac bar refers to the Last Glacial Maximum (LGM), and the light pink bar to the Holocene.

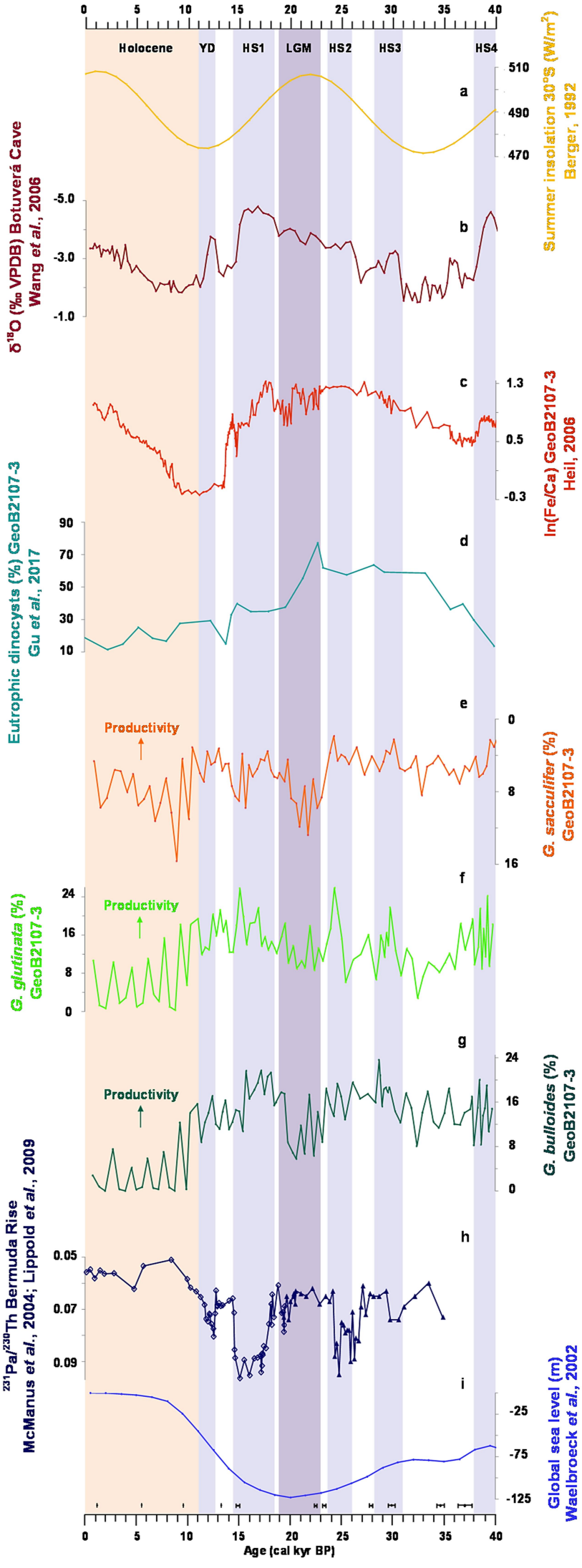

Figure 25 – Marine and terrestrial proxy records from core GeoB2107-3 compared with other records. **(a)** Precession-driven February austral summer insolation (30°S) (W/m^2) (BERGER, 1992); **(b)** Stalagmite oxygen isotope record ($\delta^{18}O$) from Botuverá Cave (WANG *et al.*, 2006); **(c)** Major elements intensity (Fe/Ca ratios) from core GeoB2107-3 (HEIL, 2006); Relative abundances of: **(d)** Eutrophic dinocyst from core GeoB2107-3 (GU *et al.*, 2017); **(e)** Oligotrophic *G. sacculifer;* **(f)** Eutrophic *G. glutinata*; and **(g)** *G. bulloides* planktonic foraminifera (this study); **(h)** Bermuda Rise $^{231}Pa/^{230}Th$ records, a proxy for the AMOC strength (open square: McMANUS *et al.*, 2004; solid triangle: LIPPOLD *et al.*, 2009); **(i)** Global sea-level record (WAELBROECK *et al.*, 2002). Black symbols at the bottom of the panel depict calibrated radiocarbon ages. The blue bars correspond to Heinrich Stadials (HS) and the Younger Dryas (YD) (SARNTHEIN *et al.*, 2001), the lilac bar refers to the Last Glacial Maximum (LGM), and the light pink bar to the Holocene.

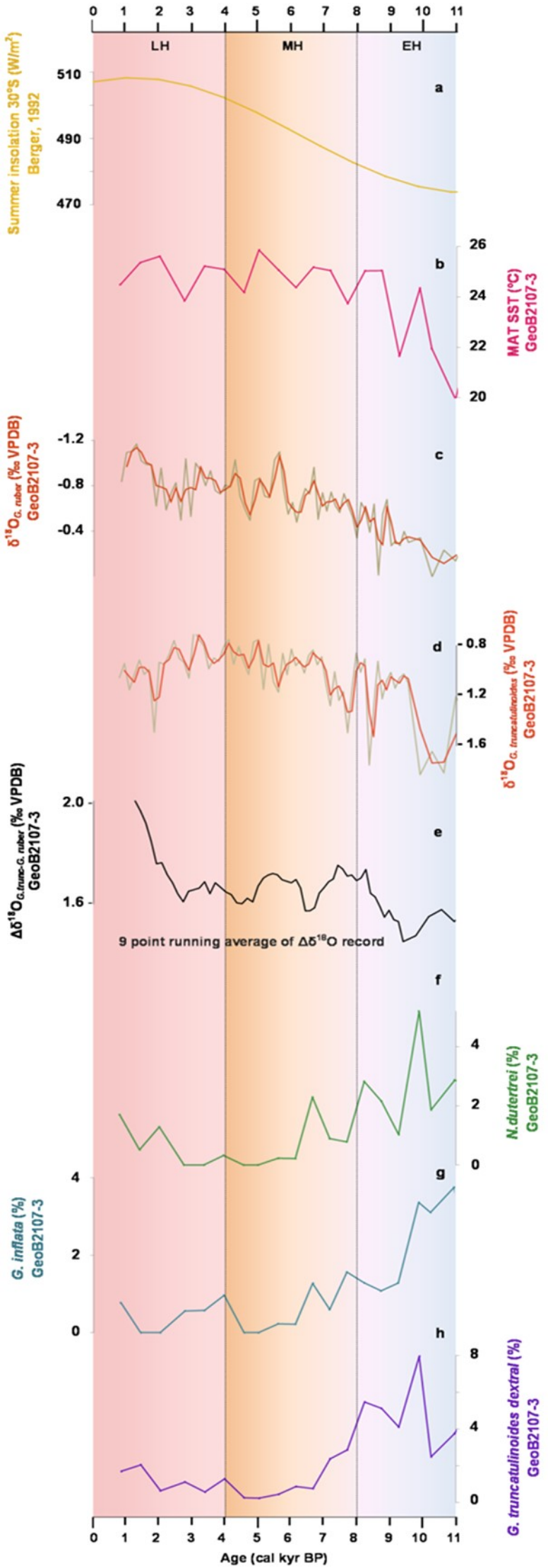

Figure 26 – Relative abundances of planktonic foraminiferal species from core GeoB2107-3 plotted together with other proxy records.
(a) Precession-driven February austral summer insolation (30°S) (W/m^2) (BERGER, 1992);
(b) Modern Analog Technique (MAT)-derived sea surface temperature estimates (this study);
Foraminiferal stable oxygen isotope records (and respective five-point running average) from:
(c) *G. ruber* (white) ($\delta^{18}O_{G.ruber}$);
(d) *G. truncatulinoides* ($\delta^{18}O_{G.\ truncatulinoides}$) (this study);
(e) Stable oxygen isotope difference (nine-point running average) between the deep- and shallow-dwelling planktonic foraminifera *G. truncatulinoides* and *G. ruber* ($\Delta\delta^{18}O_{G.truncatulinoides\text{-}G.\ ruber}$), a proxy for upper ocean stratification (this study);
Relative abundances of the planktonic foraminiferal species:
(f) *N. dutertrei*;
(g) *G. inflata*; and
(h) *G. truncatulinoides* (this study).
The bluish-lilac bar refers to the Early Holocene (EH), the pinkish-orange bar corresponds to the Mid Holocene (MH), and the dark pink bar depicts the Late Holocene (LH) (WALKER *et al*., 2012).

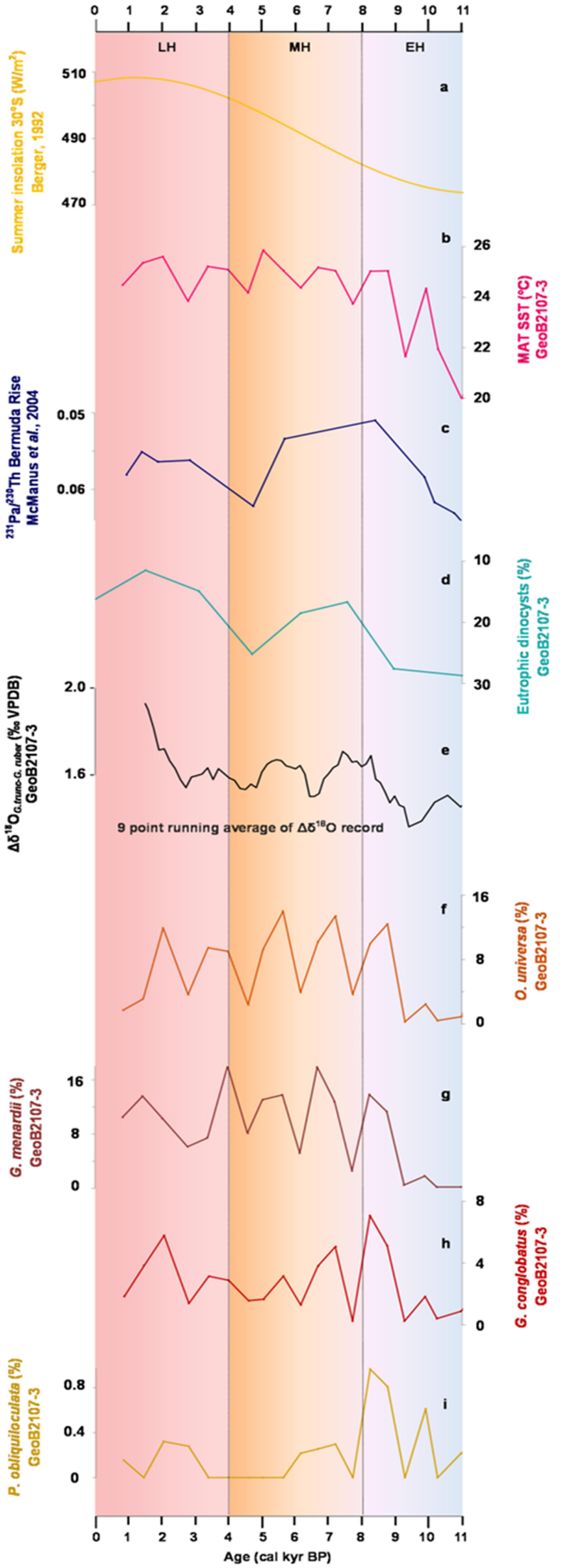

Figure 27 – Relative abundances of Agulhas faunal species from core GeoB2107-3 plotted together with other proxy records. **(a)** Precession-driven February austral summer insolation (30°S) (W/m^2) (BERGER, 1992); **(b)** Modern Analog Technique (MAT)-derived sea surface temperature estimates (this study); **(c)** Bermuda Rise $^{231}Pa/^{230}Th$ record, proxy for AMOC strength (McMANUS *et al.*, 2004); **(d)** Relative abundances of eutrophic dinocysts from core GeoB2107-3 (GU *et al.*, 2017); **(e)** Stable oxygen isotope difference (nine-point running average) between the deep- and shallow-dwelling planktonic foraminifera *G. truncatulinoides* and *G. ruber* ($\Delta\delta^{18}O_{G.truncatulinoides\text{-}G.\ ruber}$), a proxy for upper ocean stratification (this study);
Relative abundances of Agulhas faunal species:
(f) *O. universa*;
(g) *G. menardii;*
(h) *G. conglobatus;*
(i) *P. obliquiloculata*;
(this study).
The bluish-lilac bar refers to the Early Holocene (EH), the pinkish-orange bar corresponds to the Mid Holocene (MH), and the dark pink bar depicts the Late Holocene (LH) (WALKER *et al.*, 2012).

Chapter 6

Discussion

6.1 Last Glacial-Interglacial Cycle

At glacial-interglacial timescale, the reconstruction of paleoceanographic conditions in the upper water column shows that lowest temperatures prevailing over the glacial were followed by a steep rise (ca. 4^{o}C) at the onset of the Holocene (Fig. 24b). Overall, rather lower salinity was also yielded along the glacial in comparison to the Holocene (Fig. 24c). Parallel to this long-term trend of temperature and salinity, enhanced primary productivity along the glacial was succeeded by a marked decrease after the Holocene inception, as signalled by a conspicuous drop in abundance of *G. glutinata* and *G. bulloides* (Fig. 24f; g). After this transitional period, full interglacial conditions established in the study area, with a pronounced productivity decline and the dominance of warmer oligotrophic waters, typical for the modern western South Atlantic (MULITZA *et al*., 1998; WEFER *et al*., 2004).

It is hypothesised here that the long-term trend depicted in the proxy records is tightly related to the dynamics of the BC, which dictates the pace of a mesoscale upwelling system along the southern Brazilian margin together with the seaward displacement of BCC coastal waters off CSM. The CSM constitutes the southerly portion of such upwelling system, which comprises many other important upwelling zones spreading to the south of 20^{o}S, where the SACW is incorporated to the BC and cyclonic vortices are formed. Those upwelling zones are located around cape areas off (i) Vitória (20^{o}S) (SCHMID *et al*., 1995; GAETA *et al*., 1999); (ii) Cape São Tomé (22°S) (CALADO *et al*., 2010; PALÓCZY *et al*., 2013); (iii) Cape Frio (23°S) (CAMPOS; VELHOTE; SILVEIRA, 2000; CASTELÃO; BARTH, 2006); including (iv) Cape Santa Marta (28^{o}S) (CAMPOS *et al*., 2013; BRANDINI *et al*., 2014). Unlike all those upwelling zones extending northward, the region offshore CSM is further impacted by the outflow of PPW waters (Fig. 15a) (PIOLA *et al.,* 2005; MÖLLER *et al.*, 2008).

As it is observed in the modern subtropical western South Atlantic, reconstructions of such upwelling system evolution over the last 140 cal kyr BP also underline the role of the BC dynamics governing past shifts in upper water properties and in the nutrient enrichment of such oligotrophic waters (TOLEDO *et al.*, 2008; SOUTO *et al*., 2011; PORTILHO- RAMOS *et al*., 2015; LESSA *et al*., 2017). Those findings also reiterate the impact of the BC meanders and vortices on oceanographic changes over a wide extent along its pathway, reaching farther north to the core site (25-21°S). Paleostudies further suggest that those modern upwelling zones would be the remnants of an even larger western boundary upwelling system along the western South Atlantic in the past (LESSA *et al*., 2017). The impact of the BC dynamics on upper water column properties (e.g., temperature, salinity, and stratification), as well as on nutrient input and productivity under distinct background climate conditions of the last glacial and the Holocene are further discussed in the following sections.

6.2 Last Glacial

The mesoscale activity of the BC associated to its meanders and vortices entails shifts in seawater temperature. Both the SACW upwelling and the entrapment of BCC cold waters (Figs. 13a; 15a) fostered by the BC dynamics would produce cooling at (sub) surface levels. In the core site, the yielded temperature averages at surface (10 m) and at subsurface (50 m; 100 m) during the glacial (Tab. 4) are below the isotherm of 20^{o}C, which defines the modern limit between SACW and TW waters and has been applied as a parameter in upwelling regions along the Brazilian margin (CASTELÃO; CAMPOS; MILLER, 2004; PORTILHO-RAMOS *et al*., 2015). Together with the lower global temperatures, it is also likely that the enhanced upwelling and/or influx of coastal waters throughout the glacial could possibly have further contributed to the lowest temperature estimates over that time period.

Reorganisations in hydrographic conditions governed by the BC dynamics also embed changes in seawater salinity. The upwelling and seaward inflow of less saline SACW and BCC coastal waters (Fig. 13b; 15a) would result in the freshening of (sub) surface layers. Those changes impelled by the BC cyclonic vortices might likely have

accounted for the anomalously lower sea surface salinity depicted in the proxy records along most of the glacial (Fig. 24c). It would not be expected that the overall long-term trend of lower ice-volume corrected salinity estimates (i.e., excluding the global salinity signal resulting from the ice volume effect) would have been produced by local changes in the hydrological regime induced by orbital forcing. Lower precession-driven austral summer insolation (Fig. 24a) preceding the LGM would not have possibly boosted SASM (Fig. 25b) (CRUZ *et al*., 2005; WANG *et al*., 2006) and precipitation, which is therefore not assumed to be a major forcing behind the low salinity long-term trend.

Also, the upwelling and seaward influx of nutrient-rich SACW and BCC (Fig. 13c; 15b) induced by the BC impart increased nutrient input to the euphotic zone fostering primary productivity. The higher abundance of eutrophic planktonic foraminifera (Fig. 24f; g), coeval with reduced temperatures (Fig. 24b) and salinities (Fig. 24c) over most of the glacial further suggests a tight link between changes in the upper water properties and the BC dynamics. Such assumption is also consistent with an overall opposite trend depicted in the faunal and isotopic foraminiferal records after the Holocene inception.

Apart from the impact on temperature, salinity, and nutrient content, changes triggered by the BC cyclonic vortices also embody shifts in the thermocline depth and in the upper ocean stratification. The development of cyclonic vortices would reduce the stratification of upper waters into a well-mixed surface layer. Accordingly, it would thus be expected that the yielded $\Delta\delta^{18}O$ values (Fig. 24d) would have been lower during the glacial, as compared to the Holocene, reflecting increased upwelling and vertical mixing over that period. However, the high $\delta^{18}O_{\textit{G. truncatulinoides}}$ values (Fig. 21b) imposed by coldest glacial waters at thermocline levels perhaps might have dampened the recorded $\Delta\delta^{18}O$ signal at glacial-interglacial timescale. The lowest temperatures, rather than the long-term decreased salinity, might possibly have accounted for the $\delta^{18}O_{\textit{G. truncatulinoides}}$ signature, signalling to denser subsurface waters along the glacial.

Hence, the proxy record for upper ocean stratification likely might not have captured the long-term pattern depicted in the MAT-derived temperature (Fig. 24b), and in salinity

(Fig. 24c) estimates, as well as in the productivity changes displayed by the eutrophic planktonic foraminiferal records (24f; g). The dissimilarity between upper ocean stratification and the other proxy records at glacial-interglacial timescale might as well possibly imply that not only upwelling, but also other oceanographic processes would have forced the long-term changes observed in the study area.

It is inferred here that local rivers discharge (BRANDINI *et al*., 2014) and PPW northward intrusions, analogous to modern winter conditions (Fig. 15a; b) (MÖLLER *et al*., 2014), might also have accounted for the colder, less saline and nutrient-enriched waters at shallower depths. An increased influence of those coastal waters transported by the BCC is further suggested by the high Fe/Ca values (Fig. 25c) (HEIL, 2006) and the enhanced percentages of eutrophic dinocysts (Fig. 25d) (GU *et al*., 2017) recorded in the study site over the glacial. Both proxies have been related to fluvial runoff and continental-sourced nutrient influx (GU *et al*., 2017).

Indeed, the stronger nutrient supply induced by the BCC would have been favoured by the lower sea level (Fig. 25i) (CLARK *et al*., 2009) and progressive exposure of the continental shelf along the last glacial, redirecting terrigenous input further offshore (LANTZSCH *et al*., 2014). Together with the seaward displacement of the coastline and the PPW strengthening propelled by intensified cold fronts, BCC nutrient-rich shelf waters were to be further captured by the coastal lobe of the BC cyclonic vortex and impelled seaward, entraining into the surface oceanic waters overlaying the continental slope and the study area (MATANO *et al*., 2014). Such condition might have been provisionally reversed along the LGM, when a major shelf narrowing resulting from sea level retreat (Fig. 25i) would have likely restrained the vorticity of the BC (see section 6.2.1) and the northward intrusion of PPW distant nutrient-rich coastal waters (PALMA; MATANO; PIOLA, 2008; LANTZSCH *et al*., 2014). Yet, that environmental setting would have not prevailed throughout the glacial period.

The presence of cold, less saline and nutrient-rich shallower waters in the study site along most of the last glacial is therefore interpreted as indicative of (i) BC meandering

flow promoting shelf break upwelling and (ii) increased BCC-delivered terrigenous input off CSM.

6.2.1 Last Glacial Maximum

During the LGM, however, a steep temperature rise (ca. 2^{o}C) (Fig. 24b) and salinity increase (Fig. 24c) is accompanied by a sharp decrease in abundance of eutrophic symbiont-barren planktonic foraminifera (Fig. 24f; g) and a peak of tropical symbiont-bearing species (Fig. 24e), marking an interval of prevailing oligotrophic conditions. Enhanced sea surface temperature and salinity coeval with the lowest percentage of *G. bulloides* within the glacial (5.8%), and an outstanding drop of *G. glutinata* (8.9%), as well as a peak of *G. sacculifer* (13%) suggest the dominance of warmer, salty and oligotrophic TW. Over that period, colder nutrient-rich SACW waters would have been restricted to greater depths, as it is also depicted in the temperature estimates (≥ 20^{o}C) for 10 m and 50 m (Tab. 4). In addition, concurrently enhanced upper water column stratification (Fig. 24d) would mirror the development of both strong thermocline and nutricline, thereby limiting the nutrient supply to the upper sunlit layer. Altogether, those changes reflect a sudden decrease in the local upwelling regime and in the mesoscale activity of the BC, leading to a sharp productivity decline.

A temperature rise alone might have been partially fostered by an increased warming of the BC linked to the enhanced incoming solar radiation (PROVOST; GARCIA; GARÇON, 1992; SILVEIRA *et al*., 2000) during the LGM, when precession-driven austral summer insolation (30^{o}S) reached its maximum (Fig. 24a) (BERGER; LOUTRE, 1991). Increased SST over the LGM has also been formerly detected nearby (27^{o}-24^{o}S) both in planktonic foraminiferal Mg/Ca (CARLSON *et al*., 2008b; SANTOS *et al*., 2017a) and coccolithophore alkenone (LOURENÇO *et al*., 2016) records. Likewise, an early warming prior to the last deglaciation has also been found in the eastern subtropical South Atlantic (MARTINEZ-MÉNDEZ *et al*., 2010). It has been suggested that, superimposed to changes in orbital parameters, a shoaled AMOC during the LGM might have impaired the efficiency of the northward export of heat, and salt, which would be stored in the South Atlantic subtropical gyre. In the western South

Atlantic, the heat and salt excess would have been redirected southward by an intensified flow of the BC (CARLSON *et al*., 2008b; SANTOS *et al*., 2017a).

A regional warming associated to AMOC disturbances potentially could have applied to the study area, contributing to amplify the climatic response to the insolation signal, as the orbital forcing alone would not explain such an abrupt temperature rise observed over the LGM. Yet, distinct tracers of AMOC strength and geometry (McMANUS *et al*., 2004; LIPPOLD *et al*., 2009; BÖHM *et al*., 2015; HOWE *et al*., 2016a; b) indicate that only a relatively shoaled overturning in the Atlantic (AMOC 'cold mode') would have prevailed during the LGM (BÖHM *et al*., 2015; LYNCH-STIEGLITZ, 2017). Such slight change in the AMOC along the LGM (Fig. 24h) could not solely explain the enhanced temperatures, and salinities, recorded in the study site over this period (Fig 24b; c). Besides, a time lag between the temperature rise (Fig. 24b) and changes in the AMOC strength (Fig. 24h) is also observed. Further, it would rather be expected that a reduced AMOC would correlate to a strengthened BC, intensifying its meandering flow and fostering productivity in the study area. Therefore, it is assumed that other forcing would have been at stake, inducing the changes recorded during the LGM.

Superimposed to changes in insolation and in the AMOC mode, the eustatic sea level reached ca.125 m below pre-industrial level during the LGM (WAELBROECK *et al*., 2002) (Fig 24i). The LGM sea level closely corresponds to the shelf break depth (ca.120 m) along that southern portion of the Brazilian margin (ZEMBRUSCKI, 1979). Importantly, most outstanding changes in temperature, salinity, and stratification (increase), as well as in productivity (decrease) are observed at the very period when sea-level reached the shelf break depth (Fig. 24b; c; d; e; f; g; i). This suggests that changes in sea level during the LGM would be the overarching forcing dictating the observed shifts in the BC, thereby curbing upwelling and triggering the non-linear response reflected in abrupt temperature, salinity, stratification and productivity changes linked to an episodic dominance of TW. It is hypothesised here that maximum sea level drop would have strongly affected the vorticity of the BC, halting the development of cyclonic meanders and hindering productivity over the LGM.

Along the southern Brazilian margin, the BC system is centred on the middle continental slope (CAMPOS; VELHOTE; SILVEIRA, 2000), where the study site is located; only the coastal lobe of the BC is located near the shelf break and projected toward the coast (BILÓ *et al.*, 2014; SATO, 2015). The water depth on the continental shelf seems to affect the barotropic instability of the BC (SILVEIRA *et al*., 2000; BILÓ *et al.*, 2014; SATO, 2015). Slightly to the north off the CSM (27^{o}S), the location of the core site, modelling experiments (PALMA; MATANO, 2009; CAMPOS *et al*., 2013) show that it is the barotropic component of the alongshelf pressure gradient that generates the strongest centre of shelf-break upwelling. As suggested by a study on the meandering pattern of the Kuroshio Current (JAMES; WIMBUSH; ICHIKAWA, 1999), a lowering water depth over the shelf would hamper the boundary current flow toward the coast, enhancing the resistance for the development of cyclonic meanders. These findings agree with another study on the BC meandering flow conducted at Cape Frio (24^{o}S) (CAMPOS; GONÇALVES; IKEDA, 1995), which also suggests that a reduced water depth along the shelf would alter the potential vorticity of the BC. Changes in the bathymetry therefore may curb the development and amplitude of the BC cyclonic vortices (PALMA; MATANO, 2009; SATO, 2015), which would require stronger wind forcing to promote coastal upwelling (PALÓCZY *et al*., 2014), inhibiting both shelf break and coastal upwelling.

Reduced upwelling seems to have taken place even under a relatively strengthened BC, induced by the AMOC cold mode and a narrowed continental shelf over the LGM, as supported by modelling studies on the South Atlantic large-scale circulation (CLAUZET *et al.*, 2007). Besides, as suggested by hydrographic data (CASTELÃO; CAMPOS; MILLER, 2004) and modelling experiments (CAMPOS *et al*., 2013) off the CSM, shifts in ocean conditions are much slower under NE favourable-upwelling winds than under SW downwelling-favourable wind forcing. For this reason, coastal upwelling events would demand more prolonged episodes of pronounced NE winds (MIRANDA, 1982; GIBBS; MIDDLETON; MARCHESIELLO, 1998), which might not have sufficed to promote coastal upwelling over this period of sea-level drop. Moreover, a narrowed shelf would have further contributed to halt the incidence of coastal upwelling over the LGM.

It is also expected that the influence of distant nutrient-rich coastal waters transported by the BCC would be reduced in the study area during the LGM, as a major shelf narrowing would have induced a PPW retreat together with the southward displacement of the BC (PALMA; MATANO; PIOLA, 2008; LANTZSCH *et al*., 2014). That is indeed suggested by the decreasing trend in Fe/Ca ratios (Fig. 25c) (HEIL, 2006) and sharp drop of eutrophic dinocysts (Fig. 25d) (GU *et al*., 2017) recorded in the core site along the LGM. The reduced productivity further indicates that the ensuing lower carbonate content would not be responsible for the Fe/Ca decreasing trend over the LGM.

Hence, shifts in the environmental conditions and in mesoscale processes controlling the development of the BC cyclonic vortices would seemly have modulated the observed changes in the study area along the LGM. Those shifts would have induced remarkable changes in the upper water column, resulting in increased temperature, salinity and stratification; also restraining the oceanic- and continental-sourced nutrient inflow toward the continental slope (MATANO *et al*., 2014; BRANDINI *et al*., 2014), leading to a pronounced productivity decline.

6.2.2 Heinrich Stadials

For the first time, changes in productivity have been recorded in the western subtropical South Atlantic during HS throughout the last glacial. The results of the present study show that all HS (HS4-HS1) events are marked by enhanced abundance of the eutrophic species *G. glutinata* (Fig. 24f) and some also of *G. bulloides* (HS3; HS1) (Fig. 24g). Coeval with the highest abundances of eutrophic planktonic foraminifera, lower $\Delta\delta^{18}O_{G.truncatulinoides\text{-}G.ruber}$ values (Fig. 24d) are also recorded along some HS periods suggesting weaker upper ocean stratification (MULITZA *et al*., 1997).

The most outstanding changes are found during HS1, a period of major AMOC slowdown (Fig. 24h), when peaks of eutrophic planktonic foraminifera (Fig. 24f; g) are accompanied by the lowest $\Delta\delta^{18}O$ values (Fig. 24d). Both the increased productivity and the most prominent reduction in the upper-water-column stratification during HS1

suggest a resumption of the upwelling regime after the LGM. This condition would have also been favoured by a major meltwater pulse at 19 cal kyr BP that likely occurred in the North Atlantic in response to Northern Hemisphere ice-sheet melting, and the ensuing sea-level rise following the LGM (Fig. 24i), at the onset of the last deglaciation (CLARK *et al*. 2009).

Parallel to changes in ocean conditions, reorganisations in the atmospheric circulation would have also intensified the SAMS/SACZ activity (Fig. 25b) (CRUZ *et al*., 2005; WANG *et al*., 2006; STRÍKIS *et al*., 2015). That would have led to increased river discharge and terrigenous nutrient influx toward the study area, impelled by a strengthened BC, further enhancing productivity during HS. This is indeed supported by the increased sedimentation rates within some HS events recorded in the core site (Fig. 16), and also formerly reported farther south (ca. 32^{o}S) in the subtropical western South Atlantic (CAMPOS *et al*., 2017).

Taken together, those results suggest that the weakened AMOC of HS (Fig. 24h) and the sea-level rise preceding HS1 (Fig. 24i) strengthened the southward meandering flow of the BC, boosting the development of cyclonic vortices and promoting both upwelling and the seaward entrapment of BCC nutrient-rich coastal waters (CAMPOS *et al*., 2013; MATANO *et al*., 2014; BRANDINI *et al*., 2014). The development of cyclonic vortices would also reduce the stratification of upper waters into a well-mixed surface layer, as indicated by low $\Delta\delta^{18}O$ values during HS1 (Fig. 24d), further propitiating the nutrient input to the euphotic zone. Those conditions would foster marine productivity, favouring the occurrence of phytoplankton blooms (Fig. 15b) and resulting in the enhanced abundances of non-symbiont, herbivorous planktonic foraminiferal species displayed by the proxy records.

During events of weakened AMOC and impaired northward transport of heat and salt, intensified BC would redirect the excess of heat and salt southward. It would therefore be expected that millennial-scale changes in temperature and salinity would be mirrored in the MAT estimates and $\delta^{18}O_{ivc\text{-}ssw}$ proxy records. However, unlike the abrupt shifts in productivity, no clear millennial-scale trend is detected in the paleotemperatures derived

from planktonic foraminiferal assemblages (Fig. 24b). Likewise, the $\delta^{18}O_{ivc\text{-}ssw}$ values do not show a distinct millennial-scale pattern (Fig. 24c).

In the western subtropical South Atlantic, SST millennial-scale changes do not seem to be as dominant as they are in the northern high latitudes and in the western tropical South Atlantic (BARD *et al*., 2000; JAESCHKE *et al*., 2007; SANTOS *et al*., 2017). Also, as modelling studies suggest (DAHL; BROCCOLI; STOUFFER, 2005; WEBER *et al*., 2014), warming in the western South Atlantic during meltwater events in the northern high latitudes would mostly prevail at intermediate depths. Thus, the MAT-derived proxy for temperature may not have been sensitive enough to capture the rather subtle changes in the upper water column. Strong SST increases though have been reported for HS1 in planktonic foraminiferal Mg/Ca records of the western (CHIESSI *et al*., 2015) and eastern (BARKER *et al*., 2009) subtropical South Atlantic. Yet, millennial-scale changes of temperature in the upper subtropical western South Atlantic during other HS events would likely have played only a marginal role along the last glacial cycle (SANTOS *et al*., 2017a). Besides, changes of temperature in periods of strengthened BC fostering upwelling and the seaward inflow of coastal waters toward the study site would instead produce cooling at (sub) surface levels, further dampening the temperature signal in the study area.

Despite the absence of a clear millennial-scale signal in the salinity estimates, high frequency variability in the $\delta^{18}O_{ivc\text{-}ssw}$ values is recorded during HS1. Indeed, enhanced salinity in the (sub) tropical western South Atlantic seems to be a pervasive feature over that period, as it has been reported both northward (WELDEAB; SCHNEIDER; KÖLLING, 2006; TOLEDO; COSTA; PIVEL, 2007) and southward (CHIESSI *et al.*, 2015) to the study area. Along with the impact of a weakened AMOC, higher salinity during HS1 would also have been boosted by the enhanced inflow of the Agulhas salty waters into the Atlantic over the termination of the last glacial cycle (PEETERS *et al.*, 2004). It has been suggested (SCUSSOLINI *et al.*, 2015) that the increasing salinity associated with the reinvigoration of the Agulhas leakage (Fig. 10) would mostly prevail at thermocline levels, being transported by SACW waters through the South Atlantic gyre (Fig. 14) (TOMCZAK; GODFREY, 2003; SANTOS *et al*., 2017b).

Unlike other HS, the salinity peaks recorded during HS1 in the core site would possibly mirror the upwelling of anomalous saltier SACW. On the other hand, concomitant reorganisations in the atmospheric circulation boasting the SASM (CRUZ *et al*., 2005; WANG *et al*., 2006; STRÍKIS *et al*., 2015), and thereby enhancing both fluvial runoff and freshening, might possibly have acted in the opposite direction to the ocean circulation shifts forcing instead salinity increases. Such oscillations might have likely produced the intermittent signal depicted in the $\delta^{18}O_{ivc\text{-}ssw}$ record over HS1 (Fig. 24c). During other HS periods of sluggish AMOC, a strengthened BC meandering flow would have rather induced upper layer freshening.

6.2.3 Younger Dryas

The most conspicuous change observed over the YD was a pronounced salinity decline (Fig. 24c). Such outstanding salinity change initiates after HS1, at ca. 14 cal kyr BP, further decreasing throughout the B-A until it reaches a low during the YD. Marked salinity decrease starting at the same time period (~14 kyr) was also recorded in distinct core site locations along the tropical (WELDEAB; SCHNEIDER; KÖLLING, 2006; TOLEDO; COSTA; PIVEL, 2007) and subtropical western South Atlantic (TOLEDO; COSTA; PIVEL, 2007; CHIESSI *et al*., 2015). Such a far-reaching feature might not be possibly explained by local changes in the hydrological regime alone. Besides, distinct proxy records rather indicate a sudden decline in local precipitation rates at the boundary of HS1/B-A, as depicted in a sharp SASM decrease signalled by stalagmite $\delta^{18}O$ records from the surrounding continent (Fig. 25b) (WANG *et al.,* 2006) and outstanding drop in the Fe/Ca ratios recorded in the study site (Fig. 25c) (HEIL, 2006). Hence, precipitation might not have likely induced the salinity low over that period, acting instead in the opposite direction. Also, rising global temperatures fostering deglacial warming would otherwise enhance evaporation, further resulting in higher salinity.

It has been rather suggested that the anomalous salinity decrease in the western South Atlantic would have been largely forced by the progressive northward export of salt throughout the last deglaciation, fuelling the recovery of the AMOC ‘warm mode’

(Fig. 24h) (TOLEDO; COSTA; PIVEL, 2007; CHIESSI *et al*., 2008). As modelling studies also suggest (KNORR; LOHMANN, 2003; BEAL *et al.*, 2011), warm and salty waters from the Indian Ocean entering the South Atlantic with the reestablishment of Agulhas leakage would undergo enhanced atmospheric heat loss along its northward pathway, becoming increasingly more saline. As saltier waters are advected northwards, the excess of salt reaching the North Atlantic would foster the production of the NADW, intensifying the Atlantic overturning strength and resulting in the AMOC resumption (GORDON *et al.*, 1992; WEIJER *et al*., 2002; KNORR; LOHMANN, 2003; BEAL *et al*., 2011).

The trend toward the AMOC reinvigoration along the B-A is briefly interrupted, however, during the YD (Fig. 24h) (McMANUS *et al*., 2004; LIPPOLD *et al*., 2009; BÖHM *et al*., 2015). It is likely that the increased meridional heat transport producing warming in the North Atlantic over the B-A would have forced the retreat of northern hemisphere ice sheets, resulting in a meltwater discharge and causing rather opposing effect in the AMOC strength during the YD (KNORR; LOHMANN, 2003). Nevertheless, no consensus exists as yet about unequivocal sources triggering the YD (CARLSON, 2008a; BROECKER *et al*., 2010).

In the study site, such disturbance in the AMOC was accompanied by changes in marine productivity. A drop by nearly half in the eutrophic planktonic foraminiferal abundances (Fig. 24f; g) signalled a period of decreased productivity. Unlike HS, however, productivity changes in the core site over the YD were not so clearly detectable and would seemly correlate to the reduced magnitude of this shorter event restraining the AMOC slowdown (Fig. 24h) (McMANUS *et al*., 2004; BÖHM *et al*., 2015; LYNCH-STIEGLITZ, 2017).

Hence, the AMOC disturbance during the YD supposedly would not have been strong enough to severely impact the BC dynamics, curbing upwelling and terrigenous input toward the study area. Such condition is further suggested by the increased upper ocean stratification in comparison to HS1 (Fig. 24d). Productivity would have been relatively reduced therefore even under increasingly higher sea levels (Fig. 24i) and enhanced

SASM mirrored in stalagmite $\delta^{18}O$ records from the adjacent continent (Fig. 25b) (WANG *et al*., 2006) likely fostering river discharge and continental-sourced nutrient input.

6.3 Holocene

6.3.1 Early Holocene

The onset of the Holocene was marked by the lowest temperatures (Fig. 26b) and the weakest upper ocean stratification of the interglacial (Fig. 26e). Those conditions were also accompanied by the highest percentages of *N. dutertrei*, *G. inflata*, and *G. truncatulinoides* (Fig. 26f-h), coeval with the lowest abundances of oligotrophic *O. universa*, *G. menardii*, and *G. conglobatus* (Fig. 27f-h). Cooler, nutrient-rich waters and weaker stratified water column over this period suggest a remnant upwelling fostering productivity, to some extent, at the inception of the Holocene. Further, the highest percentage of eutrophic dinocysts (Fig. 27d) recorded in the study area would also signal an increased riverine nutrient input along this period (GU *et al*., 2017). Altogether, such environmental setting would mirror a relatively strengthened BC, fuelling the regional upwelling system and seaward entrainment of nutrient-rich coastal waters prior to a complete recovery of the AMOC (Fig. 27c) and to the advent of full interglacial conditions.

A southward displacement of the STF boosting the Agulhas leakage (BARD; RICKABY, 2009; BEAL *et al*., 2011) supposedly would have propitiated the repopulation of the Agulhas fauna in the Atlantic over this period (PEETERS *et al*., 2004; CALEY *et al*., 2012). In the study area, however, remnants of a mesoscale upwelling producing turbulence and mixing in the surface layer would likely have curbed the development of obligatory symbiont-bearing species, such as *O. universa* (Fig. 27f) and *G. conglobatus* (Fig. 27h) (HEMLEBEN; SPINDLER; ANDERSON, 1989; SCHIEBEL; HEMLEBEN, 2005; KUCERA, 2007) at the rise of the Holocene.

Turbid upwelled waters and reduced ambient light levels would have inhibited symbiont photosynthetic activity (ORTIZ; MIX; COLLIER, 1995), preventing both species to develop. Eventually, the dietary preference for zooplanktonic copepods and ciliates of both *O. universa* and *G. conglobatus* carnivorous specialists (HEMLEBEN; SPINDLER; ANDERSON, 1989; KEMLE-VON MÜCKE; HEMLEBEN, 1999; KUCERA, 2007) might have favoured their growth at times of upwelling and relatively higher productivity. However, those species are rather adapted to oligotrophic conditions and experience lower standing stocks under light limitation (ORTIZ; MIX; COLLIER, 1995). They are therefore outnumbered by herbivorous species, such as *N. dutertrei*, *G. inflata*, and *G. trucatulinoides*, under upwelling regimes and phytoplankton blooms (HEMLEBEN; SPINDLER; ANDERSON, 1989; ORTIZ; MIX; COLLIER, 1995; SCHMIDT *et al*., 2006). The rising temperatures reaching optimal levels (~22^{o}C) for both warm-water species *O. universa* and *G. conglobatus* (BÉ, DUPLESSY, 1976; SCHMIDT *et al*., 2006; KUCERA, 2007) might also have allowed them to thrive. Yet, reduced symbiotic photosynthesis would not have enabled those species to flourish under such transient conditions at the onset of the Holocene.

Unlike those obligatory symbiont-bearing species, *P. obliquiloculata* and *G. menardii* harbour symbionts on a non-permanent basis, and thus are typically facultative symbiont-bearing species (HEMLEBEN; SPINDLER; ANDERSON, 1989; SCHIEBEL; HEMLEBEN, 2005; KUCERA, 2007). Also, both *P. obliquiloculata* and *G. menardii* are mainly herbivorous, preying mostly on phytoplankton (chrysophytes and diatoms) (HEMLEBEN; SPINDLER; ANDERSON, 1989; XU *et al*., 2005; LIN *et al.*, 2006). Distinct nutrition strategies would possibly have enabled these non-obligatory symbiont species to develop under relative upwelling. Yet, marked increase in abundance is only recorded by *P. obliquiloculata* with the Holocene inception (Figs. 20a; d; 27g; i).

Earlier reappearances and later disappearances of *P. obliquiloculata* during glacial-interglacial transitions, as compared to *G. menardii*, seem to be a rather pervasive feature in the Atlantic Ocean (PRELL; DAMUTH, 1978; FLOWER; KENNETT, 1990; XU *et al*., 2005). In fact, records from both the tropical (BROECKER; PENA, 2014)

and the subtropical (PIVEL *et al*., 2013) South Atlantic indicate a late occurrence of *G. menardii* after the onset of the Holocene. So far, the causes for the delayed reappearance of *G. menardii* in the Atlantic still remain unclear (CALEY *et al*., 2012; PIVEL *et al*., 2013; BROECKER; PENA, 2014).

Past changes in the distribution of both species most likely reflect a broader adaptive tolerance of *P. obliquiloculata* to environmental changes, as it is indicated by the distinct distribution patterns of both species in the modern ocean (PRELL; DAMUTH, 1978; CULLEN; PRELL, 1984; FLOWER; KENNETT, 1990; XU *et al*., 2005). The species *P. obliquiloculata* is able to sustain wider temperature ranges, while *G. menardii* usually requires much warmer conditions to thrive (LE; MIX; SHACKLETON, 1995; XU *et al*., 2005; SCHMIDT *et al*., 2006; KUCERA, 2007). Also, as a stenohaline species, *G. menardii* is less tolerant to high salinity levels (CULLEN; PRELL, 1984; XU *et al*., 2005) and is usually associated with rather stable thermocline and well stratified upper water column (FAIRBANKS; WIEBE 1980; FAIRBANKS *et al*., 1982; HEMLEBEN; SPINDLER; ANDERSON, 1989).

Contrasting tolerance limits between the thermocline-dwelling *G. menardii* and *P. obliquiloculata* (XU *et al*., 2005; FARMER *et al*., 2007; ZHANG *et al*., 2018) depicted in the abundances of those species at the onset of the Holocene are consistent with the *G. truncatulinoides* $\delta^{18}O$ signature, which also mirrors the thermocline conditions (MULITZA *et al*., 1997; CLÉROUX *et al*., 2009). Over that period, anomalously high *G. truncatulinoides* $\delta^{18}O$ values (~1.8‰) characteristic of glacial climate were recorded in the study site (Fig. 26d).

The *G. truncatulinoides* isotopic configuration at the rise of the Holocene would possibly imply much lower temperatures remaining at thermocline level. This condition would have lasted until the AMOC fully recovered its strength (Fig. 27c). Much colder thermocline over this period is also suggested by the highest relative abundance of the deep-dwelling species *G. inflata* (CHIESSI *et al*. 2007) recorded in the study site (Fig. 26g). Noteworthy, high *G. inflata* $\delta^{18}O$ values (~1.8‰) were also reported in the vicinities of the study area (24°S) at the onset of the Last Interglacial (~130 kyr)

(SANTOS *et al*., 2017b). Such glacial-like pattern in the thermocline despite the advent of interglacial background conditions would seemly be imposed by increased northward export of heat, favouring the AMOC overshoot (KNORR; LOHMANN, 2003; BEAL *et al*., 2011; SANTOS *et al*., 2017b).

Also, higher $\delta^{18}O$ values could entail a rather saltier thermocline resulting from a massive contribution of salty (sub) surface waters from the Indian Ocean under reinvigorated Agulhas leakage (SCUSSOLINI *et al*., 2015; SANTOS *et al*., 2017b). Indeed, a sharp increase in salinity is depicted in the core site at the Holocene inception (Fig. 24c). The prevalence of a salty thermocline in the core site would also be signalled by the enhanced abundance of *P. obliquiloculata* (Fig. 27i), which is considered a reliable tracer of high-salinity waters (WANG; ZHANG; MIN, 1985; LI; JIAN; WANG, 1997; UJIIÉ; UJIIÉ, 1999; JIAN *et al*., 2000; XU *et al.*, 2005).

Either way, much colder and/or saltier thermocline would likely have prevented *G. menardii* to thrive under such unfavourable conditions. In spite of reinvigorated Indian-Atlantic interoceanic exchange (PEETERS *et al*., 2004; CALEY *et al*., 2012), those environmental settings supposedly would have halted the early reseeding of *G. menardii* in this portion of the western South Atlantic.

Instead, cooler nutrient-rich waters would have favoured deep-dwelling herbivorous species, such as *G. inflata*, *G. truncatulinoides*, and *N. dutertrei* (Fig. 26f-h) (CHIESSI *et al*., 2007; FARMER *et al*., 2007; CLÉROUX *et al*., 2009), which show highest abundances under productive environments (HEMLEBEN; SPINDLER; ANDERSON, 1989; ORTIZ; MIX; COLLIER, 1995; MALLO *et al*., 2017; SCHIEBEL; HEMLEBEN, 2017). Overall maximum abundances of those species between ~11 and 9 cal kyr BP have also been recorded in the vicinities and to the north of the study area (TOLEDO; COSTA; PIVEL, 2007; PIVEL *et al*., 2013). Relatively increased productivity might also have further enabled an earlier reappearance of the herbivorous subsurface-dwelling species *P. obliquiloculata* (Fig. 27i) (HEMLEBEN; SPINDLER; ANDERSON, 1989; XU *et al*., 2005; LIN *et al.*, 2006).

At ~9.4 cal kyr BP, that glacial-like configuration in the thermocline was abruptly interrupted, as signalled by a sharp decrease in the *G. truncatulinoides* $\delta^{18}O$ values (Fig. 26d). That shift was followed by a steep decline in abundance of *G. truncatulinoides* (Fig. 26h). Interestingly, an outstanding drop in *G. truncatulinoides* $\delta^{18}O$ values at ~9.4 kyr was also found in distinct locations of the North Atlantic (CLÉROUX *et al*., 2009). As suggested by CLÉROUX *et al*. (2009), that common signal would possibly embody an upward migration of *G. truncatulinoides* to a remarkably shallower water depth in response to the enhanced sediment input stemming from deglacial ice melting. It has been argued that such condition might have limited light levels, thereby confining chlorophyll maximum concentration to shallower depths and constraining that species to live in a remarkably shallow habitat (CLÉROUX *et al*., 2009).

It is likely that such environmental setting would not only have affected the asymbiont species *G. truncatulinoides* (BÉ; TOLDERLUND, 1971; FAIRBANKS; WIEBE, 1980; HEMLEBEN; SPINDLER; ANDERSON, 1989), but might have also impacted other deep-dwelling herbivorous species, such as *N. dutertrei*, *G. inflata* (Fig. 26f-h), and even *P. obliquiloculata* and *G. menardii* (Fig. 27g; i), which are commonly associated with the chlorophyll maximum depth (FAIRBANKS; WIEBE 1980; RAVELO; FAIRBANKS, 1992; SCHIEBEL; HEMLEBEN, 2017).

In the study site, a stepwise increase in the sedimentation rates (from 2.7 to 7.5 cm/kyr) is indeed recorded within this time period (Fig. 16) and it is also consistent with enhanced continental runoff (Fig. 27d). Those changes are also in line with relatively increased upwelling producing deep mixing and weakest upper ocean stratification (Fig. 27e), fostering productivity and chlorophyll maximum at shallower levels. Such conditions would be followed, however, by a transient period toward full interglacial settings.

The *G. truncatulinoides* isotopic configuration (Fig. 26d) would thus likely embed an outstanding temperature rise at subsurface level, subsequently halting the development of *G. inflata*, *N. dutertrei*, and *G. truncatulinoides* (Fig. 26f-h), which usually inhabit cooler, deeper water depths (CHIESSI *et al*. 2007; FARMER *et al*. 2007; CLÉROUX *et*

al., 2009). Enhanced warming in the thermocline would favour instead the development of warm water species, such as *G. menardii*, *O. universa* and *G. conglobatus* after this time period (Fig. 27f-h). Yet, only when such unstable conditions finally settle and both warm (Fig. 27b) and well stratified upper water column (Fig. 27e) may prevail, would a faunal turnover take place signalling a transition toward interglacial-like conditions.

Paleonutrient records from the same location (27°S) also indicate that oceanographic conditions were not stable along the inception of the Holocene, and that the interglacial mode of the Atlantic overturning circulation (AMOC 'warm mode') would not be fully established by then (CAME; OPPO; CURRY, 2003). Background climatic conditions modulating the waxing and waning of continental ice sheets over the glacial-interglacial transition (GROOTES *et al*., 2003) would still have affected full AMOC recovery at the beginning of the Holocene. Maximal summer insolation in the northern latitudes was reached at ~11 cal kyr BP; yet, remnants of large glaciers still persisted in North America until ~9 cal kyr BP (WANNER *et al*., 2008). Thus, while the Agulhas leakage in the southern latitudes would have acted to strengthen the AMOC, northern latitudes ice melting in response to a warming trend would operate in the opposite way, causing the AMOC reduction (BEAL *et al*., 2011). As paleonutrient records suggest, deep-water geometry in the Atlantic would only have achieved an interglacial configuration at ~9 cal kyr BP, after summer insolation at high northern latitudes had reached its maximum (WANNER *et al*., 2008) and Holocene warmth in North Atlantic was completely set (CAME; OPPO; CURRY, 2003).

As also inferred by the changes recorded in study site, only after ~9 cal kyr BP full interglacial conditions would be finally reached. Along with the full AMOC recovery (Fig. 27c), markedly weakened BC meandering flow would have hampered SACW upwelling and the influx of BCC coastal waters toward the core site, as depicted in a sharp decline of eutrophic dinocysts (Fig. 27d) (GU *et al*., 2017). Those changes would result in strong upper ocean stratification (Fig. 27e) and a steep temperature rise (Fig. 27b). Although enhanced temperatures would have been formerly recorded at the onset of the Holocene, steady warming would only have been established by then. Together with the establishment of more stable conditions, both the obligatory (*O. universa*,

G. conglobatus) and facultative (*G. menardii*, *P. obliquiloculata*) symbiont-bearing species start to thrive (Fig. 27f-i). Conversely, oligotrophic conditions concurrently with warmer and well stratified upper water column would lead to a sharp drop in the relative abundances of *N. dutertrei*, *G. inflata*, and *G. trucatulinoides* (Fig. 26f-h).

Reduced mixing and the development of a strong thermocline would diminish water turbidity and enhance ambient light levels, favouring symbiont photosynthetic activity and enabling both the symbiont-bearing species *G. conglobatus* (Fig. 27h) and *O. universa* (Fig. 27f) to flourish (ORTIZ; MIX; COLLIER, 1995). Also, reduced upwelling and a well-developed thermocline would further favour the development of the subsurface dwelling *P. obliquiloculata* and *G. menardii* (Fig. 27i; g), which proliferate when chlorophyll maximum concentration coincides with the thermocline depth (FAIRBANKS; WIEBE 1980; RAVELO; FAIRBANKS, 1992; SCHIEBEL; HEMLEBEN, 2017). Together with the increased availability of food, conspicuous warming of subsurface waters resulting from the reduced upwelling and influx of cooler coastal waters would have propitiated optimum conditions for those tropical species to develop (BÉ, 1977; HEMLEBEN; SPINDLER; ANDERSON, 1989; WATKINS; MIX; WILSON, 1996; SCHMIDT, *et al*., 2006; SCHIEBEL; HEMLEBEN, 2017).

The chlorophyll maximum concentration coinciding with the thermocline depth might also have fostered the growth of herbivorous subsurface-dwelling *N. dutertrei*, *G. inflata* and especially the asymbiont species *G. trucatulinoides* (BÉ, 1977; HEMLEBEN; SPINDLER; ANDERSON, 1989; LIN *et al*., 2006). However, increased stratification would halt the development of *G. trucatulinoides* (Fig. 26h), as it would hamper penetration of juveniles into the photic zone, reducing their abundance (MULITZA *et al*. 1997; CLÉROUX *et al*. 2009). Under reduced mixing, the facultative symbiont-bearing species *N. dutertrei* and *G. inflata* may also have benefited from symbiotic photosynthesis (HEMLEBEN; SPINDLER; ANDERSON, 1989; SCHIEBEL; HEMLEBEN, 2005; KUCERA, 2007). But progressively higher temperatures would likely have further contributed for the lowering abundances of both species (Fig. 26f; g) (YAMASAKI; ODA, 2003; LIN *et al*., 2006; CHIESSI *et al*., 2007; SCHMIDT *et al*., 2006). As *P. obliquiloculata* and *G. menardii*, all those

herbivorous species mainly feed on algal prey (BÉ, 1977; HEMLEBEN; SPINDLER; ANDERSON, 1989; LIN *et al.*, 2006). Yet, under more favourable conditions for *P. obliquiloculata* and *G. menardii*, both would likely outcompete *G. trucatulinoides*, *N. dutertrei*, and *G. inflata* (UJIIÉ *et al*., 2003; LIN *et al.*, 2006), thereby enjoying higher food supply and being more adapted to thrive along the early Holocene.

Abrupt changes in the oceanographic conditions leading to a faunal turnover after the onset of the Holocene were also recorded nearby of the study area (25^{o}S) (PIVEL *et al*., 2013). Those records not only indicate a late reappearance of *G. menardii*, but also a marked decrease in abundances of *G. trucatulinoides*, *N. dutertrei*, and *G. inflata*. Similarly to the findings of the present study, the delayed establishment of full interglacial conditions depicted both in the faunal (PIVEL *et al*., 2013) and in the isotopic (SANTOS *et al*., 2017b) composition of planktonic foraminifera seem to be closely related to the full reactivation of the AMOC interglacial (i.e., 'warm') mode.

6.3.2 Mid Holocene

Along the Mid Holocene, however, shifts in the oceanic conditions at ~5 cal kyr BP seem to interrupt a progressive trend of temperature increase (Fig. 27b) and strongly stratified water column (Fig. 27e). Those changes are accompanied by a sudden decline in the abundances of species typical for warm and well stratified waters (Fig. 27f-i), and by a sharp reduction in the AMOC strength (Fig. 27c).

Unlike the onset of the Holocene, most conspicuous changes would have occurred at the surface level, in comparison to subsurface depths, as depicted in the *G. ruber* (Fig. 26c) and *G. truncatulinoides* $\delta^{18}O$ records (Fig. 26d). A marked increase in *G. ruber* $\delta^{18}O$ values would likely signal an interval of relative cooling provisionally halting an increased warming trend, as it is suggested by the MAT estimates (Fig. 27b). Those changes in the isotopic configuration would possibly mirror the cooling of the surface layer resulting from the enhanced PPW northward intrusion during the Mid Holocene. Such condition is inferred from distinct core records located off CSM and extending further north (22-27^{o}S) (GYLLENCREUTZ *et al*., 2010), as well as farther south

(~32°S) (RAZIK *et al*., 2013) to the study site. An increased seaward influx of PPW coastal waters entrapped by the BC meandering flow and reaching the study area is also indicated by the higher percentages of eutrophic dinocysts recorded over this time period (Fig. 27d).

During the Mid Holocene, northward incursions of PPW (GYLLENCREUTZ *et al*., 2010; RAZIK *et al*., 2013) would have been propelled by invigorating and more frequent southwesterly winds resulting from the strengthening and northward shift of the westerly wind belt (JENNY; WILHELM, VALERO-GARCÉS, 2003; LAMY *et al*., 2010). A northward PPW displacement would have also been favoured by a widened continental shelf stemming from sea level rise (Fig. 24i) (WAELBROECK *et al*., 2002; ANGULO; LESSA; SOUZA, 2006). Enhanced fluvial discharge would have been further induced by an intensification of the SASM (Fig. 25b) driven by increasingly higher precession-driven austral summer (30°S) insolation (Figs. 25a; 27a) (CRUZ *et al*., 2005; WANG *et al*., 2006). A northward shift of both the southern westerly winds and the STF would cause a contraction of the subtropical gyre, reducing the Agulhas leakage and, as a consequence, the AMOC strength (Fig. 27c) (SIJP; ENGLAND, 2008; BIASTOCH *et al*., 2009; BEAL *et al*., 2011).

Those shifts in the oceanic and atmospheric conditions would have strongly affected the Agulhas fauna distribution during the Mid Holocene (Fig. 27f-i). Both the increased cooling and mixing in the upper layer, disrupting a stable and well stratified water column would likely have impacted those warm-water species. Changes in the environmental conditions during the Mid Holocene, however, seem to have especially affected *P. obliquiloculata* (Fig. 27i). The abundance and distribution of this species is known to be largely controlled by seawater salinity, as *P. obliquiloculata* usually proliferate in highly saline waters (PRELL; DAMUTH, 1978; WANG; ZHANG; MIN, 1985; LI; JIAN; WANG, 1997; UJIIÉ; UJIIÉ, 1999; JIAN *et al*., 2000; XU *et al*., 2005). The salinity decrease fostered by the freshwater input from glaciers melting (WELDEAB; SCHNEIDER; KÖLLING, 2006; TOLEDO; COSTA; PIVEL, 2007), and by the enhanced seaward inflow of fresh PPW waters (GYLLENCREUTZ *et al*., 2010;

RAZIK *et al*., 2013) might have severely curbed the development of *P. obliquiloculata*, preventing the species to thrive along this time period.

6.3.3 Late Holocene

During the Late Holocene, changes in the orbital parameters resulted in a progressive decline of summer insolation in the northern hemisphere after 5 cal kyr BP. Cooling in the northern latitudes due to orbital forcing and highest austral summer insolation, in turn, would lead to the strengthening of northerly trade winds and to a southward displacement of the ITCZ (WANNER, *et al.,* 2008), intensifying the SASM (Fig. 25b) (CRUZ *et al*., 2005; WANG *et al*., 2006). Orbital forcing would also induce the increased activity of El Niño-Southern Oscillation (ENSO) (MOY *et al*., 2002; REIN *et al.*, 2005). Along with the enhanced amplitude and frequency of ENSO events, increasingly higher precession-driven austral summer insolation (Fig. 27a) would further foster precipitation.

The large-scale changes in the atmospheric circulation over the Late Holocene would have inhibited PPW northward incursions (GYLLENCREUTZ *et al*., 2010; RAZIK *et al*., 2013), in spite of the enhanced precipitation (PIOLA *et al*., 2005; MÖLLER *et al*., 2008). Besides, the sudden AMOC recovery along this period (Fig. 27c) likely coupled with a weakened BC might also have possibly hampered the seaward export of riverine runoff (Fig. 27d), despite the development of ENSO activity (MOY *et al*., 2002) and intensified SASM (CRUZ *et al*., 2005). Such conditions would have further restrained terrigenous sediment input to the core site, as mirrored by a slight drop (from 7.5 to 6.5 cm/kyr) of the sedimentation rate after the Mid Holocene (Fig. 16). A reduced presence of cooler waters at surface levels is also suggested by marked negative excursions in the *G. ruber* $\delta^{18}O$ records after ~3 cal kyr BP (Fig. 26c). Conversely, reduced upwelling and ensuing cooling at thermocline levels, as well as the influx of more saline subsurface waters modulated by the Agulhas leakage, possibly may have accounted for the enhanced *G truncatulinoides* $\delta^{18}O$ values (Fig. 26d) over this period.

Thereafter, increasingly higher precession-driven austral summer insolation (Fig. 27a) would then result in rising temperatures (Fig. 27b). Together with the resumption of the AMOC, a reduced BC would further curb upwelling, favouring strong stratification in the upper water column (Fig. 27e). Altogether, such favourable setting would have provided best conditions for the development of symbiont-bearing species (Fig. 27f-i), typical for warmer, oligotrophic waters of modern western South Atlantic. The diminished influence of freshwater discharge from both riverine runoff (Fig. 27d) and glaciers meltwater would further have favoured the growth of *P. obliquiloculata*.

Chapter 7

Conclusions

The reconstruction of past changes in the upper subtropical western South Atlantic over the last 40 kyr reveals, for the first time, increases in primary production during HS. Peaks in the abundance of eutrophic planktonic foraminiferal species are accompanied by weakened upper ocean stratification during some HS. Conversely, a productivity decline along the LGM, the YD, and most remarkably after the Holocene inception is indicated by the marked drop of eutrophic planktonic foraminiferal abundance. All those time periods of productivity decreases are coeval with enhanced upper ocean stratification. The paleoproductivity evolution under distinct glacial and interglacial boundary conditions suggests that primary productivity is modulated by the dynamics of the BC, which dictates the pace of a mesoscale upwelling system. The results also suggest that productivity changes governed by the BC are coupled to disturbances in the AMOC. During events of weakened AMOC, a strengthened BC meandering flow would boost the development and amplitude of cyclonic vortices, promoting upwelling. Additionally, invigorated BC meandering vortices over periods of AMOC slowdown would also foster the seaward entrapment of BCC nutrient-rich coastal waters, further enhancing primary production. The findings of this study therefore corroborate the notion of a tight coupling between marine productivity changes and AMOC disturbances, which would have led to the termination of the last glacial cycle.

The reconstruction of past oceanographic changes further suggests that rather overall glacial-like conditions would have prevailed at the onset of the Holocene, before complete reinvigoration of the AMOC. Along this time period, a remnant upwelling regime sustained by a relatively strengthened BC would have produced surface mixing, lower temperatures and weak stratification likely preventing the Agulhas fauna to thrive. Also, a glacial-like configuration in the thermocline, possibly mirroring an enhanced northward export of heat bolstering AMOC overshoot, would probably have accounted for the late reappearance of *G. menardii*. Full interglacial settings would have only established after ~9 kyr, when warmth and background climatic conditions in

the high northern latitudes completely settled and the AMOC fully recovered. Along with a full AMOC recovery, correlated weakened BC and reduced upwelling would have propitiated the development of a strong thermocline allowing Agulhas fauna to flourish. During the course of the Mid Holocene, however, full interglacial conditions were abruptly interrupted, accompanying a sudden reduction of the AMOC. Those abrupt changes might have marked an interval of relatively reinvigorated BC favouring the seaward inflow of enhanced northward PPW intrusions and also resulting in a conspicuous Agulhas fauna decline, before the Late Holocene and modern interglacial conditions finally set. Overall, the findings of the present study suggest that the impact of the AMOC on the subtropical western South Atlantic would have played a critical role not only over boundary conditions of the last glacial, but also throughout the glacial-interglacial transition and even under full background interglacial conditions.

Acknowledgements

This work has been accomplished with the joint institutional and scientific support from the Oceanographic Institute and the School of Arts and Humanities of the University of São Paulo, Brazil, in collaboration with the MARUM - Center for Marine Environmental Sciences of the University of Bremen, Germany. This study was financed in part by the *Coordenação de Aperfeiçoamento de Pessoal de Nível Superior - Brasil* (CAPES) - Finance Code 001.

I acknowledge the support from the coordinator of the post-graduation program of the Oceanographic Institute (IOUSP), my supervisor, and from all professors, reviewers, technicians, assistants and colleagues that greatly contributed to the accomplishment of this task. In a special way, I warmly thank my family and friends who immensely helped me to overcome the hardest moments throughout this challenging endeavour.

References

ALLEY, R. B. ***Ice-core evidence of abrupt climate changes***. Proceedings of the National Academy of Sciences – PNAS, v. 97, p. 1331–1334, 2000.

ANDERSON, R. F. *et al.* ***Wind-driven upwelling in the Southern Ocean and the deglacial rise in atmospheric CO_2***. Science, v. 323, p. 1443-1448, 2009.

ANGULO, R. J.; LESSA, G. C.; SOUZA, M. C. ***A critical review of mid- to late-Holocene sea-level fluctuations on the eastern Brazilian coastline***. Quaternary Science Reviews, v. 25, p. 486-506, 2006.

ANTONOV, J. I. *et al*. ***World Ocean Atlas 2010: Salinity***. In: S., Levitus, (Ed.), NOAA Atlas NESDIS 69, v. 2, p. 184. Washington, DC: US Government Printing Office, 2010.

ARCHER, D. *et al*. ***The importance of ocean temperature to global biogeochemistry***. Earth and Planetary Science Letter, v. 222, p. 333-348, 2004.

ARZ, H. W. *et al*. ***Millennial-scale changes of surface- and deep-water flow in the western tropical Atlantic linked to Northern Hemisphere high-latitude climate during the Holocene***. Geology, v. 29, p. 239-242, 2001.

ASP, N. E. *et al.* ***Geology and hypsometry of river basins at central-northern Santa Catarina (Brazil): Implications for the coastal zone***. Quaternary and Environmental Geosciences, v. 01, p. 98-108, 2009.

BARD, E. *et al.* ***Hydrological impact of Heinrich events in the subtropical northeast Atlantic***. Science, v. 289, p. 1321-1324, 2000.

BARD, E.; RICKABY, R. E. M. ***Migration of the subtropical front as a modulator of glacial climate***. Nature, v. 460, p. 380-393, 2009.

BARKER, S. *et al*. ***Interhemispheric Atlantic seesaw response during the last deglaciation***. Nature, v. 457, p. 1097-1103, 2009.

BÉ, A. W. H. **An ecological, zoogeographic and taxonomic review of recent planktonic foraminifera**. In: A. T. S. Ramsay (Ed.), Oceanic Micropaleontology, p. 100. London, UK: Academic Press, 1977.

BÉ, A. W. H.; DUPLESSY, J. C. ***Subtropical convergence fluctuations and Quaternary climates in the middle latitudes of the Indian Ocean***. Science, v. 194, p. 419-422, 1976.

BÉ, A. W. H.; TOLDERLUND, D. S. ***Distribution and ecology of living planktonic foraminifera in surface waters of the Atlantic and Indian oceans***. In: B. M. Funnell; W. R. Riedel (Eds.), Micropaleontology of Oceans, p. 105-149. London, UK: Cambridge University Press, 1971.

BEAL, L. M. *et al.* ***On the role of the Agulhas system in ocean circulation and climate***. Nature, v. 472, p. 429-436, 2011.

BERGER, A. ***Orbital variations and insolation***. Database IGBP PAGES/World Data Center for Paleoclimatology. Data Contribution Series # 92-007. NOAA/NGDC Paleoclimatology Program, USA, 1992.

BERGER, A.; LOUTRE, M. F. ***Insolation values for the climate of the last 10 million years***. Quaternary Science Reviews, v. 10, p. 297-317, 1991.

BERGER, W. H.; WEFER, G. ***Klimageschichte aus Tiefseesedimenten – Neues vom Ontong-Java- Plateau (Westpazifik)***. Naturwissenschaften, v. 79, p. 541-550, 1992.

BERNARDELLO, R. *et al*. ***Response of the ocean natural carbon storage to projected twenty-first-century climate change***. Journal of Climate, v. 27, p. 2033-2053, 2014.

BIASTOCH, A. *et al*. ***Increase in Agulhas leakage due to pole-ward shift of the Southern Hemisphere westerlies***. Nature, v. 462, p. 495-498, 2009.

BILÓ, T. C. *et al.* ***Methods for estimating the velocities of the Brazil Current in the pre-salt reservoir area off southeast Brazil (23^{o}S-26^{o}S)***. Ocean Dynamics, v. 64, p. 1431-1446, 2014.

BLEII U. *et al*. ***Report and preliminary results of METEOR Cruise 23/2, Rio de Janeiro-Recife, 27.02.-19.03.1993***. In: Berichte aus dem Fachbereich Geowissenschaften, Technical Report, v. 43, p. 133. Bremen, Germany: Universität Bremen, 1994.

BLUNIER, T.; BROOK, E. J. ***Timing of millennial-scale climate change in Antarctica and Greenland during the last glacial period***. Science, v. 291, p. 109-112, 2001.

BÖHM, E. *et al*. ***Strong and deep Atlantic meridional overturning circulation during the last glacial cycle***. Nature, v. 517, p. 73-76, 2015.

BRAGA, E. S. *et al*. ***Nutrients distribution over the southeastern South Atlantic continental shelf from Mar del Plata (Argentina) to Itajaí (Brazil): Winter–summer aspects***. Continental Shelf Research, v. 28, p. 1649-1661, 2008.

BRANDINI, F. P. *et al*. ***Deep chlorophyll maximum and plankton community response to oceanic bottom intrusions on the continental shelf in the South Brazilian Bight***. Continental Shelf Research, v. 89, p. 61-75, 2014.

BROECKER, W. S. ***Paleocean circulation during the last deglaciation: A bipolar seesaw?*** Paleoceanography, v. 13, p. 119-121, 1998.

BROECKER, W. S. *et al*. ***Putting the Younger Dryas cold event into context***. Quaternary Science Reviews, v. 29, p. 1078-1081, 2010.

BROECKER, W. S.; PENA, L. D. ***Delayed Holocene reappearance of G. menardii***. Paleoceanography, v. 29, p. 291-295, 2014.

BROVKIN, V. *et al*. ***Lowering of glacial atmospheric CO_2 in response to changes in oceanic circulation and marine biogeochemistry***. Paleoceanography, v. 22, p. 1-14, 2007.

CAI, W. ***Antarctic ozone depletion causes an intensification of the Southern Ocean super-gyre circulation***. Geophysical Research Letters, v. 33, L03712, 2006.

CALADO, L. *et al*. ***Eddy-induced upwelling of Cape São Tomé (22°S, Brazil)***. Continental Shelf Research, v. 30, p. 1181-1188, 2010.

CALEY, T. *et al.* ***Agulhas leakage as a key process in the modes of Quaternary climate changes***. PNAS – Proceedings of the National Academy of Sciences, v. 109, p. 6835-6839, 2012.

CAME, R. E.; OPPO, D. W.; CURRY, W. B. ***Atlantic Ocean circulation during the Younger Dryas: Insights from a new Cd/Ca record from the western subtropical South Atlantic***. Paleoceanography, v. 18, p. 1086, 2003.

CAMPOS, E. J. D.; GONÇALVES, J. E.; IKEDA, Y. ***Water mass characteristics and geostrophic circulation in the South Brazil Bight: Summer of 1991***. Journal of Geophysical Research, v. 100, p. 537-550, 1995.

CAMPOS, E. J. D.; VELHOTE, D.; SILVEIRA, I. C. A. ***Shelf break upwelling driven by Brazil Current cyclonic meanders***. Geophysical Research Letters, v. 27, p. 751-754, 2000.

CAMPOS, M. C. *et al.* ***$\delta^{13}C$ decreases in the upper western South Atlantic during Heinrich Stadials 3 and 2***. Climate of the Past, v. 13, p. 345-358,2017.

CAMPOS, P. C. *et al*. ***Seasonal variability and coastal upwelling near Cape Santa Marta (Brazil)***. Journal of Geophysical Research, v. 118, p. 1420-1433, 2013.

CARLSON A. E. ***The Younger Dryas Climate Event***. In: S. A. Elias (Ed.), The Encyclopedia of Quaternary Science, v. 3, p. 126-134. Amsterdam, Netherlands: Elsevier, 2013.

CARLSON, A. E. ***Why there was not a Younger Dryas-like event during the penultimate deglaciation?*** Quaternary Science Reviews, v. 27, p. 882-887, 2008a.

CARLSON, A. E. *et al*. S***ubtropical Atlantic salinity variability and Atlantic meridional circulation during the last deglaciation***. Geology, v. 36, p. 991-994, 2008b.

CARLSON, A. E.; WINSOR, K. ***Northern Hemisphere ice-sheet responses to past climate warming***. Nature Geoscience, v. 5, p. 607-613, 2012.

CARVALHO, L. M. V.; JONES, C.; LIEBMANN, B. ***The South Atlantic Convergence Zone: intensity, form, persistence and relationships with intraseasonal to interannual activity and extreme rainfall***. Journal of Climate, v. 17, p. 88-109, 2004.

CASTELÃO, R. M.; BARTH, J. A. ***Upwelling around Cabo Frio, Brazil: The importance of wind stress curl***. Geophysical Research Letters, v. 33, L03602, 2006.

CASTELÃO, R. M.; CAMPOS, E. J. D.; MILLER, J. L. ***A modelling study of coastal upwelling driven by wind and meanders of the Brazil Current***. Journal of Coastal Research, v. 20, p. 662-671, 2004.

CHAPMAN, M. R.; SHACKLETON, N. J. ***Global ice-volume fluctuations, North Atlantic ice-rafting events, and deep-ocean circulation changes between 130 and 70 ka***. Geology, v. 27, p. 795-798, 1999.

CHIESSI, *et al*. ***Signature of the Brazil-Malvinas Confluence (Argentine Basin) in the isotopic composition of planktonic foraminifera from surface sediments***. Marine Micropaleontology, v. 64, p. 52-66, 2007.

CHIESSI, C. M. *et al*. ***South Atlantic interocean exchange as the trigger for the Bolling warm event***. Geology, v. 36, p. 919-922, 2008.

CHIESSI, C. M. *et al.* ***Thermal evolution of the western South Atlantic and the adjacent continent during Termination 1***. Climate of the Past, v. 11, p. 915-929, 2015.

CIRANO, M. *et al.* ***A circulação oceânica de larga-escala na região oeste do Atlântico Sul com base no modelo de circulação global OCCAM***. Revista Brasileira de Geofísica, v. 24, p. 209-230, 2006.

CLARK, P. U. *et al*. ***The Last Glacial Maximum***. Science, v. 325, p. 710-714, 2009.

CLAUZET, G. *et al.* ***A numerical study of the South Atlantic circulation at the Last Glacial Maximum***. Palaeogeography, Palaeoclimatology, Palaeoecology, v. 253, p. 509-528, 2007.

CLÉROUX, C. *et al*. ***Evidence for calcification depth change of Globorotalia truncatulinoides between deglaciation and Holocene in the western Atlantic Ocean***. Marine Micropaleontology, v. 73, p. 57-61, 2009.

CONKRIGHT, M. E. *et al*. ***World Ocean Atlas 2001: objective analyses, data statistics, and figures***. National Oceanographic Data Center, Silver Spring, MD, 17, CD-ROM documentation, 2002.

CROWLEY, T. J. ***North Atlantic Deep Water cools the Southern Hemisphere***. Paleoceanography, v. 7, p. 489-497, 1992.

CRUZ JR., F. W. *et al*. ***Insolation-driven changes in atmospheric circulation over the past 116,000 years in subtropical Brazil***. Nature, v. 434, p. 63-66, 2005.

CULLEN, J. L.; PRELL, W. L. ***Planktonic foraminifera of the northern Indian Ocean: distribution and preservation in surface sediments***. Marine Micropaleontology. v. 9, p. 1-52, 1984.

DAHL, K. A.; BROCCOLI, A. J.; STOUFFER, R. J. ***Assessing the role of North Atlantic freshwater forcing in millennial scale climate variability: a tropical Atlantic perspective***. Climate Dynamics, v. 24, p. 325-346, 2005.

DANSGAARD, W. *et al*. ***North Atlantic climatic oscillations revealed by deep Greenland ice cores***. In: J. E. Hansen; T. Takahashi (Eds), Climate processes and climate sensitivity, v. 29 p. 288-298. Washington, D.C: American Geophysical Union, 1984.

DE VRIES, P.; WEBER, S. L. ***The Atlantic freshwater budget as a diagnostic for the existence of a stable shut down of the meridional overturning circulation***. Geophysical Research Letters, v. 32, L09606, 2005.

EPICA COMMUNITY MEMBERS. ***One-to-one coupling of glacial climate variability in Greenland and Antarctica***. Nature, v. 444, p. 195-198, 2006.

FAIRBANKS, R. G. *et al.* ***Vertical distribution and isotopic fractionation of living planktonic foraminifera from the Panama Basin***. Nature, v. 298, p. 841-844, 1982.

FAIRBANKS, R. G.; WIEBE, P. H. ***Foraminifera and chlorophyll maximum: Vertical distribution, seasonal succession, and paleoceanographic significance***. Science, v. 209, p. 1524-1526, 1980.

FARMER, E. C. *et al.* ***Corroborating ecological depth preferences of planktonic foraminifera in the tropical Atlantic with the stable oxygen isotope ratios of core top specimens***. Paleoceanography, v. 22, PA3205, 2007.

FERREIRA, F. *et al*. ***Zoneamento paleoclimático do Quaternário da Bacia de Santos com base em foraminíferos planctônicos.*** Revista Brasileira de Paleontologia, v. 15, p. 173-188, 2012.

FLORES, J-A.; GERSONDE, R.; SIERRO, F. J. ***Pleistocene fluctuations in the Agulhas Current Retroflection based on the calcareous plankton record***. Marine Micropaleontology. v. 37, p. 1-22, 1999.

FLOWER, B. P.; KENNETT, J. P. ***The Younger Dryas cool episode in the Gulf of Mexico***. Paleoceanography, v. 5, p. 949-961, 1990.

GAETA, S. A.; BRANDINI, F. P. ***Produção primária do fitoplâncton na região entre o Cabo de São Tomé (RJ) e o Chuí (RS)***. In: C.L.B. Rossi-Wongtschowski; L.S-P. Madureira (Eds.), O ambiente oceanográfico da plataforma continental e do talude na região Sudeste-Sul do Brasil, p. 219-264. São Paulo, Brazil: Edusp, 2006.

GAETA, S.A. *et al*. ***The Vitória Eddy and its relation to the phytoplankton biomass and primary productivity during the austral fall of 1995***. Archive of Fishery and Marine Research, v. 47, p. 253-270, 1999.

GANACHAUD, A.; WUNSCH, C. ***Large-scale ocean heat and freshwater transports during the world ocean circulation experiment***. Journal of Climate, v. 16, p. 696-705, 2003.

GARZOLI, S. L.; MATANO, R. ***The South Atlantic and the Atlantic meridional overturning circulation***. Deep-Sea Research II. Topical Studies in Oceanography, v. 58, p. 1837-1847, 2011.

GEBBIE, G. ***How much did Glacial North Atlantic Water shoal?*** Paleoceanography, v. 29, p. 190-209, 2014.

GIBBS, M. T.; MIDDLETON, J. H.; MARCHESIELLO, P. ***Baroclinic response of Sydney shelf waters to local and deep ocean forcing***. Journal of Physical Oceanography, v. 28, p. 178-190, 1998.

GIRAUDEAU, J. ***Planktonic foraminiferal assemblages in surface sediments from the southwest African continental margin***. Marine Geology, v. 110, p. 47-62, 1993.

GORDON, A. L. *et al*. ***Thermocline and intermediate water communication between the South Atlantic and Indian Oceans***. Journal of Geophysical Research, v. 97, p. 7223-7240, 1992.

GRIMM, A. M.; VERA, C. S.; MECHOSO, C. R. ***The South American monsoon system***. In: C. P. Chang; B. Wang; N.-C.G Lau (Eds.), The global monsoon system: research and forecast. Geneva, Switzerland: World Meteorological Organization, 2005.

GRUBER, N.; SARMIENTO, J. ***Large-scale biogeochemical-physical interactions in elemental cycles: Biological-physical interactions in the sea***. In: A. R. Robinson; J. J. McCarthy; B. J. Rothschild (Eds.), The Sea: Ideas and Observations on Progress in the Study of the Seas, v. 12, p. 337-399. New York, NY: Wiley and Sons, 2002.

GU, F. *et al*. ***Long-term vegetation, climate and ocean dynamics inferred from a 73,500 years old marine sediment core (GeoB2107-3) off southern Brazil***. Quaternary Science Reviews, v. 172, p. 55-71, 2017.

GYLLENCREUTZ, R. *et al.* ***Mid- to Late-Holocene paleoceanographic changes on the southeastern Brazilian shelf based on grain size records***. The Holocene, v. 20, p. 863-875, 2010.

HASTENRATH, S. ***Climate dynamics of tropics***. London, UK: Kluwer Academic Publishers, 1991.

HAYS, J. D.; IMBRIE, J.; SHACKLETON, N. J. ***Variations in the Earth's orbit: pacemaker of the Ice Ages***. Science, v. 194, p. 1121-1132, 1976.

HEIL, G. ***Abrupt climate shifts in the western tropical to subtropical Atlantic region during the last glacial***. Doctoral dissertation. Bremen, Germany: Universität Bremen, 2006.

HEINRICH, H. ***Origin and consequences of cyclic ice rafting in the northeast Atlantic Ocean during the past 130,000 years***. Quaternary Research, v. 29, p.142-152, 1988.

HEMLEBEN, C.; SPINDLER, M.; ANDERSON, O. R. ***Modern planktonic foraminifera***. New York, NY: Springer-Verlag, 1989.

HENDRY, K. R. *et al*. ***Abrupt changes in high-latitude nutrient supply to the Atlantic during the last glacial cycle***. Geology, v. 40, p. 123-126, 2012.

HERTZBERG, J. E. *et al*. ***Evidence for a biological pump driver of atmospheric CO_2 rise during Heinrich Stadial 1***. Geophysical Research Letters, v. 43, p. 12242-12251, 2016.

HOWE, J. N. W. *et al.* ***Antarctic intermediate water circulation in the South Atlantic over the past 25,000 years***. Paleoceanography, v. 31, p. 1302-1314, 2016a.

HOWE, J. N. W. *et al.* ***North Atlantic Deep Water production during the Last Glacial Maximum***. Nature Communications, v. 7, 11765, 2016b.

HUT, G. ***Consultants group meeting on stable isotope reference samples for geochemical and hydrological investigations***, p. 42. Vienna, Austria: International Atomic Energy Agency, 1997.

JAESCHKE, A. *et al*. ***Coupling of millennial-scale changes in sea surface temperature and precipitation off northeastern Brazil with high-latitude climate shifts during the last glacial period***. Paleoceanography, v. 22, PA4206, 2007.

JAMES, C.; WIMBUSH, M.; ICHIKAWA, H. ***Kuroshio meanders in the East China Sea***. Journal of Physical Oceanography, v. 29, p. 259-272, 1999.

JENNY, B.; WILHELM, D.; VALERO-GARCÉS, B. L. ***The southern Westerlies in Central Chile: Holocene precipitation estimates based on a water balance model for Laguna Aculeo (33°50' S)***. Climate Dynamics, v. 20, p. 269-280, 2003.

JIAN, Z. *et al*. ***Holocene variability of the Kuroshio Current in the Okinawa Trough, northwestern Pacific Ocean***. Earth and Planetary Science Letter, v. 184, p. 305-319, 2000.

JUGGINS, S. ***C2 Version 1.5 User guide. Software for ecological and palaeoecological data analysis and visualization***. Newcastle, UK: Newcastle University, 2007.

KEMLE-VON-MÜCKE, S.; HEMLEBEN, C. ***Planktic foraminifera.*** In: D. Boltovskoy (Ed.), South Atlantic zooplankton. Leiden, Netherlands: Backhuys Publishers, 1999.

KINDLER, P. *et al*. ***Temperature reconstruction from 10 to 120 kyr b2k from the NGRIP ice core***. Climate of the Past, v. 10, p. 887-902, 2014.

KNORR, G.; LOHMANN, G. ***Southern Ocean origin for the resumption of Atlantic thermohaline circulation during deglaciation***. Nature, v. 424, p. 532-536, 2003.

KOHFELD, K. E. *et al*. ***Southern Hemisphere westerly wind changes during the Last Glacial Maximum: Paleo-data synthesis***. Quaternary Science Review, v. 68, p. 76-95, 2013.

KOWSMANN, R. O.; COSTA, M. P. A. ***Sedimentação quaternária da margem continental brasileira e das áreas oceânicas adjacentes***. In: H. A. F. Chaves (Ed.), Geomorfologia da margem continental brasileira e das áreas oceânicas adjacentes. Série Projeto REMAC, v. 8, p. 51-55. Rio de Janeiro, RJ: CENPES/PETROBRÁS, 1979.

KROOPNICK, P. ***The distribution of ^{13}C of ΣCO_2 in the world oceans***. Deep Sea Research, Part A, v. 32, p. 57-84, 1985.

KUCERA, M. ***Planktonic foraminifera as tracers of past oceanic environments***. In: C. Hillaire-Marcel; A. de Vernal (Eds.), Developments in Marine Geology, v.1, p. 213-62. Amsterdam, Netherlands: Elsevier, 2007.

KUCERA, M. *et al.* ***Multiproxy approach for the reconstruction of the glacial ocean surface (MARGO)***. Quaternary Science Reviews, v. 24, p. 813-819,2005.

LAMY, F. *et al*. ***Holocene changes in the position and intensity of the southern westerly wind belt***. Nature Geoscience, v. 3, p. 695-699, 2010.

LANTZSCH, H. *et al*. ***The high-supply, current-dominated continental margin of southeastern South America during the late Quaternary***. Quaternary Research, v. 81, p. 339-354, 2014.

LE, J.; MIX, A. C.; SHACKLETON, N. J. ***Late Quaternary paleoceanography in the eastern equatorial Pacific Ocean from planktonic foraminifers: A high-resolution record from ODP Site 846***. In: N. G. Pisias *et al.* (Eds.), Proceedings of the Ocean Drilling Program, Scientific Results, v. 138, p. 675-694. College Station, TX: Ocean Drilling Program, 1995.

LESSA, D. V. O. *et al.* ***Offshore expansion of the Brazilian coastal upwelling zones during Marine Isotope Stage 5***. Global and Planetary Change, v. 158, p. 13-20, 2017.

LEVY, M. *et al*. ***Physical pathways for carbon transfers between the surface mixed layer and the ocean interior***. Global Biogeochemestry Cycles, v. 27, p. 1001-1012, 2013.

LI, B.; JIAN, Z.; WANG, P. ***Pulleniatina obliquiloculata as a paleoceanographic indicator in the southern Okinawa Trough during the last 20,000 years***. Marine Micropaleontology. v. 32, p. 59-69, 1997.

LIN, Y-S. *et al*. ***The Holocene Pulleniatina minimum event revisited: Geochemical and faunal evidence from the Okinawa Trough and the upper reaches of the Kuroshio Current***. Marine Micropaleontology. v. 59, p. 153-170, 2006.

LIPPOLD, J. *et al.* ***Does sedimentary $^{231}Pa/^{230}Th$ from the Bermuda Rise monitor past Atlantic meridional overturning circulation?*** Geophysical Research Letters, v. 36, L12601,2009.

LOCARNINI, R. A. *et al*. ***World Ocean Atlas 2013*: Temperature**. In: S. Levitus; A. Mishonov (Eds.), NOAA Atlas NESDIS 73, v. 1, p. 40. Washington, DC: US Government Printing Office, 2013.

LOURENÇO, R A. *et al*. ***Organic biomarker records spanning the last 34,800 years from the southeastern Brazilian upper slope: Links between sea surface temperature, displacement of the Brazil Current, and marine productivity***. Geo-Marine Letters, v. 36, p. 361-369, 2016.

LUMPKIN, R.; SPEER, K. ***Global ocean meridional overturning***. Journal of Physical Oceanography, v. 37, p. 2550-2562, 2007.

LYNCH-STIEGLITZ, J. ***The Atlantic meridional overturning circulation and abrupt climate change***. Annual Review of Marine Science, v. 9, p. 83-104, 2017.

MacAYEAL, D. R. ***Binge/purge oscillations of the Laurentide ice sheet as a cause of the North Atlantic's Heinrich events***. Paleoceanography, v. 8, p. 775-784, 1993.

MAHIQUES, M. M. *et al*. ***Hydrodynamically driven patterns of recent sedimentation in the shelf and upper slope off southeast Brazil***. Continental Shelf Research, v. 24, p.1685-1697, 2004.

MALLO, M. *et al.* ***Low planktic foraminiferal diversity and abundance observed in a spring 2013 west-east Mediterranean Sea plankton tow transect***. Biogeosciences, v. 14, p. 2245-2266, 2017.

MARINOV, I. *et al*. ***The Southern Ocean biogeochemical divide***. Nature, v. 441, p. 964-967, 2006.

MARIOTTI, V. *et al*. ***Marine productivity response to Heinrich events: A model-data comparison***. Climate of the Past, v. 8, p. 1581-1598, 2012.

MARTÍNEZ-MÉNDEZ, G. *et al.* ***Contrasting multiproxy reconstructions of surface ocean hydrography in the Agulhas Corridor and implications for the Agulhas leakage during the last 345,000 years***. Paleoceanography, v. 25, PA4227, 2010.

MASLIN M.; SEIDOV D.; LOWE J. J. ***Synthesis of the nature and causes of rapid climate transitions during the Quaternary***. In: D. Seidov; B. J. Haupt; M. Maslin (Eds.) The oceans and rapid climate change: Past, present and future, Geophysical Monograph Series, v. 126, p. 9-52. Washington, DC: American Geophysical Union, 2001.

MATANO, R. P. *et al*. ***The salinity signature of the cross-shelf exchanges in the Southwestern Atlantic Ocean: Numerical simulations***. Journal of Geophysical Research, v. 119, p. 7949-7968, 2014.

MATSUURA, Y. ***Contribuição ao estudo da estrutura oceanográfica da região sudeste entre Cabo Frio (RJ) e Cabo de Santa Marta Grande (SC)***. Ciência e Cultura, v. 38, p. 1439-1450, 1986.

McMANUS, J. F. *et al*. ***Collapse and rapid resumption of Atlantic meridional circulation linked to deglacial climate changes***. Nature, v. 428, p. 834-837, 2004.

MENVIEL, L. *et al.* ***Atlantic-Pacific seesaw and its role in outgassing CO_2 during Heinrich events. Paleoceanography***, v. 29, p. 58-70, 2014.

METCALFE, B. *et al*. ***Late Pleistocene glacial–interglacial shell-size–isotope variability in planktonic foraminifera as a function of local hydrography***. Biogeosciences, v. 12, p. 4781-4807, 2015.

MIRANDA, L. B. ***Análise de massas de água da plataforma continental e da região oceânica adjacente: Cabo de São Tomé (RJ) e Ilha de São Sebastião (SP)***. In: C. L. Rossi-Wongtschowski; L. S. Madureira (Eds.), O ambiente oceanográfico da plataforma continental e do talude na região Sudeste-Sul do Brasil, p. 466. São Paulo, Brazil: Edusp, 1982.

MIX, A. C. ***Influence of productivity variations on long-term atmospheric CO_2***. Nature, v. 337, p. 541–544, 1989.

MOHTADI, M. *et al*. ***North Atlantic forcing of tropical Indian Ocean climate***. Nature, v. 509, p. 76-80, 2014.

MÖLLER, O. O. *et al.* ***The effects of river discharge and seasonal winds on the shelf off southeastern South America***. Continental Shelf Research, v. 28, p.1607-1624, 2008.

MONNIN, E. *et al*. ***Atmospheric CO_2 concentration over the last glacial termination***. Science, v. 291, p. 112-114, 2001.

MORRISON, A. K.; FRÖLICHER, T. L.; SARMIENTO, J. L. ***Upwelling in the Southern Ocean***. ***Physics Today***, v. 68(1), 27, 2015.

MOY, C. M. *et al*. ***Variability of El Niño/ Southern Oscillation activity at millennial timescales during the Holocene epoch***. Nature, v. 420, p. 162-165, 2002.

MULITZA, S. *et al.* ***Planktonic foraminifera as recorders of past surface-water stratification***. Geology, v. 25, p. 335-338, 1997.

MULITZA, S. *et al.* ***Temperature: ^{18}O relationships of planktonic foraminifera collected from surface waters***. Palaeogeography, Palaeoclimatology, Palaeoecology, v. 202, p. 143-152, 2003.

MULITZA, S. *et al.* ***Temperature sensitivity of planktonic foraminifera and its influence on the oxygen isotope record***. Marine Micropaleontology, v. 33, p. 223-240, 1998.

NAIDU, P. D.; BABU, C. P.; RAO, C. H. M. ***Upwelling record in the sediments of the western continental margin of India***. Deep-Sea Research, v. 39, p. 715-723, 1992.

NOERNBERG, M. A.; KAMPEL, M.; BRANDINI, F. P. ***Estudo da variabilidade temporal da concentração de clorofila estimada por satélite na plataforma continental catarinense: latitude 26º 46' S***. Anais XIII Simpósio Brasileiro de Sensoriamento Remoto, p. 4635-4642. Florianópolis, Brazil: INPE. 2007.

NORTH GREENLAND ICE CORE PROJECT MEMBERS. ***High-resolution record of Northern Hemisphere climate extending into the last interglacial period***. Nature, v. 431, p. 147-151, 2004.

NUNES, M. V; VIVIERS, M.; LANA, C. C. ***Bacias sedimentares brasileiras: Bacia de Santos***. Fundação Paleontológica Phoenix, v. 66, p.1-6, 2004.

ODA, M.; YAMASAKI, M. ***Sediment trap results from the Japan Trench in the Kuroshio domain: Seasonal variations in the planktonic foraminiferal flux***. Journal of Foraminiferal Research, v. 35, p. 315-326, 2005.

OESCHGER, H. *et al*. ***Late glacial climate history from ice cores***. In: J. E. Hansen; T. Takahashi (Eds), Climate processes and climate sensitivity, v. 29, p. 299-306. Washington, D.C: American Geophysical Union, 1984.

OLSON, D. B. *et al*. ***Temporal variations in the separation of Brazil and Malvinas Currents***. Deep-Sea Research, v. 35, p. 1971-1990, 1988.

ORTIZ, J. D.; MIX, A. C.; COLLIER, R. W. ***Environmental control of living symbiotic and asymbiotic foraminifera of the California Current***. Paleoceanography, v. 10, p. 987-1009, 1995.

PALMA, E. D.; MATANO, R. P. Disentangling the upwelling mechanisms of the South Brazil Bight. Continental Shelf Research, v. 29, p. 1525-1534, 2009.

PALMA, E. D.; MATANO, R. P.; PIOLA, A. R. ***A numerical study of the Southwestern Atlantic shelf circulation: Stratified ocean response to local and offshore forcing***. Journal of Geophysical Research, v. 113 (C11010), 2008.

PALÓCZY, A. *et al.* ***Coastal upwelling off Cape São Tomé (22°S, Brazil): the supporting role of deep-ocean processes***. Continental Shelf Research, v. 89, p. 38-50, 2014.

PEETERS, F.; BRUMMER, G.; GANSSEN, G. ***Stable isotope composition of Globigerina bulloides and Globigerinoides ruber (planktic foraminifera) in modern surface the NW Arabian Sea***. Global and Planetary Change, v. 34, p. 269-291, 2002.

PEETERS, F. *et al.* ***Vigorous exchange between the Indian and Atlantic oceans at the end of the past five glacial periods***. Nature, v. 430, p. 661-665, 2004.

PETERSON, C. D.; LISIECKI, L. E.; STERN J. V. ***Deglacial whole-ocean $\delta^{13}C$ change estimated from 480 benthic foraminiferal records***. Paleoceanography, v. 29, p. 549-563, 2014.

PETERSON, R. G., *et al.* ***Lagrangian measurements in the Malvinas Current***. In: G. Wefer *et al.* (Eds.), The South Atlantic: present and past circulation, p. 239-247. Berlin, Germany: Springer-Verlag, 1996.

PETERSON, R. G.; STRAMMA, L. ***Upper-level circulation in the South Atlantic Ocean***. Progress in Oceanography, v. 26, p. 1-73, 1991.

PETIT, J. R. *et al*. ***Climate and atmospheric history of the past 420,000 years from the Vostok ice core, Antarctica***. Nature, v. 399, p. 429-436, 1999.

PIOLA, A. R. *et al.* ***The influence of the Plata River discharge on the western South Atlantic shelf***. Geophysical Research Letters, 32(1), L01603, 2005.

PIVEL, M. A. G. *et al*. ***The Holocene onset in the southwestern South Atlantic***. Palaeogeography, Palaeoclimatology, Palaeoecology, v. 374, p. 164-172, 2013.

PORTILHO-RAMOS, R. C. *et al*. ***Methane release from the southern Brazilian margin during the last glacial***. Nature Scientific Reports, v. 8(1), 5948, 2018.

PORTILHO-RAMOS, R. C. *et al*. ***Variability of the upwelling system in the southeastern Brazilian margin for the last 110,000 years***. Global and Planetary Change, v. 135, p. 179-189, 2015.

PRELL, W. L.; DAMUTH, J. E. ***The climate-related diachronous disappearance of Pulleniatina obliquiloculata in Late Quaternary sediments of the Atlantic and Caribbean***. Marine Micropaleontology, v. 3, p. 267-277, 1978.

PROVOST, C.; GARCIA, O.; GARÇON, V. ***Analysis of satellite sea surface temperature time series in the Brazil-Malvinas Current confluence region: dominance of the annual and semi-annual periods***. Journal of Geophysical Research, v. 97, p. 841-858, 1992.

RAHMSTORF, S. ***Abrupt climate change***. In: J. Steele; S. Thorpe; K. Turekian (Eds.) Encyclopedia of Ocean Sciences, p. 1-6. London, UK: Academic Press, 2001.

RAHMSTORF, S., ***Ocean circulation and climate during the past 120,000 years***. Nature, v. 419, p. 207-214, 2002.

RAHMSTORF, S. ***Thermohaline ocean circulation***. In: S. A. Elias (Ed.), Encyclopedia of Quaternary Sciences, Amsterdam, Netherlands: Elsevier, 2006.

RAVELO, A. C.; FAIRBANKS, R. G. ***Oxygen isotopic composition of multiple species of planktonic foraminifera: Recorders of the modern photic zone temperature gradient***. Paleoceanography, v. 7, p. 815-831, 1992.

RAZIK, S. *et al.* ***Depositional provinces, dispersal, and origin of terrigenous sediments along the SE South American continental margin***. Marine Geology, v. 363, p. 261-272, 2015.

RAZIK, S. *et al*. ***Interaction of the South American Monsoon System and the Southern Westerly Wind Belt during the last 14 kyr***. Palaeogeography, Palaeoclimatology, Palaeoecology, v. 374, p. 28-40, 2013.

REIMER, P. J. *et al*. ***Intcal09 and Marine09 radiocarbon age calibration curves, 0-50,000 years cal BP***. Radiocarbon, v. 51, p. 1111-1150, 2009.

REIMER, P. J. *et al*. ***IntCal13 and Marine13 radiocarbon age calibration curves 0-50,000 years cal BP***. Radiocarbon, v. 55, p. 1869-1887, 2013.

REIN, B. *et al.* ***El Niño variability off Peru during the last 20,000 years***. Paleoceanography 20, PA4003, 2005.

ROCHA, J. *et al*. ***Continental margin sedimentation off Brazil: Southern Brazil***. Contributions to Sedimentology, part 5, v. 4, p. 117-150, 1975.

RUDDIMAN, W. F. Earth's climate: Past and future. New York, USA: W.H. Freeman and Company (2nd Edition), 2008.

SANTOS, T. P. *et al.* ***Prolonged warming of the Brazil Current precedes deglaciations***. Earth and Planetary Science Letters, v. 463, p. 1-12, 2017a.

SANTOS, T. P. *et al*. ***The impact of the AMOC resumption in the western South Atlantic thermocline at the onset of the Last Interglacial***. Geophysical Research Letters, v. 44, p. 547-554, 2017b.

SARMIENTO, J. L. *et al*. ***High-latitude controls of thermocline nutrients and low latitude biological productivity***. Nature, v. 427, p. 56–60, 2010.

SARNTHEIN, M. *et al*. ***Fundamental modes and abrupt changes in North Atlantic circulation and climate over the last 60 ky: Concepts, reconstructions and numerical modeling***. In: P. Schäfer *et al.* (Eds.), The Northern North Atlantic: A changing environment, p. 365-410. Berlin, Germany: Pergamon, 2001.

SATO, R. M. ***The Brazil Current cyclonic meandering off Cape Santa Marta (28.5°S)***. Master thesis, p. 1-90. São Paulo, Brazil: University of São Paulo, 2015.

SCHEFFER, M.; BROVKIN, V.; COX, P. M. ***Positive feedback between global warming and atmospheric CO_2 concentration inferred from past climate change***. Geophysical Research Letters, v. 33, L10702, 2006.

SCHIEBEL, R.; HEMLEBEN, C. ***Modern planktic foraminifera***. Paläontologische Zeitschrift, v. 79, p. 135-148, 2005.

SCHIEBEL, R.; HEMLEBEN, C. ***Planktic foraminifers in the modern ocean***. Berlin, Germany: Springer-Verlag, 2017.

SCHMID, C. *et al.* T***he Vitória Eddy and its relation to the Brazil Current***. Journal of Physical Oceanography, v. 25, p. 2532-2546, 1995.

SCHMIDT, D. N. *et al*. ***Biogeography and evolution of body size in marine plankton***. Earth-Science Reviews, v. 78, p. 239-266, 2006.

SCHMITTNER, A.; LUND, D. C. ***Early deglacial Atlantic overturning decline and its role in atmospheric CO_2 rise inferred from carbon isotopes (^{13}C)***. Climate of the Past, v. 11, p. 135-152, 2015.

SCHMITTNER, A.; SAENKO, O. A.; WEAVER, A. J. ***Coupling of the hemispheres in observations and simulations of glacial climate change***. Quaternary Science Reviews, v. 22, p. 659-671, 2003.

SCUSSOLINI, P. *et al.* ***Saline Indian Ocean waters invaded the South Atlantic thermocline during glacial termination II***. Geology, v. 43, p. 139-142, 2015.

SEN GUPTA, A. *et al*. ***Projected changes to the Southern Hemisphere Ocean and sea ice in the IPCC AR4 climate models***. Journal of Climate, p. 22, v. 3047-3078, 2009.

SIGMAN, D. M.; BOYLE, E. A. ***Glacial/interglacial variations in atmospheric carbon dioxide***, Nature, v. 407, p. 859-869, 2000.

SIJP, W. P.; ENGLAND, M. H. ***The effect of a northward shift in the southern hemisphere westerlies on the global ocean***. Progress in Oceanography, v. 79, p. 1-19, 2008.

SILVEIRA, I. C. A. *et al*. ***A Corrente do Brasil ao largo da costa leste brasileira***. Revista Brasileira de Oceanografia, v. 48, p. 171-183,2000.

SKINNER, L. C. *et al*. ***Ventilation of the deep Southern Ocean and deglacial CO_2 rise***. Science, v. 328, p. 1147-1151, 2010.

SOUTO, D. D. *et al*. ***Marine sediments from southeastern Brazilian continental shelf: a 1200 year record of upwelling productivity***. Palaeogeography, Palaeoclimatology, Palaeoecology, v. 299, p. 49-55, 2011.

STOCKER, T. F. ***The seesaw effect***. Science, v. 282, p. 61-62, 1998.

STOCKER, T. F.; JOHNSEN, S. J. ***A minimum thermodynamic model for the bipolar seesaw***. Paleoceanography, v. 18, PA000920, 2003.

STOMMEL, H. ***Thermohaline convection with two stable regimes of flow***. Tellus, v. 13, p. 224-230, 1961.

STRAMMA, L.; ENGLAND, M. ***On the water masses and mean circulation of the South Atlantic Ocean***. Journal of Geophysical Research, v. 104, p. 20863-20883, 1999.

STRÍKIS, N. M. *et al*. ***Timing and structure of Mega-SACZ events during Heinrich Stadial 1***. Geophysical Research Letters, v. 42, p. 5477-5484, 2015.

STUIVER, M.; REIMER, P. J.; REIMER, R. W. ***CALIB 7.1*** [www program] http://calib.org. accessed 2017-3-3], 2017.

TALLEY L. D. *et al.* ***Descriptive physical oceanography: an introduction***, 6th edition, p. 560. Boston, USA: Elsevier, 2011.

THOMSEN, L. *et al.* ***The oceanic biological pump: rapid carbon transfer to depth at continental margins during winter***. Scientific Reports, v. 7, 10763, 2017.

TOLEDO, F. A. L.; COSTA, K. B.; PIVEL, M. A. G. ***Salinity changes in the western tropical South Atlantic during the last 30 kyr***. Global and Planetary Change, v. 57, p. 383-395, 2007.

TOLEDO, F. A. L. *et al*. ***Tracing past circulation changes in the western South Atlantic based on planktonic foraminifera***. Revista Brasileira de Paleontologia, v. 11, p. 169-178, 2008.

TOMCZAK, M.; GODFREY, J. S. ***Regional Oceanography: An introduction***, p. 402. Delhi, India: Daya Publishing House, 2003.

TORN, M. S.; HARTE, J. ***Missing feedbacks, asymmetric uncertainties, and the underestimation of future warming***. Geophysical Research Letters, v. 33, L10703, 2006.

UJIIÉ, Y. *et al.* ***Spatial and temporal variability of surface water in the Kuroshio source region, Pacific Ocean, over the past 21,000 years: evidence from planktonic foraminifera***. Marine Micropaleontology, v. 49, p. 335-364, 2003.

UJIIÉ, Y.; ISHITANI Y. ***Evolution of a planktonic foraminifer during environmental changes in the tropical oceans***. PLoS ONE, v. 11(2), 2016.

UJIIÉ, H.; UJIIÉ, Y. ***Late Quaternary course changes of the Kuroshio Current in the Ryukyu Arc region, northwestern Pacific Ocean***. Marine Micropaleontology, v. 37, p. 23-40, 1999.

VELLINGA, M.; WOOD, R. A. ***Global climatic impacts of a collapse of the Atlantic thermohaline circulation***. Climate Change, v. 54, p. 251-267, 2002.

VERA, C. S.; VIGLIAROLO, P. K.; BERBERY, E. H. ***Cold season synoptic-scale waves over subtropical South America***. Monthly Weather Review, v.130, p. 684-699, 2002.

VÖLKER, C.; KÖHLER, P. ***Responses of ocean circulation and carbon cycle to changes in the position of the Southern Hemisphere westerlies at Last Glacial Maximum***. Paleoceanography, v. 28, p. 726-739, 2013.

WAELBROECK, C. *et al*. ***Sea-level and deep water temperature changes derived from benthic foraminifera isotopic records***. Quaternary Science Reviews, v. 21, p. 295-305, 2002.

WALKER, M. J. C. *et al*. ***Formal subdivision of the Holocene Series/Epoch: a Discussion Paper by a Working Group of INTIMATE (Integration of ice-core, marine and terrestrial records) and the Sub-commission on Quaternary Stratigraphy (International Commission on Stratigraphy)***. Journal of Quaternary Science, v. 27, p. 649-659, 2012.

WANG, X. *et al*. ***Interhemispheric anti-phasing of rainfall during the last glacial period***. Quaternary Science Reviews, v. 25, p. 3391-3403,2006.

WANG, P.; ZHANG, J.; MIN, Q. ***Distribution of foraminifera in surface sediments of the East China Sea***. In: P. Wang *et al*. (Eds.), Marine Micropaleontology of China, p. 34-69. Beijing, China: Springer-Verlag, 1985.

WANNER, H. *et al*. ***Mid-to Late Holocene climate change: an overview***. Quaternary Science Reviews, v. 27, p. 1791-1828, 2008.

WATKINS, J. M.; MIX, A. C.; WILSON, J. ***Living planktic foraminifera: tracers of circulation and productivity regimes in the central equatorial Pacific***. Deep-Sea Research II, v. 43, p. 1257-1282, 1996.

WEBER, M. E. *et al*. ***Millennial-scale variability in Antarctic ice-sheet discharge during the last deglaciation***. Nature, v. 510, p. 134-138, 2014.

WEFER, G.; MULITZA, S.; RATMEYER, V. ***The South Atlantic in the Late Quaternary: Reconstruction of material budgets and current systems***. Berlin, Germany: Springer-Verlag, 2004.

WEIJER, W. *et al*. ***Response of the Atlantic overturning circulation to South Atlantic sources of buoyancy***. Global and Planetary Change, v. 34, p. 293-311, 2002.

WELDEAB, S.; SCHNEIDER, R. R.; KÖLLING, M. ***Deglacial sea surface temperature and salinity increase in the western tropical Atlantic in synchrony with high latitude climate instabilities***. Earth and Planetary Science Letters, v. 241, p. 699–706, 2006.

XU, J. *et al.* ***Response of planktonic foraminifera to glacial cycles: Mid-Pleistocene change in the southern South China Sea***. Marine Micropaleontology, v. 54, p. 89-105, 2005.

YAMASAKI, M.; ODA, M. ***Sedimentation of planktonic foraminifera in the East China Sea: Evidence from a sediment trap experiment***. Marine Micropaleontology, v. 49, p. 3-20, 2003.

ZEMBRUSCKI, S. G. ***Geomorfologia da margem continental sul brasileira e das bacias oceânicas adjacentes***. In: H. A. F. Chaves (Ed.), Geomorfologia da margem continental brasileira e das áreas oceânicas adjacentes. Série Projeto REMAC, v. 7, p. 129-177. Rio de Janeiro, Brazil: CENPES/PETROBRÁS, 1979.

ZHANG, P. *et al*. ***Geochemical characteristics from tests of four modern planktonic foraminiferal species in the Indonesian Throughflow region and their implications***. Geoscience Frontiers, in press. [http://schbylg.com/360/science/article/pii/S1674987118300471] (accessed September, 2018).

ZHANG, R.; DELWORTH, T. L. ***Simulated tropical response to a substantial weakening of the Atlantic thermohaline circulation***. Journal of Climate, v. 18, p. 1853-1860, 2005.

ZHOU, J.; LAU, K. M. ***Does a monsoon climate exist over South America?*** Journal of Climate, v. 11, p. 1020-1040, 1998.